University of Alberta

Oil sand middling processing using a flotation column.

by

Jessica Vandenberghe

A thesis submitted to the Faculty of Graduate Studies and Research in partial fulfillment of the requirements for the degree of Master of Science

in

Chemical & Mining Engineering

Department of Chemical and Materials Engineering

Edmonton, Alberta

Spring 2003

National Library of Canada
Acquisitions and Bibliographic Services
395 Wellington Street
Ottawa ON K1A 0N4
Canada

Bibliothèque nationale du Canada
Acquisitions et services bibliographiques
395, rue Wellington
Ottawa ON K1A 0N4
Canada

Your file Votre référence

Our file Notre référence

The author has granted a non-exclusive licence allowing the National Library of Canada to reproduce, loan, distribute or sell copies of this thesis in microform, paper or electronic formats.

L'auteur a accordé une licence non exclusive permettant à la Bibliothèque nationale du Canada de reproduire, prêter, distribuer ou vendre des copies de cette thèse sous la forme de microfiche/film, de reproduction sur papier ou sur format électronique.

The author retains ownership of the copyright in this thesis. Neither the thesis nor substantial extracts from it may be printed or otherwise reproduced without the author's permission.

L'auteur conserve la propriété du droit d'auteur qui protège cette thèse. Ni la thèse ni des extraits substantiels de celle-ci ne doivent être imprimés ou autrement reproduits sans son autorisation.

0-612-82358-X

Canada

University of Alberta

Library Release Form

Name of Author: Jessica Vandenberghe

Title of Thesis: Oil sand middling processing using a flotation column

Degree: Master of Science

Year this Degree Granted: 2003

Permission is hereby granted to the University of Alberta Library to reproduce single copies of this thesis and to lend or sell such copies for private, scholarly or scientific research purposes only.

The author reserves all other publication and other rights in association with the copyright in the thesis, and except as herein before provided, neither the thesis nor any substantial portion thereof may be printed or otherwise reproduced in any material form whatever without the author's prior written permission.

Jessica Vandenberghe

#601, 9903 – 104 Street
Edmonton, AB T5K 0E4
Canada

Submitted: 01/02/03

University of Alberta

Faculty of Graduate Studies and Research

The undersigned certify that they have read, and recommend to the Faculty of Graduate Studies and Research for acceptance, a thesis entitled *Oil sand middling processing using a flotation column* submitted by Jessica Vandenberghe in partial fulfillment of the requirements for the degree of Master of Science in Chemical & Mining Engineering.

Dr. Zhenghe Xu
(Supervisor)

Dr. Jacob Masliyah
(Supervisor)

Dr. Jozef Szymanski
(External committee member)

Oct 8/02

This thesis is dedicated to my parents, Mrs. Anna Zinterer and Mr. Murray Zinterer, as well as to my husband, Mr. Mark Vandenberghe, for their support, patience and encouragement.

ABSTRACT

Flotation columns may benefit the oil sand industry by improving grade and recovery when processing middlings. Preliminary testing was conducted with a laboratory flotation column for two-phase systems over a bubble size range of 250 to 1100 μm. A correlation between exponent "m" in the drift flux equation, $j_{gf} = U_t \alpha_g (1 - \alpha_g)^m$, and bubble Reynolds number was established, where j_{gf}, U_t, α_g, and "m" are the drift flux, terminal velocity of a bubble, gas volume fraction, and an exponent depending on flow conditions, respectively. The correlation is valid for a Reynolds number range of 5 to 70. After preliminary testing, the column was tested to ensure little difficulty when processing oil sands. Next, in-plant tests at Suncor Energy Inc. using a feed stream of oil sand middlings were completed to investigate the effects of the feed, recirculation, air, and wash water flow rates on bitumen recovery.

ACKNOWLEDGEMENTS

I would like to thank both my supervisors, Dr. Zhenghe Xu and Dr. Jacob Masliyah, for their guidance and encouragement throughout the course of this thesis.

I would also like to extend thanks to Dr. Jaewon Choung, for his support, advice, and help throughout the project. My gratitude also extends to the Oil Sands group and the staff in the Department of Chemical and Materials Engineering at the University of Alberta.

My thanks also goes to my family for their support and encouragement, as well as to my loving husband, Mr. Mark Vandenberghe, for always being there for me.

I would like to thank all the industrial support that I received while conducting the tests at Syncrude Research Centre in Edmonton, Alberta and at Suncor Energy Inc. oil sands plant in Fort McMurray, Alberta.

Finally, I would like to thank the NSERC Industrial Research Chair in Oil Sands Engineering for the funding that made this thesis project possible.

TABLE OF CONTENTS

1.0 INTRODUCTION 1

2.0 LITERATURE REVIEW 5

2.1 Different types of flotation devices 5

2.2 Modifications of the conventional flotation column 11

2.3 Flotation column characteristics 17

2.4 Drift flux analysis 21

3.0 TWO-PHASE MODEL SYSTEM TESTS 32

3.1 Bubbly zone theory 32

3.2 Froth zone theory 36

3.3 Equipment and set-up 39

3.4 Materials and procedures 41

3.5 Results and discussion 42

3.6 Conclusions 51

4.0 BITUMEN FLOTATION TESTS 52

4.1 Equipment and set-up 52

4.2 Materials and procedures 55

4.2.1 Sample analysis 55

4.3 Experimental techniques 57

4.3.1 Tests at the University of Alberta 57

4.3.2 Syncrude Research Centre tests 58

4.3.3 Suncor in-plant tests 60

4.4 Results and discussion 62

4.4.1 Tests at the University of Alberta 62

4.4.2 Syncrude Research Centre tests 65

4.4.3 Suncor in-plant tests 70

4.5 Conclusions 77

5.0 CONCLUSIONS 79

6.0 RECOMMENDATIONS 80

REFERENCES 82

APPENDIX A: Bubbly region calculations 87

A.1 Sample calculations to find the bubble diameter in the bubbly zone 88

A.2 Visual Basic program 94

APPENDIX B: Froth region calculations 98

B.1 Sample calculations to find the gas volume fraction in the froth zone 99

B.2 Visual Basic program 102

APPENDIX C: Calibration equations 105

C.1 Pump calibration 106

C.2 Air rotameter calibration 107

C.3 Summary of all the calibration equations 108

APPENDIX D: Methyl isobutyl carbinol (MIBC) information 111

D.1 Material Safety Data Sheet (MSDS) 112

D.2 General information on frothers 115

APPENDIX E: Flotation column operating procedures 116

E.1 Two-phase system test operating procedure 117

E.2 Bitumen flotation test operating procedure 118

APPENDIX F: Two-phase system test data 120

F.1 Two-phase system test data 121

APPENDIX G: Dean Stark method 127

G.1 Dean Stark method 128

APPENDIX H: HAZOP for flotation column 132

H.1 HAZOP for flotation column 133

APPENDIX I: Bitumen flotation test data 134

I.1 Tests at the University of Alberta 135

I.2 Syncrude Research Centre tests 135

I.3 Suncor in-plant tests 137

LIST OF TABLES

Table 2-1.	Summary of empirical relations of exponent "m" reported in literature.	30
Table 3-1.	Properties of the process water used for the two-phase system tests.	41
Table 4-1.	Operating conditions for the initial bitumen flotation tests completed at the University of Alberta.	64
Table 4-2.	Results for the bitumen flotation tests conducted at the Syncrude Research Centre.	69
Table 4-3.	Summary of the pilot plant conditions at the Syncrude Research Centre during the bitumen flotation tests.	70
Table 4-4.	Summary of the results from the bitumen flotation tests conducted at Suncor (sample analysis completed at the University of Alberta).	74
Table C-1.	Data gathered to calibrate the Matheson I/P wash water pump used for the two-phase system tests.	106
Table C-2.	Calibration data for the Matheson air rotameter used in the two phase system test.	108
Table C-3.	Summary of all the calibration equations used for the corresponding test.	109
Table F-1.	Raw data for two-phase system tests.	121
Table F-2.	Results for the two-phase system tests.	122

Table F-3. Data used in generating Figure 3-6, a comparison between the bubbly zone measured and calculated average bubble diameters. 123

Table F-4. Data used in generating Figure 3-7, the relationship between gas flux and the bubbly zone bubble diameter. 124

Table F-5. Bubbly zone data used in generating Figure 3-9, relationship between exponent "m" and bubble Reynolds number. 125

Table F-6. Data used to generate Figure 3-10, the relationship between Reynolds number and bubble diameter in the froth zone. 126

Table I-1. The raw data collected for the University bitumen flotation tests. 135

Table I-2. The resultant data collected for the University bitumen flotation tests. 135

Table I-3. Raw data for bitumen flotation tests conducted at the Syncrude Research Centre. 136

Table I-4. Resultant data for bitumen flotation tests conducted at the Syncrude Research Centre. 136

Table I-5. Pilot plant conditions on the same day as the bitumen flotation tests, including ore type, grade, and fines, as well as chemical type and concentration. 137

Table I-6 Raw data for the tests completed at Suncor. 138

Table I-7. Raw data for feed sample analysis completed at the University of Alberta for all the tests conducted at Suncor. 139

Table I-8. Raw data for the underflow sample analysis completed at the University of Alberta for the flotation tests conducted at Suncor. 140

Table I-9. Results from the tests conducted at Suncor.

LIST OF FIGURES

Figure 2-1. Schematic of a conventional cylindrical flotation column. 7

Figure 2-2. The two main zones within a flotation column, the bubbly and froth zones. 8

Figure 2-3. The column design used in this thesis study. 15

Figure 2-4. A schematic of the air sparger used in this thesis study. 16

Figure 2-5. An example of drift flux analysis used to predict the bubbly and froth zone gas volume fractions for a given j_g and j_f. 24

Figure 2-6. An example of the drift flux analysis when the bubbly and froth zones have sufficiently different Reynolds numbers and how to predict the bubbly and froth zone gas volume fractions for a given j_g and j_f. 25

Figure 2-7. Variation of operating lines on the depending flow pattern in a flotation column. 26

Figure 3-1. Flowchart of the iterative process used to calculate bubble diameter based on gas volume fraction. 34

Figure 3-2. Flowchart of the froth zone calculations used to determine gas hold-up based on an average bubble diameter in the froth zone. 38

Figure 3-3. A schematic of the flotation column used for this study, including dimensions. 40

Figure 3-4. A snapshot of the bubbly zone during a process water test, indicating that the bubbles are spherical in shape. 43

Figure 3-5. A snapshot of the froth zone during a process water test, illustrating that the bubbles are spherical in shape. 43

Figure 3-6. A comparison between the measured and calculated average bubble diameters in the bubbly zone for all the tests. 44

Figure 3-7. The relationship between gas flux and bubble diameter in the bubbly zone for all the tests. 45

Figure 3-8. An example of a process water test where exponent "m" was adjusted such that the system characteristic curve and the operating line intersected at the locations of the pre-determined gas volume fractions. 46

Figure 3-9. A plot of between exponent "m" and bubble Reynolds number for the bubbly zone. 47

Figure 3-10. A plot of the relationship between froth zone Reynolds number and bubble diameter. 48

Figure 3-11. Comparison between the trial and error and calculated exponent "m" values for the bubbly and froth zones for all the tests. 49

Figure 3-12. An example of the drift flux analysis for a 7.8 ppm MIBC aqueous solution test, using the new correlations. 50

Figure 4-1. Schematic of the flotation column used in the bitumen flotation tests. The column was operated in a continuous mode. 53

Figure 4-2. Schematic of the air sparger used in the bitumen flotation tests. 53

Figure 4-3. Schematic of the experimental set-up used for tests at the University of Alberta. 57

Figure 4-4. Schematic of the flotation column set-up used for the bitumen flotation tests conducted at the Syncrude Research Centre. 59

Figure 4-5. Schematic of the flotation column set-up used for the bitumen flotation tests at Suncor. 61

Figure 4-6. An example of the bitumen accumulation on the 20 L sample pail that was used to transport the process middling to the University of Alberta. 63

Figure 4-7. The feed stirrers used to create a more homogenous feed for the University of Alberta tests. 63

Figure 4-8. An example of the samples taken during the University of Alberta tests. 65

Figure 4-9. The feed screen as it was plugged during the bitumen flotation tests at Syncrude Research Centre, allowing for flow from only the bottom of the screen. 66

Figure 4-10. An example of the froth along with the wash water distributor and launder used to direct the froth stream. 68

Figure 4-11. An example of the feed slurry when air was pre-maturely introduced before entering the flotation column. 71

Figure 4-12. An example of the feed slurry without pre-mature air introduction, before it entered the flotation column. 72

Figure 4-13. An example of the feed and tailings samples for Test 1 conducted at Suncor. 75

Figure 4-14. The froth during Test 13 where no wash water was introduced. 77

Figure C-1. Calibration curve used for the wash water pump. 107

Figure C-2. Calibration curve for the Matheson air rotameter used in the two-phase system tests. 108

Figure G-1. Schematic of separation process used in the Dean Stark method. 129

LIST OF NOMENCLATURE

A	cross-sectional area of the flotation column, m^2
C_D	drag coefficient for terminal velocity, dimensionless
d_{32}	Sauter mean bubble diameter, m
d_b	bubble diameter, m
d_{bCALC}	calculated bubble diameter, m
d_{bi}	bubble diameter of bubble *i*, m
d_{bv}	volumetric mean bubble diameter, m
d_c	diameter of the flotation column, m
d_{sb}	statistical mean bubble diameter, m
g	gravitational constant, m/s^2
h	the height difference between liquid levels in the two adjacent manometers, m
j	total flux, m/s
j_f	liquid flux (or superficial velocity), m/s
j_g	gas flux (or superficial velocity), m/s
j_{gf}	drift flux of a gas-liquid system, m/s
L	the total distance between the two adjacent manometer ports, m
m	a parameter that depends on flow conditions, dimensionless
m_b^{feed}	mass flow rate of bitumen in the feed stream, kg/s
m_b^{froth}	mass flow rate of bitumen in the froth stream, kg/s
$m_b^{tailings}$	mass flow rate of bitumen in the tailings stream, kg/s

m_s^{feed}	mass flow rate of solids in the feed stream, kg/s
m_s^{froth}	mass flow rate of solids in the froth stream, kg/s
$m_s^{tailings}$	mass flow rate of solids in the tailings stream, kg/s
m_w^{feed}	mass flow rate of water in the feed stream, kg/s
m_w^{froth}	mass flow rate of water in the froth stream, kg/s
$m_w^{tailings}$	mass flow rate of water in the tailings stream, kg/s
$m_w^{washwater}$	mass flow rate of water in the wash water stream, kg/s
n_i	number of bubbles having bubble diameter d_{bi}
Q_g	net gas volumetric flow rate, m^3/s
Re_b	Reynolds number based on terminal velocity of a single bubble, dimensionless
Re_{bs}	Reynolds number based on slip velocity, dimensionless
$Re_{froth\ zone}$	Reynolds number for in the froth zone, dimensionless
U_{gf}	relative or slip velocity, m/s
U_{gfCALC}	calculated relative (or slip) velocity, m/s
U_t	terminal velocity of a single bubble or settling velocity of a single particle in an infinite stationary liquid, m/s
U_{tCALC}	calculated value of terminal velocity of a single bubble or settling velocity of a single particle in an infinite stationary liquid, m/s
v_f	liquid velocity relative to a stationary observer, m/s
v_g	gas velocity relative to a stationary observer, m/s

Greek Letters

Δ	difference in parameters, dimensionless
α_f	liquid volume fraction, dimensionless
α_g	gas volume fraction, dimensionless
α_{gCALC}	calculated gas volume fraction, dimensionless
ρ	density, kg/m^3
ρ_b	density of a bubble, kg/m^3
ρ_f	density of the liquid phase, kg/m^3
ρ_g	density of the gas phase, kg/m^3
σ	surface tension, N/m
μ_f	viscosity of the liquid phase, Pa s

1.0 INTRODUCTION

The Athabasca oil sands in Northern Alberta, Canada represent the largest known source of oil sand in the world. In the past, oil sand was mined using draglines, bucketwheels, and conveyors. Currently, the mining operations are shifting towards more mobile equipment such as trucks and shovels. Once the oil sand has been mined, it is fed into crushers where the major lumps and rocks are crushed into smaller, more manageable sizes. After crushing it is either mixed with hot water and transported via hydrotransport pipelines or moved via conveyors to tumblers where hot water and caustic are added. The hydrotransport pipelines or tumblers initiate the three major steps necessary in separating bitumen from oil sand: bitumen liberation, aeration, and bitumen-air attachment. Hydrotransport pipelines are favored over tumblers because they are more convenient and economical. In the case of tumblers, the oil sand must first be transported over a large distance from the mine to the extraction plant via conveyors before entering the tumblers. In both cases, the bitumen is liberated by shear action and often bitumen separation is accelerated by introducing additives such as caustic or diesel oil and by increasing the slurry temperature to lower the bitumen viscosity. The next step in the extraction process is aeration. Air is entrained in mixing boxes and within the tumblers through air/slurry contact at the free slurry interface. In hydrotransport pipelines, additional air is injected via nozzles. With the bitumen liberated and air bubbles available, the bitumen will either coat, engulf, or attach as a separate droplet to an air bubble, depending on system properties, mainly temperature. The slurry, at this stage, is pumped into large gravity separation vessels where the air-bitumen aggregates float upwards and accumulate at the top of the vessels, while the denser particles settle

out as an underflow stream, which is referred to as tailings. The froth collected at the top of the vessels by overflow is further processed while the tailings are sent to a tailings pond where water is recovered and recycled back into the process. Although the majority of the bitumen is floated in the gravity separation vessels, there are small droplets that neither sink nor float and consequently accumulate in the middle of the vessel. A middling stream is taken from the vessel to be further processed by a flotation device, such as a Denver cell, and it is here that the use of a flotation column may be beneficial. Flotation columns have a good possibility of improving both bitumen recovery and grade since columns have proven aeration techniques that would work well in collecting finer bitumen droplets.

Flotation columns can be applied to many different industrial situations. In the mineral and coal industries, columns are replacing conventional flotation machines such as scavengers and cleaners (Finch & Dobby, 1990). Burnstein & Flint (2000) summarized several ways flotation columns are useful in the environmental sector. They listed applications such as hydrocarbon removal from water, resulting in a by-product recovery; reprocessing of existing mineral waste dumps; site run-off treatments; soil decontamination treatments; and possible effluent treatments. The aforementioned applications are just a few ways in which flotation columns can be used to benefit the environment. Flotation columns have also been successfully introduced to process tailings in the oil sand industry. Oil sand tailings often contain fine and coarse sands along with other minerals such as titanium and zirconium, of which flotation columns can remove the heavier materials. Ityokumbul et al. (1988) showed that use of batch bubble

columns, a type of flotation column, results in a rapid recovery of the aforementioned minerals. Flotation columns can also be used to recover bitumen from the tailings, but the recovery rate is much slower than that of the heavier minerals and it may not be economical.

A wide variety of industries have demonstrated the benefits of using flotation columns. The main benefits are: improved recovery, higher product grades, significant energy and maintenance savings, higher sensitivities, low capital and operating costs, and adaptability to computer process control (Pal & Masliyah, 1989; Finch & Dobby, 1990). Since flotation columns have many advantages and a high degree of flexibility, there is a good possibility of successfully extending flotation column use to areas within the oil sand industry such as: low-grade feed, high fines ore, transition ore, and processing middlings. In all of these examples, current methods have difficulties in floating the bitumen, but a flotation column that generates sufficiently small air bubbles in a cost efficient manner may increase both bitumen recovery and grade.

Before applying flotation columns to the oil sand industry, preliminary testing to characterize a column is necessary. This study characterized a flotation column using the drift flux analysis developed by Wallis (1969) for the two-phase systems of air and either industrial process water or aqueous solutions of low concentration methyl isobutyl carbinol (MIBC) in de-ionized water. Characterizing the column allowed the effects of changing air and/or liquid flow rates on the flow characteristics in the bubbly and froth regions to be predicted. A correlation for exponent "m", used in the drift flux system

characterizing equation, was established to predict the bubbly and froth zone gas volume fractions. The initial two-phase system tests were also performed to determine the size range of air bubbles that the gas sparger could produce. By knowing the minimum bubble diameter, insight into how well the column would process oil sands was gained. With the knowledge of the bubble diameter limitations and flow characteristics, the column was made ready to recover bitumen from oil sand middlings.

The main objective of this study is to explore the use of a flotation column to improve bitumen recovery when processing oil sand middlings. To determine the operating conditions optimum for bitumen recovery, the effects of varying the feed, recirculation, air, and wash water rates on bitumen recovery were evaluated. Since the extraction process is fairly similar for all oil sand processing plants, the results from the in-plant tests at both the Syncrude Research Centre and Suncor Energy Inc. were generalized to include most of the oil sand industry.

2.0 LITERATURE REVIEW

2.1 Different types of flotation devices

Flotation is based on the concept of buoyancy difference although the separation is based on differences in surface wettability. There are many different ways to design flotation devices to achieve the goal of removing impurities from a medium. Finch (1995) categorized the three main types of flotation devices as: mechanical cells, reactor/separator cells, and flotation columns. All three flotation systems must accomplish two functions: the attachment of particles to gas bubbles and the subsequent separation of the bubble-particle aggregates from the medium.

Mechanical cells induce flotation by mechanically agitating the slurry and often consist of several stages including: roughing, scavenging, cleaning, and cleaner scavenging (Gray et al., *2002*). Like most improved flotation devices, recently developed mechanical cells use wash water to reduce the amount of entrained particles in the froth by creating a downward flow back into the bubbly zone. As the wash water flows downwards, it sweeps away the smaller hydrophilic particles that entered the froth due to drag from the loaded bubble-particle aggregates. These mechanical cells also use froth boosting to develop a deeper and more stable froth. A deeper froth has the benefit of improved froth stability and better froth drainage, resulting in a higher selectivity of the product particles and an improved overall froth grade. In comparison to other flotation devices, mechanical flotation machines tend to have lower selectivity, but higher flotation rates (Xu et al., 1996a). An example of a mechanical cell is the HG tank cell developed

by Outokumpu (Green & Cox, 1993). In this particular design, an adjustable booster cone is used to limit the space that froth can occupy. By adjusting the height position of the cone and consequently the froth depth, the grade is improved. As well, the solids removal rate is improved by changing the available surface area (Finch, 1995).

The second type of flotation device is the reactor/separator cell. As mentioned previously, the two main functions of a flotation device are to attach hydrophobic particles to gas bubbles and subsequently separate the resultant aggregates from the medium. A reactor/separator cell physically separates these two functions such that the reactor enhances bubble – particle attachment and the separator facilitates the separation. Since the functions are separated, a better overall performance is achieved because of: increased particle collection rates, increased unit column capacity, and reduced column height (Xu et al., 1996a). Examples of reactor-separator devices include the Jameson cell, the pneumatic cell, the contact cell, and the Centrifloat.

The third and last category of flotation devices is flotation columns. In the past, the only flotation column design available was the conventional column design, as illustrated in Figure 2-1. The Column Flotation Company of Canada first introduced this design in 1981 for the Les Mines Gaspés (Quebec, Canada) to help with molybdenum (Mo) cleaning. In a conventional column, feed is usually introduced just below the interface of the bubbly and froth zones while gas is introduced at the bottom of the column via a gas sparger. As the bubble rises from the bottom of the column, it collides with the downward traveling particles creating a countercurrent flow.

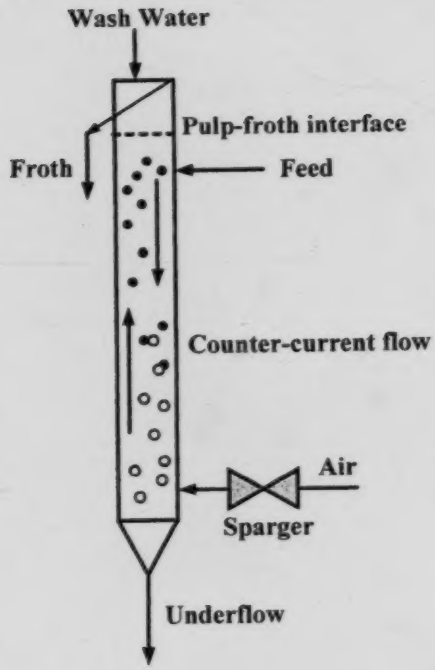

Figure 2-1. Schematic of a conventional cylindrical flotation column.

Once collision occurs, the hydrophobic particles have a tendency to attach to the rising bubbles and the resulting aggregates proceed to the top of the column where they are collected. The countercurrent flow enhances the probability of contact between the hydrophobic particles and gas bubbles. Typically, columns operate with small bubbles (d_b < 3 mm) and low gas flow rates (< 4 cm/s). Continuous countercurrent operation is generally used with an intermediate solids concentration of 10 to 15% v/v and a particle size < 100 μm (Banisi et al., 1995a).

The two main zones within a flotation column are the bubbly zone and the froth zone as shown in Figure 2-2.

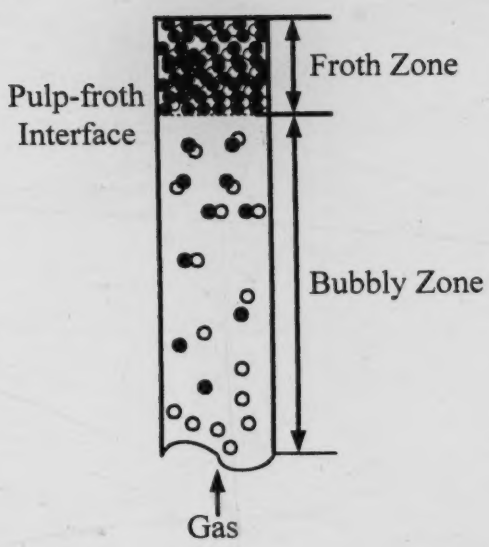

Figure 2-2. The two main zones within a flotation column, the bubbly and froth zones.

The bubbly zone is the region where gas bubbles attach to hydrophobic particles. After the bubble-particle aggregates rise through the bubbly zone, they eventually meet with the pulp-froth interface and enter the second region, the froth zone. Falutsu (1994) stated that the main methods for solid material to enter the froth zone are by attachment to gas bubbles, entrainment in the liquid behind gas bubbles or aggregates, mechanical entrapment in the aggregates due to partial slime coating or flocculation, and finally by carrier flotation (finer particles attach to coarser particles). Upon contact with the interface, the aggregates rapidly decelerate and the particles may detach from the gas bubbles. Particles return to the bubbly zone through three main mechanisms: bubble coalescence, particle detachment, and liquid drainage (Falutsu, 1994). If the particles manage to remain attached to the gas bubbles, they cross the interface and enter the froth zone. Once in the froth zone, possible detachment may also occur from liquid drainage,

bias water, slippage, or oscillation factors (Falutsu, 1994). There is a possibility of reattachment in the froth zone as well, although the probability is quite low. Once the aggregates enter the froth, they continue to the top of the froth bed where they are removed as a product.

Although the froth zone mainly consists of hydrophobic particles, entrained hydrophilic particles often cross the interface as well. To improve the froth grade, wash water can be introduced to rinse the entrained hydrophilic particles back to the bubbly zone. By removing entrained particles from the froth, overall froth quality increases (Pal & Masliyah, 1989; Yianatos et al., 1986). Froth properties also depend on wash water distribution, which in turn is affected by the design of the wash water distributor and its positioning (Yianatos & Bergh, 1995). The defining parameter of wash water is bias, which is defined as the difference between the fresh water added near the top of the froth and the fresh water that goes into the concentrate (Yianatos & Bergh, 1995). A more common definition of bias is the net water flow rate across the pulp-froth interface. Positive bias represents net water flow from the froth zone across the interface to the bubbly zone. The advantages of bias include the ability to stabilize the froth by compensating for water drainage due to gravity and the prevention of solids entrainment by replacing the feed water with fresh water (Yianatos & Bergh, 1995).

The froth zone is affected by parameters such as wash water rate, froth depth, bubble residence time, and dropback. Dropback particles are the fraction of solids that enter the froth zone attached to gas bubbles but eventually return to the bubbly zone

(Falutsu, 1994). Dropback needs to be considered when modeling the froth zone, since solid particles greatly affect the froth structure and stability. To have a higher grade product with sufficient selectivity, ideally no hydrophilic solid particles should be carried over with the froth product.

To apply flotation columns to industry, the column must be easily scaled from laboratory to industrial size. Most scaling is based on chemical kinetics, mainly the axial dispersion model which involves the two parameters of the flotation rate constant and the solids vessel dispersion number (Xu et al., 1996b; Dobby & Finch, 1986). Often the model used for a laboratory system cannot be applied to the industrial size system and each must be modeled separately. Furthermore, the bubbly and froth zones are also modeled separately. The bubbly zone can be modeled by a first order rate process, which depends on the rate constant, particle retention time, and degree of axial mixing in the bubbly zone (Finch & Dobby, 1991). The froth zone can be simulated using a plug flow model including a first order kinetic process to describe the solid dropback (Yianatos et al., 1998). Other froth zone models have been developed for both two-phase froths (Yianatos, 1987) and three phase froths (Ross & Van Deventer, 1988). Yianatos et al. (1986) took a different froth modeling approach and separated the froth into an upper and lower zone. The upper zone acted like a packed bubble bed (gas volume fraction > 0.74), while the lower zone acted like an expanded bubble bed (0.20 < gas volume fraction < 0.74). Solid particle behavior is best modeled using a sedimentation dispersion model (Ityokumbul, 1996). In both the bubbly and froth zones, recovery is an important parameter and often has a model that is proportional to particle residence time, which in

turn depends on aeration dynamics. In scaling a bench scale column to industrial size, the control system must be adaptable to computer process control application. Persechini et al. (2000) showed that the controlled variables (froth layer height, bias, and froth zone gas volume fraction) and the manipulated variables (wash water, air, and non-floated fraction flow rates) could be modeled using a linear multivariate model. The application of computer process control techniques allows for easy adjustment of variables such as column flow rate and pulp-froth interface level.

2.2 Modifications of the conventional flotation column

Most conventional columns are cylindrical, but tests have been conducted with rectangular columns as well (Alexander & Shah, 1976; Akita & Yoshida, 1973). If a cylindrical column diameter is equal to one side of a square column, the effects are virtually equal and the geometry of the column is unimportant. Akita & Yoskida (1973) found that the liquid phase mass transfer coefficient used to define the liquid axial dispersion coefficient is the same in either situation. In addition to the cross-sectional shape of a column, height is often an issue as well. Ityokumbul (1996) proposed that height should be estimated based on mass transfer. Some evidences indicate that the particle-collection process occurs at a relatively constant height within a cylindrical column and is independent of actual recovery zone height (Ityokumbul, 1996). Most columns use a height to diameter ratio of approximately 5:1, although there is insufficient evidence indicating this ratio is the most effective (Ityokumbul, 1996).

A modified flotation column, first utilized by Falutsu & Dobby (1989) and later tested by Rubio (1996), separates the bubbly and froth regions in order to increase the flotation rate and reduce the amount of dropback and entrained particles. When separating the bubbly and froth zones in the modified flotation column, recoveries were found to increase beyond those achieved by other flotation methods.

Flotation columns have undergone improvement in the area of axial mixing by introducing various types of baffling or column packing material. When axial mixing occurs, the aggregates do not float directly to the top of the column but swarm about on the way to the froth zone instead, thus increasing the time for the aggregates to float and be collected. Packed columns are effective in reducing axial mixing for ultrafine particle flotation, but tend to have plugging problems when coarser particles are processed (Yang, 1988). The main advantage of using packing is that deeper froth zones can be supported and as a consequence, selectivity characteristics are enhanced (Killmeyer et al., 1989; Honaker & Paul, 1995). The Leeds column (Degner & Sabey, 1988) is an example of a design that minimizes axial mixing by using fixed and moveable rods within the column interior. By creating smaller compartments between the rods, axial mixing is reduced and consequently product recovery is improved. Kawatra & Eisele (1995) tried the combination of packing and horizontal baffles to have the advantage of handling both ultrafine and coarser particles while reducing axial mixing. Results showed that the lower baffles increased residence time while the upper baffles controlled bubble size by preventing coalescence. The overall design for this column seems promising with respect to improved recovery.

Flotation columns have been improved in the areas of air introduction, bubble generation, bubble-particle contact, and axial mixing (Mohanty & Honaker, 1999). All these areas are associated with the type and method of gas introduction, commonly in the form of gas spargers. The purpose of a gas sparger is to produce small gas bubbles at a high rate (Dobby & Finch, 1986), thus the type of gas sparger used in a flotation column greatly affects the probability of bubble-particle attachment. For a given volume of gas, by creating smaller bubbles a larger quantity of bubbles are generated, increasing the probability of bubble-particle collisions along with the particle collection rate. The superficial gas velocity also affects particle collection because when a gas bubble rises faster, the probability of collision and attachment increases. Gas velocity does have an upper limit though. The gas rate limitation can be identified by the loss of bubbly flow, loss of a visible pulp-froth interface, and loss of wash water positive bias (Xu et al., 1989). Keeping in mind the upper limit to gas velocity, smaller gas bubbles can be produced to create an increase in flotation rate, but unfortunately selectivity is not necessarily improved (Dobby & Finch, 1991). Smaller bubbles also help improve froth grade and stability by entraining fewer particles in their wake due to smaller drag forces. Froth stability increases as well since smaller bubbles allow for better froth drainage due to availability of water pathways between the froth bubbles. Finally, a smaller diameter bubble also decreases the probability of gas bubble coalescence (Mohanty & Honaker, 1999). If gas bubbles coalesce before the bubbles and particles attach, the amount of surface area available is reduced which in turn decreases the probability of collision and ultimately, overall recovery.

In research completed by Dobby & Finch (1991), the main types of bubble generation techniques are mechanical shear contacting, static shear contacting, sparging through a porous media with or without high external shear force, and jetting. Mechanical shearing often generates bubbles with a diameter of 0.5 to 1.0 mm and is a technique used in conventional mechanical flotation devices. Static shear contacting is based on high velocity contact between the slurry and the gas phase. Examples of devices that use this type of sparger include the Davera cells, packed columns, and in-line mixers within pipelines. The technique of sparging through a porous medium is the most common method because it involves a simple design that creates bubbles of sufficiently small diameter. Generally, the porous medium is made out of rubber or fabric. This type of sparger can either include or exclude a high external shear force through the porous medium. Examples of devices that use high external shear force spargers include the Bhar cells, air sparged hydrocyclones, and Flotaire gas sparging systems. If a high external shear force is not used, there is a risk of plugging the pores with solids or precipitates. The final bubble generating technique to mention is jetting. Basically, a gas stream is jetted from an orifice into a liquid, or vice versa where the slurry is jetted at a high velocity into a gas stream instead. Jetting is used in the Jameson cell and the Jet Flotation Cell (Dobby & Finch, 1991).

In this thesis project, a flotation column is tested to recover bitumen from oil sands. Although both mechanical cells and reactor/separator cells are proven useful, flotation columns would better suit the oil sand industry since they tend to occupy smaller

space, have low capital and operating costs, and do not require large amounts of maintenance for moving parts.

The column used for this experimental investigation, shown in Figure 2-3, does not conform to the conventional column arrangement in which feed is introduced near the pulp-froth interface and air is introduced via a gas sparger at the bottom of the column.

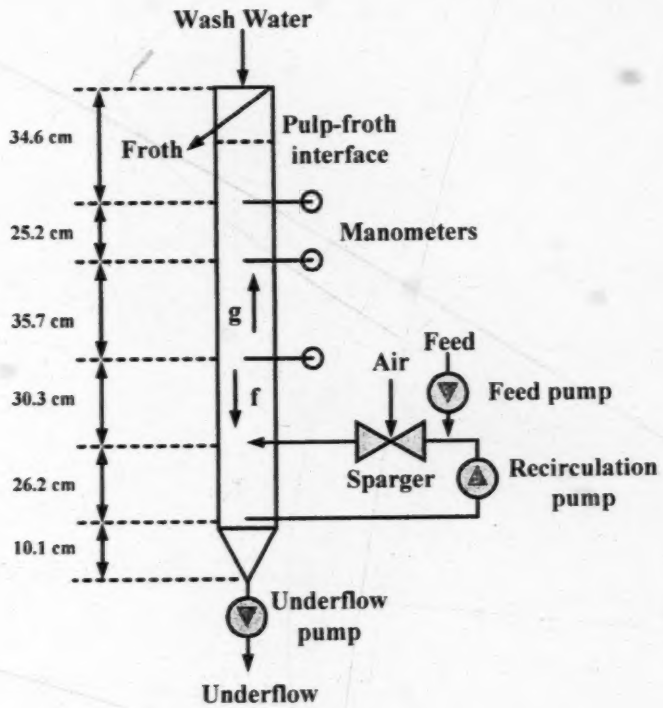

Figure 2-3. The column design used in this thesis study.

Instead, the column used for this thesis study features a recirculation line that aerates the feed before it enters the column. The slurry enters the recirculation line close to the tailings port and is reintroduced approximately 30 cm above the bottom of the column. The air sparger is installed within the recirculation line and feed can be introduced

immediately before the sparger. The air sparger used in these experiments is shown in Figure 2-4. As illustrated, the air-slurry mixture must proceed through a narrow orifice (3.1 mm).

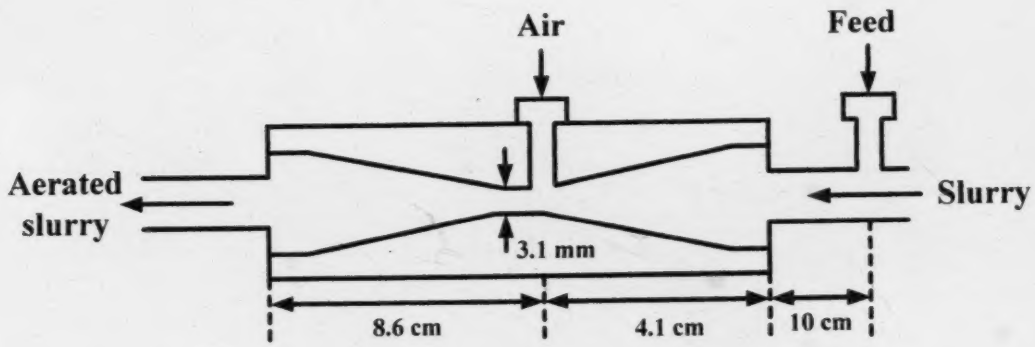

Figure 2-4. A schematic of the air sparger used in this thesis study.

By reducing the cross-sectional area within the sparger, the slurry velocity at the narrowest point becomes very high causing a large decrease in the corresponding slurry pressure. If the drop in pressure is below the pressure of water vaporization and/or air saturation, cavities of water vapor will form and air will migrate to fill these cavities. In the presence of hydrophobic particles, cavitation and gas nucleation occur more favorably on hydrophobic particles, such as bitumen droplets, allowing for a more effective aeration. This mechanism is limited by two factors, the first being that the recirculation rate and consequently the slurry velocity in the narrow gap must be high enough to reduce the pressure below the water vaporization pressure. The second limitation is that the supersaturation limit of the slurry only allows a certain amount of air to be dissolved. Fortunately, this type of air sparger also produces small diameter bubbles by a second mechanism. At the throat region of the orifice, the Reynolds number is sufficiently high

such that the slurry is in the turbulent region. Due to the turbulence and subsequent shear forces, the formation of large bubbles is avoided. Both these mechanisms contribute to the production of small air bubbles, which in turn increases the probability of air-bitumen attachment. Xu et al. (1996a) tested a similar type of feed-line aeration system, which significantly improved column flotation performance over conventional methods. With this type of in-line aeration system, better bitumen flotation recovery is anticipated.

2.3 Flotation column characteristics

To identify whether flotation columns can be successfully applied to the oil sand industry, the interactions within the bubbly and froth zones in the column must be further studied.

A flotation column can operate in three flow regimes: bubbly, churn turbulent or slug flow (Shah et al., 1982). The bubbly flow regime, defined by uniform sized bubbles with equal radial distribution, is optimum for flotation columns. By observing the relationship between gas volume fraction and superficial gas velocity, the flow regime can be identified (Finch & Dobby, 1990). At lower superficial gas velocities the relationship between superficial gas velocity and gas volume fraction is linear and the flotation column is operating in the bubbly regime. At a certain gas velocity unique to each column, the ratio of gas hold-up and gas flow rate reaches its maximum. At superficial velocities higher than this value corresponding to the maximum ratio, the column moves from the bubbly to churn-turbulent flow regime.

Mixing in the bubbly zone reduces the probability of collision and as a consequence causes the column recovery and selectivity to decrease. Often column flow behavior is modeled to help understand the impact of mixing. Models usually depend on the parameters of mean residence time and vessel dispersion number (Dobby & Finch, 1985). In general, a first order kinetic approach is used to model attachment in the bubbly zone, although a hydrodynamic model for plug flow including axial dispersion may be used as well (Yianatos et al., 1998). Particle collection is considered to be a first order effect with respect to solids concentration. To model the behavior of the mineral particles within the bubbly zone, the model by Ross & Van Deventer (1988) can be used.

Gas hold-up reflects a change in bubble velocity. For a given volumetric gas flow rate, an increase in bubble velocity causes a decrease in the gas hold-up (Banisi et al., 1995b). Gas hold-up is affected by several operating parameters, some of which include: gas sparger type, frother characteristics and concentration, air flow rate, slurry flow rate, solids content, and bubbly zone mixing patterns (Tavera et al., 2001). Upon addition of solids to a system, gas hold-up generally decreases because of an increase in bubble velocity caused by wake stabilization. When a bubble rises behind a loaded bubble, it is influenced by the liquid flow in the wake of the leading bubble (Banisi et al., 1995b). Gas hold-up also decreases with solid addition due to a change in radial hold-up and flow profiles within the column.

Gas hold-up can be measured in two ways: either by the difference in pressure between two manometers or by conductivity probes. Manometer methods for gas hold-up measurements are based on the water head pressure difference within a certain portion of the column. The conductivity probe methods for gas hold-up measurements, on the other hand, are based on the fact that liquid conductivity decreases when non-conducting gas bubbles are introduced (Mattenella & Zapiola, 2001). Tavera et al. (2001) found that the gas hold-up distribution is not uniform across the cross section of a column, but rather it is higher in the centre of the column than at the walls. Gas hold-up measurements can also be affected by slurry density, which in turn depends on particle size, particle density, and liquid velocity (Dobby et al., 1988). Gorain (1997) stated that gas hold-up defines bubble flow density (bubble surface-area flux), which is a function of flotation kinetics. Usually in two-phase systems the effects of bubble density are negligible, but in a mineral system bubble density is important and must be taken into account. The bulk density of the slurry is also affected by column diameter since mixing effects increase with column diameter. If baffles are installed to reduce axial mixing, bulk density may still vary between baffled sections and must still be considered.

In a flotation column, the knowledge of the generated bubble size is very useful. Bubble diameter can be found from gas volume fraction or by direct measurement using digital images. Applying Sigmascan to digital images, several hundred bubbles are counted and an overall average bubble diameter is calculated. There are three conventional ways of determining an overall average bubble diameter from a range of

bubble diameters. The first definition is the Sauter mean diameter (d_{32}) (Shah et al., 1982), which is defined as:

$$d_{32} = \frac{\sum n_i d_{bi}^3}{\sum n_i d_{bi}^2} \tag{2-1}$$

where d_{bi} is the bubble diameter, n_i is the number of bubbles having diameter d_{bi}.

The second approach to define an average bubble diameter is based on volumetric mean diameter (d_{bv}) (Yianatos et al., 1988).

$$d_{bv}^3 = \frac{\sum n_i d_{bi}^3}{\sum n_i} \tag{2-2}$$

The third definition is based on regular statistical average, i.e. the statistical mean diameter (d_{sb}) given by:

$$d_{sb} = \frac{\sum n_i d_{bi}}{\sum n_i} \tag{2-3}$$

Yianatos et al. (1988) found that there is little difference between the first two definitions, with approximately 10 to 15 % error between measured and predicted bubble sizes. In other work, Gomez et al. (2000) found a small difference between the Sauter mean diameter and the statistical average diameter. From a set of bubble diameter data examined in this study, all three definitions yield approximately the same overall average bubble diameter and therefore any one of the definitions can be used.

For this study, the flotation column was operated in the bubbly flow regime. Since the column was small in diameter, there should be little flow disruption by axial mixing. Gas hold-up was measured using manometers. When using digital images to calculate an average bubble diameter, the data set was statistically averaged using equation 2-3.

2.4 Drift flux analysis

Drift flux analysis was proposed by Wallis (1969) and has been proven to be a useful tool to characterize flotation columns. Wallis described the drift flux as "the volumetric flux of a component relative to a surface moving at an average velocity". Drift flux analysis is used to model gas volume fraction in the bubbly and froth zones as influenced by column operating conditions.

By definition, the drift flux (j_{gf}) is expressed as:

$$j_{gf} = \alpha_g (v_g - j) \tag{2-4}$$

where α_g is the gas volume fraction, v_g is the gas velocity relative to a stationary observer, and j is the total flux.

The total flux for a gas liquid two-phase system can be expressed as:

$$j = j_g - j_f \tag{2-5}$$

where j_g is the gas flux and j_f is the liquid flux. Following the flotation column notation, the upward direction is taken as positive for the gas. The downward direction is taken as positive for the fluid (liquid). In our case, j_g and j_f are positive quantities.

Each flux component (or superficial velocity) can then be expressed in terms of volume fraction (α_i) and relative velocity (v_i).

$$j_f = \alpha_f v_f \tag{2-6}$$

$$j_g = \alpha_g v_g \tag{2-7}$$

where subscript f represents the liquid phase and subscript g represents the gas phase. The liquid velocity, v_f, is taken relative to a stationary observer.

Substituting equations 2-5 and 2-7 into equation 2-4 yields:

$$j_{gf} = j_g(1-\alpha_g) + j_f\alpha_g \tag{2-8}$$

This form of the drift flux, when plotted on a curve of j_{gf} versus α_g, constitutes the operating equation of a flotation column at given j_g and j_f.

Recognizing that:

$$\alpha_g + \alpha_f = 1 \tag{2-9}$$

and substituting equations 2-6, 2-7, and 2-9 into equation 2-8 yield:

$$j_{gf} = \alpha_g(1-\alpha_g)(v_g + v_f) \tag{2-10}$$

Equation 2-10 relates the drift flux, j_{gf}, to the relative (or slip) velocity of the two phases as expressed by $(v_g + v_f)$. In sedimentation and liquid fluidization, the relative velocity is uniquely related to the terminal velocity and volume fraction of the dispersed phase. From experimental studies (Lapidus & Elgin, 1957) it was found that:

$$v_g + v_f = U_{gf} = U_t f(\alpha_g) \tag{2-11}$$

where U_{gf} is the relative or slip velocity, U_t is the terminal velocity of a bubble or particle in an infinite medium, and $f(\alpha_g)$ is a function of the gas volume fraction and the dispersed phase Reynolds number.

Ityokumbul et al. (1995) summarized various forms for $f(\alpha_g)$ and the most commonly used expression is given by Richardson & Zaki (1954).

$$f(\alpha_g) = (1-\alpha_g)^{m-1} \tag{2-12}$$

where "m" is an empirical parameter that depends on the flow conditions.

Exponent "m" in this expression was defined by Richardson & Zaki (1954) to vary with bubble Reynolds number, although there are many other researchers who have suggested different empirical correlations with no common consensus among them.

Making use of equations 2-11 and 2-12, one can eliminate the relative velocity term in equation 2-10 to obtain:

$$j_{gf} = U_t \alpha_g (1-\alpha_g)^m \tag{2-13}$$

This expression states that the drift flux is a function of the terminal velocity of a bubble and the volume fraction of the dispersed phase. Equation 2-13 can be considered to be system characteristic when plotted on a j_{gf} versus α_g curve.

For design purposes, both the operating line (equation 2-8) and the system characteristics (equation 2-13) can be plotted in a figure of j_{gf} versus α_g for given values of j_f, j_g, U_{t_2} and "m". Such a plot is given in Figure 2-5.

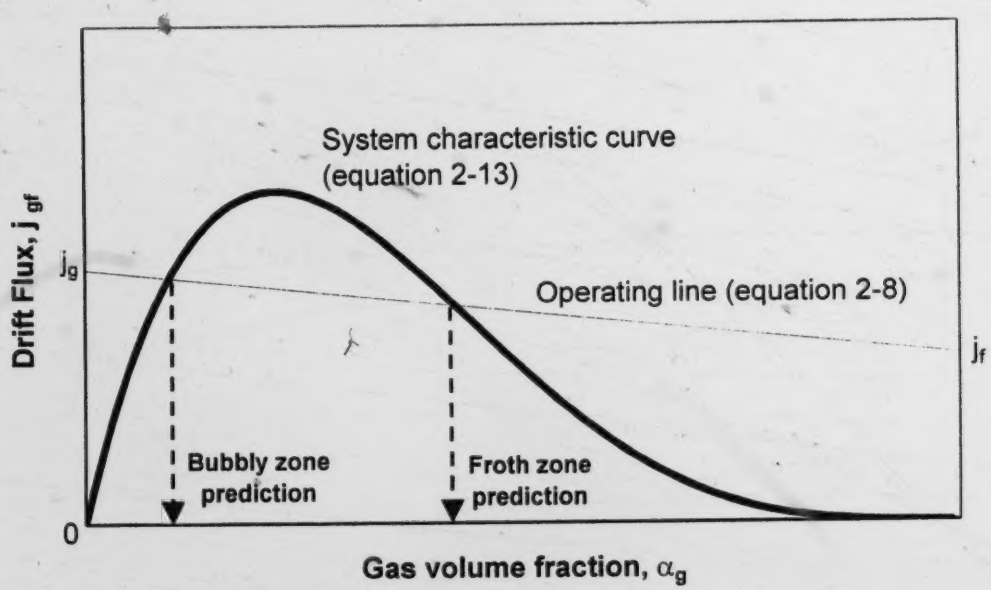

Figure 2-5. An example of drift flux analysis used to predict the bubbly and froth zone gas volume fractions for a given j_g and j_f.

The operating line shown in Figure 2-5 is typical for a flotation column operating under normal countercurrent conditions. The two curves intersect twice, the locations of which provide predictions for the gas volume fractions in the bubbly and froth zones. For

illustration purposes, "m" was taken to be constant for both zones. Such an assumption is valid when the bubble Reynolds number is very small.

In a more realistic example, the bubbly and froth zones will have different Reynolds numbers due to the difference in the bubble-bubble interactions in each zone, leading to different values for terminal velocity and exponent "m". Subsequently, the system characteristic curves can be considered unique for each zone. Figure 2-6 shows an example of the two different characteristic curves that would result along with a distinct operating line.

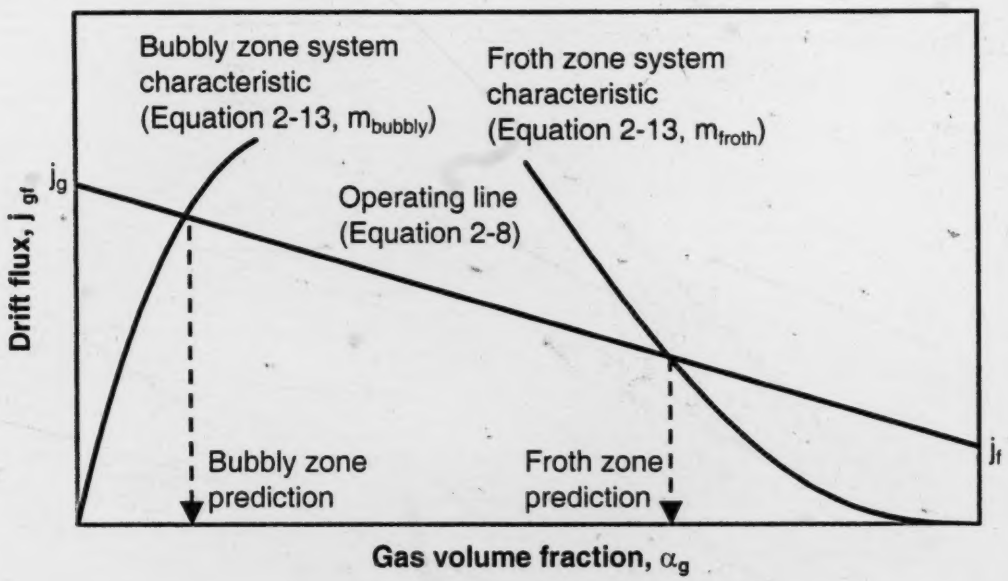

Figure 2-6. An example of the drift flux analysis when the bubbly and froth zones have sufficiently different Reynolds numbers and how to predict the bubbly and froth zone gas volume fractions for a given j_g and j_f.

In the example shown in Figure 2-6, the predictions of the gas volume fractions in the bubbly and froth zones are more accurate than by using a single characteristic curve.

When a flotation column operates under conditions other than a countercurrent flow, different operating lines would result, as shown in Figure 2-7.

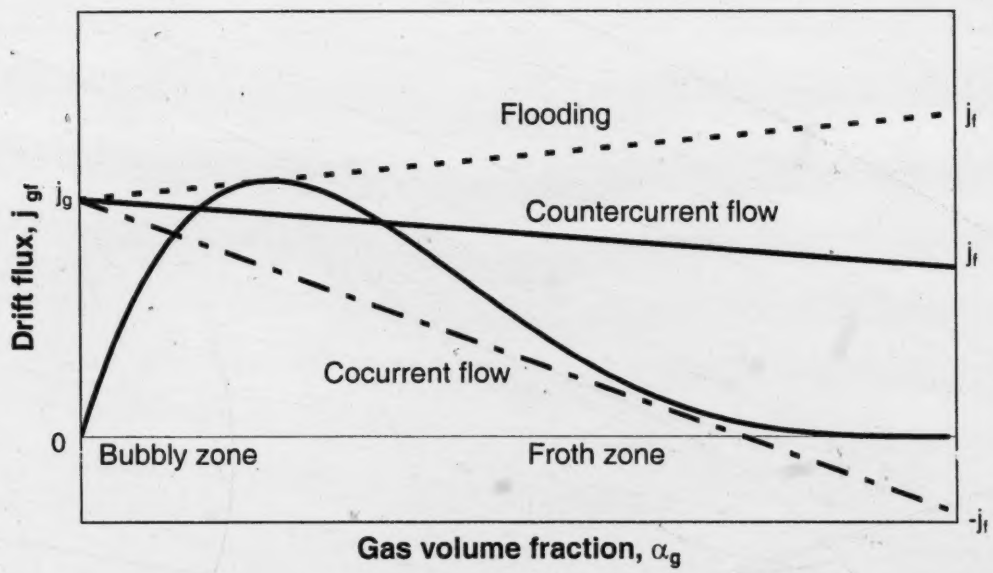

Figure 2-7. Variation of operating lines on the depending flow pattern in a flotation column.

When the column is operated under cocurrent conditions, the fluid flows in the same direction as the gas, causing the fluid flux to be negative ($-j_f$). Under the critical condition of flooding, the operating line is tangent to the system characteristic curve at a location close to the maximum drift flux in the bubbly zone. As before, the locations at which the operating line and characteristic curve intersect provide the predictions for the gas volume fractions within either the bubbly or froth zones.

In equation 2-13, the two parameters that need to be evaluated are the bubble terminal velocity and exponent "m". In both cases there are several correlations available. To estimate the terminal velocity, the drag coefficient of a bubble within a bubble swarm (C_D) needs to be determined. Two of the commonly accepted equations for the drag coefficient are given by equation 2-14 (Concha & Almendra, 1979) and by equation 2-15 (Schiller & Naumann, 1933).

$$C_D = 0.28\left(1 + 9.06\,\mathrm{Re}_b^{-0.5}\right)^2 \text{ for } \mathrm{Re_b} < 10^4 \tag{2-14}$$

$$C_D = \frac{24}{\mathrm{Re}_b}\left(1 + 0.15\,\mathrm{Re}_b^{0.687}\right) \text{ for } \mathrm{Re_b} < 800 \tag{2-15}$$

where $\mathrm{Re_b}$ is the bubble Reynolds number, which is defined as:

$$\mathrm{Re}_b = \frac{d_b U_t \rho_f}{\mu_f} \tag{2-16}$$

In equation 2-16, d_b is the bubble diameter, ρ_f is the liquid phase density, and μ_f is the liquid phase viscosity.

The drag coefficient equation can be substituted into the standard equation for terminal velocity of a solid sphere:

$$U_t = \left(\frac{4}{3}\frac{g d_b \Delta\rho}{\rho_f C_D}\right)^{\frac{1}{2}} \tag{2-17}$$

where g is the gravitational constant and $\Delta\rho$ is the change in density between the sphere and the medium.

By using equation 2-17, the assumption is made that bubbles behave like rigid spheres. This is valid for a Reynolds number less than 500 because both bubbles and rigid spheres have similar drag coefficients (Yianatos et al., 1988), but needs to be cautious at a Reynolds number greater than 500, as bubbles tend to deviate from a spherical shape. It also needs to be kept in mind that rigid spheres are unaffected by surfactant adsorption, while in reality gas bubbles adsorb surfactants onto their surfaces which will change their surface chemistry and affect the hydrodynamics of the system. Zhou et al. (1992) proposed a bubble drift flux velocity to include coefficients that account for the surfactant type (contamination factor) and concentration. These equations were shown to be valid for a gas volume fraction less than 0.3. When the gas volume fraction is above 0.3, the modified drag equations become less accurate.

Substituting the Schiller & Naumann expression for drag coefficient into equation 2-17 one obtains:

$$U_t = \frac{g(\rho_f - \rho_g)d_b^2}{18\mu_f\left(1+0.15\,\mathrm{Re}_b^{0.687}\right)} \quad \text{for } d_b < 1.5 \text{ mm} \qquad (2\text{-}18)$$

where ρ_g is the density of the gas phase and μ_f is the viscosity of the liquid phase.

Other estimates for bubble terminal velocity include Peebles & Garber (1953) and the commonly used Clift et al. (1978) correlation shown below.

$$U_t = \frac{\mu_f}{\rho_f d_b} M^{-0.149}(J - 0.857) \qquad (2\text{-}19)$$

$$M = \frac{g\mu_f^4 \Delta\rho}{\rho_f^2 \sigma^3} \tag{2-20}$$

$$J = 0.94H^{0.757} \tag{2-21}$$

$$H = \frac{4}{3} E_o M^{-0.149} \left(\frac{\mu_f}{0.009} \right)^{-0.14} \tag{2-22}$$

$$E_o = \frac{g\Delta\rho d_b^2}{\sigma} \tag{2-23}$$

where σ is the surface tension.

It was found that for bubble diameters less than 2 mm (terminal velocity less than 200 mm/s), there is little difference among the terminal velocity equations of Clift et al.; Concha and Almendra; and Schiller and Naumann (Dobby et al., 1988; Sasaki et al., 1986; Anfruns & Kitchener, 1977). For this study, the drag coefficient recommended by Schiller & Naumann (1933) was used to determine the terminal velocity of an air bubble.

The second parameter needed to evaluate the system characteristic curve is the exponent "m". Among the different correlations for exponent "m" a selected few are summarized in Table 2-1.

Table 2-1. Summary of empirical relations of exponent "m" reported in literature.

Author	Exponent "m" value
Griffith & Wallis, 1961	m = 2 for small bubbles m = 0 for large bubbles
Zuber & Hench, 1962	m = $f(d_b)$; for d_b < 0.5 mm, m = 3; for 1 mm < d_b < 2 cm, m = 1.5
Davidson & Harrison, 1966	m = 0
Turner, 1966	m = 1
Wallis, 1969	m = 2
Bhaga & Weber, 1972	m = 1
Yianatos et al., 1988	m = $f(Re_b)$
Biesheuvel & Gorissen, 1990	m = 2
Banisi & Finch, 1994	m = 3

One of the more common correlations was proposed by Richardson & Zaki (1954) and is given by:

$$m = \left(4.45 + 18\frac{d_b}{d_c}\right)\mathrm{Re}_b^{-0.1} \quad \text{for } 1 < \mathrm{Re_b} < 200 \tag{2-24}$$

$$m = 4.45\,\mathrm{Re}_b^{-0.1} \quad \text{for } 200 < \mathrm{Re_b} < 500 \tag{2-25}$$

$$m = 2.39 \quad \text{for } \mathrm{Re_b} > 500 \tag{2-26}$$

where d_c is the diameter of the flotation column.

In brief, there is no general agreement as to the value of "m" and several papers have been devoted to addressing this issue. Pal and Masliyah (1989) suggested that most literature data had been collected at low gas volume fraction (α_g) values. Referring to equation 2-13, it is clear that as α_g approaches zero, the value of $(1-\alpha_g)$ approaches one and the drift flux in equation 2-13 becomes insensitive to exponent "m". For the froth region, α_g is sufficiently large to make the drift flux sensitive to the changes in "m". Zhou and Egiebor (1993) suggested that the assumption of bubbles behaving like solid spheres over an intermediate Reynolds number range may be inaccurate. This would lead to an inadequate estimation of single bubble terminal velocity, which would then cause errors to propagate throughout the subsequent calculations. Despite the empirical nature of exponent "m", use of equation 2-13 in drift flux analysis is still a common practice and will be used for this study.

3.0 TWO-PHASE MODEL SYSTEM TESTS

The objective of this chapter is to apply the drift flux analysis to a wide range of operating conditions for a two-phase system column to develop an improved empirical relation that allows operators to predict the bubbly and froth zone characteristics. Tests were conducted with air and either process water obtained from the bitumen extraction process at Syncrude Canada Ltd. or with aqueous solutions having low concentrations of methyl isobutyl carbinol (MIBC).

3.1 Bubbly zone theory

From the bubbly zone data, calculations were performed to find the operating line, the gas volume fraction, and the system characteristic curve. The operating line defined by equation 2-8 was generated from known gas and liquid fluxes. In this study, the gas phase refers to air while the liquid or fluid phase refers to water. For the bubbly region, the gas flux was based on the air flow rate while the liquid flux was based on the liquid underflow flow rate. Gas flux was calculated using:

$$j_g = \frac{Q_g}{A} \tag{3-1}$$

where Q_g is the net gas volumetric flow rate and A is the cross-sectional area of the flotation column. The liquid flux was calculated in a similar manner.

The bubbly zone gas volume fraction was experimentally determined from measurements using differential manometers. Since the liquid phase was water, the equation for gas volume fraction reduces to:

$$\alpha_g = \frac{h}{L} \tag{3-2}$$

where h is the height difference between liquid levels in the two adjacent manometers and L is the total distance between the two adjacent manometer ports.

The final step in the drift flux analysis for the bubbly zone is to plot the system characteristic curve (equation 2-13) from known terminal velocity and exponent "m". As the terminal velocity was not measured experimentally, it was evaluated iteratively using the bubble diameter (d_b) and the gas volume fraction (α_g). Banisi and Finch (1994) summarized several iterative methods that can be used to calculate the bubble diameter from the gas volume fraction. For this study, a modified version of the approach suggested by Yianatos et al. (1988) was used and the procedure is outlined in Figure 3-1 (Yianatos et al., 1988; Banisi & Finch, 1994). The calculation involves two iterations: one for the bubble diameter evaluation and the other for the terminal velocity of a single bubble. A sample calculation and code for a Visual Basic program is shown in Appendix A to calculate bubble diameter knowing gas volume fraction within the bubbly zone.

To initiate the iterative procedure, the bubble diameter was guessed. Knowing the gas volume fraction and the gas and liquid fluxes, the relative velocity was calculated using equation 3-3.

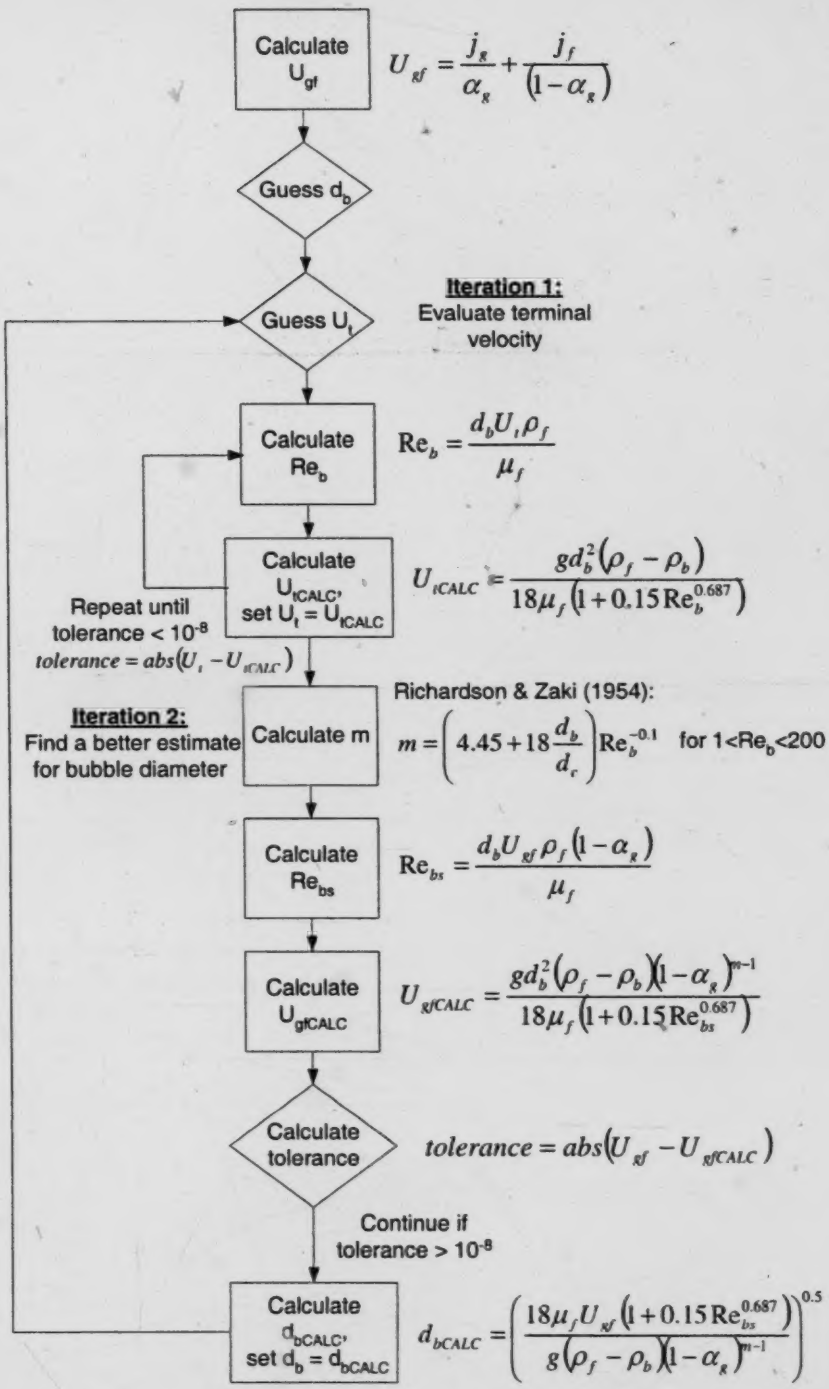
Calculate U_{gf}
$U_{gf} = \frac{j_g}{\alpha_g} + \frac{j_f}{(1-\alpha_g)}$
Guess d_b
Guess U_t
Iteration 1:
Evaluate terminal velocity
Calculate Re_b
$Re_b = \frac{d_b U_t \rho_f}{\mu_f}$
Calculate U_{tCALC}, set $U_t = U_{tCALC}$
$U_{tCALC} = \frac{g d_b^2 (\rho_f - \rho_b)}{18\mu_f (1 + 0.15 Re_b^{0.687})}$
Repeat until tolerance < 10^{-8}
$tolerance = abs(U_t - U_{tCALC})$
Iteration 2:
Find a better estimate for bubble diameter
Calculate m
Richardson & Zaki (1954):
$m = \left(4.45 + 18\frac{d_b}{d_c}\right) Re_b^{-0.1}$ for $1<Re_b<200$
Calculate Re_{bs}
$Re_{bs} = \frac{d_b U_{gf} \rho_f (1-\alpha_g)}{\mu_f}$
Calculate U_{gfCALC}
$U_{gfCALC} = \frac{g d_b^2 (\rho_f - \rho_b)(1-\alpha_g)^{m-1}}{18\mu_f (1 + 0.15 Re_{bs}^{0.687})}$
Calculate tolerance
$tolerance = abs(U_{gf} - U_{gfCALC})$
Continue if tolerance > 10^{-8}
Calculate d_{bCALC}, set $d_b = d_{bCALC}$
$d_{bCALC} = \left(\frac{18\mu_f U_{gf} (1 + 0.15 Re_{bs}^{0.687})}{g(\rho_f - \rho_b)(1-\alpha_g)^{m-1}}\right)^{0.5}$

Figure 3-1. Flowchart of the iterative process used to calculate bubble diameter based on gas volume fraction.

$$U_{gf} = \frac{j_g}{\alpha_g} + \frac{j_f}{(1-\alpha_g)} \tag{3-3}$$

At the end of the iterative process, the relative velocity, U_{gf}, was compared to the re-calculated relative velocity that was based on an initial estimate for the bubble diameter.

Using estimates for both the bubble diameter and terminal velocity, the bubble Reynolds number was calculated using:

$$\mathrm{Re}_b = \frac{d_b U_t \rho_f}{\mu_f} \tag{3-4}$$

where d_b is the diameter of a bubble, ρ_f is the density of the liquid phase, and μ_f is the viscosity of the liquid phase.

The Re_b was subsequently used to find a better estimate for the terminal velocity from a standard equation for terminal velocity of a solid sphere and the drag coefficient expression of Schiller & Naumann (1933). By using the Schiller & Naumann correlation, the assumption is made that gas bubbles behave like solid spheres. The initial terminal velocity estimate was then replaced by the calculated value and a fixed-point iteration was conducted until a tolerance of 10^{-8} was reached.

The next step is to improve on the estimated d_b value. This was achieved by using:

$$U_{gf} = \frac{g d_b^2 (\rho_f - \rho_b)(1-\alpha_g)^{m-1}}{18\mu_f (1 + 0.15\,\mathrm{Re}_{bs}^{0.687})} \tag{3-5}$$

where "m" was defined by the Richardson & Zaki (1954) correlations, given by:

$$m = \left(4.45 + 18\frac{d_b}{d_c}\right)\mathrm{Re}_b^{-0.1} \quad \text{for } 1 < \mathrm{Re}_b < 200 \tag{3-6}$$

where d_c is the diameter of the flotation column.

The expression for calculating Reynolds number using relative velocity (Re_{bs}) is given by:

$$\mathrm{Re}_{bs} = \frac{d_b U_{gf} \rho_f (1-\alpha_g)}{\mu_f} \tag{3-7}$$

The relative velocity expression, equation 3-5, was derived by Yianatos et al. (1988), which assumed multi-species hindered settling of the Masliyah (1979) model. The calculated relative velocity was compared to that calculated based on fluxes and gas volume fraction. If the tolerance between the two relative velocities was not within 10^{-8}, a new estimate for bubble diameter was calculated by rearranging the Yianatos et al. (1988) slip velocity equation. The calculated bubble diameter then replaced the initial d_b estimate and the whole iterative process was repeated until the set tolerance between the relative velocities was achieved.

With the aforementioned procedure, the terminal velocity, U_t, as required in equation 2-13 became known and the system characteristic curve was plotted.

3.2 Froth zone theory

A similar procedure was adopted for the froth region to generate the operating line. From the experimental set-up, the gas and liquid fluxes were the same as in the

bubbly zone allowing for one common operating line. In the froth zone, the gas volume fraction could not be obtained from manometer pressure drop measurements because the froth depth was too shallow. Instead, the gas volume fraction was back calculated from the measured froth zone bubble diameter. The bubble diameter in the froth zone was determined from digital images in which the diameter of 300 or more bubbles was measured using SigmaScan and an overall statistical average was determined for each test. To evaluate the gas volume fraction, calculations followed the steps and formulae shown in Figure 3-2 (Yianatos et al., 1988; Banisi & Finch, 1994). A sample calculation is shown in Appendix B, along with code for a Visual Basic program that calculates gas volume fraction in the froth zone, based on an average bubble diameter for that test.

With a known value for the bubble diameter, a fixed-point iteration with a tolerance of 10^{-8} was used to determine the Reynolds number and terminal velocity. An initial estimate for the gas volume fraction was made and the relative velocity calculated (equation 3-3). The Reynolds number based on the relative velocity (equation 3-7) was then determined and subsequently used to re-calculate the bubble diameter. This re-calculated bubble diameter was compared with the experimentally determined value. If the tolerance between the two successive bubble diameter values were not within 10^{-8}, a bisection method was used to find a new estimate for gas volume fraction and the iterative process was repeated.

The procedure in Figure 3-2 allowed the evaluation of U_t, which is needed for the plotting of the characteristic curve.

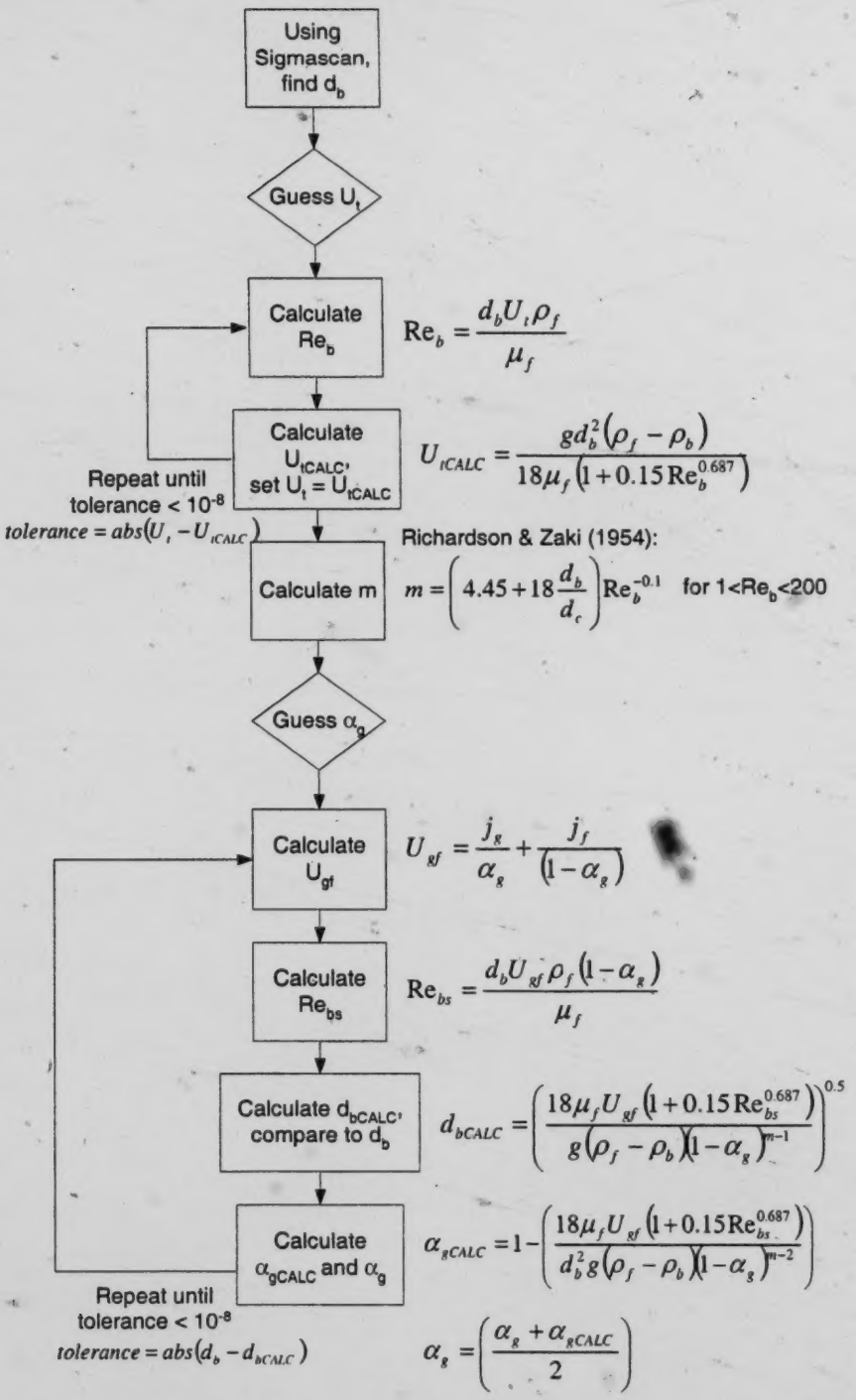
Using Sigmascan, find d_b
Guess U_t
Calculate Re_b
$Re_b = \frac{d_b U_t \rho_f}{\mu_f}$
Calculate U_{tCALC}, set $U_t = U_{tCALC}$
$U_{tCALC} = \frac{g d_b^2 (\rho_f - \rho_b)}{18 \mu_f (1 + 0.15 Re_b^{0.687})}$
Repeat until tolerance < 10^{-8}
$tolerance = abs(U_t - U_{tCALC})$
Richardson & Zaki (1954):
Calculate m
$m = \left(4.45 + 18 \frac{d_b}{d_c}\right) Re_b^{-0.1}$ for $1 < Re_b < 200$
Guess α_g
Calculate U_{gf}
$U_{gf} = \frac{j_g}{\alpha_g} + \frac{j_f}{(1 - \alpha_g)}$
Calculate Re_{bs}
$Re_{bs} = \frac{d_b U_{gf} \rho_f (1 - \alpha_g)}{\mu_f}$
Calculate d_{bCALC}, compare to d_b
$d_{bCALC} = \left(\frac{18 \mu_f U_{gf} (1 + 0.15 Re_{bs}^{0.687})}{g (\rho_f - \rho_b)(1 - \alpha_g)^{m-1}}\right)^{0.5}$
Calculate α_{gCALC} and α_g
$\alpha_{gCALC} = 1 - \left(\frac{18 \mu_f U_{gf} (1 + 0.15 Re_{bs}^{0.687})}{d_b^2 g (\rho_f - \rho_b)(1 - \alpha_g)^{m-2}}\right)$
Repeat until tolerance < 10^{-8}
$tolerance = abs(d_b - d_{bCALC})$
$\alpha_g = \left(\frac{\alpha_g + \alpha_{gCALC}}{2}\right)$

Figure 3-2. Flowchart of the froth zone calculations used to determine gas hold-up based on an average bubble diameter in the froth zone.

The exponent "m" in the system characteristic equation was considered as an adjustable parameter for both the bubbly and froth zones and was adjusted to force the characteristic curve to intersect the operating line at the pre-determined gas volume fractions. Completing this procedure for each test, two distinct exponent "m" values were obtained for either zone. The "m" values for the bubbly zone were plotted as a function of calculated bubble Reynolds number and a new correlation between the two variables was established by a non-linear fitting procedure. For the bubbly zone, the bubble hydrodynamics are significantly different from that in the froth zone. There are no singular formulae in literature to calculate bubble Reynolds number in both zones. We consider the "m" correlation established in the bubbly zone extends to the froth zone. The relation can be used to calculate corresponding Reynolds numbers of bubbles in the froth zone from the known value of "m". By correlating the calculated Reynolds number with the measured bubble diameter, an empirical correlation can be derived for estimating bubble Reynolds number in the froth zone.

3.3 Equipment and set-up

The schematic of the flotation column used for this study is shown in Figure 3-3. The column was made of glass tube with an inner diameter of 0.062 m. The height of the column was 1.62 m and the column held a volume of 4.8 L. A Masterflex L/S peristaltic pump was used for wash water addition, while a Masterflex I/P peristaltic pump was used for recirculation of the solution. A Matheson air rotameter was used for air flow measurement and control.

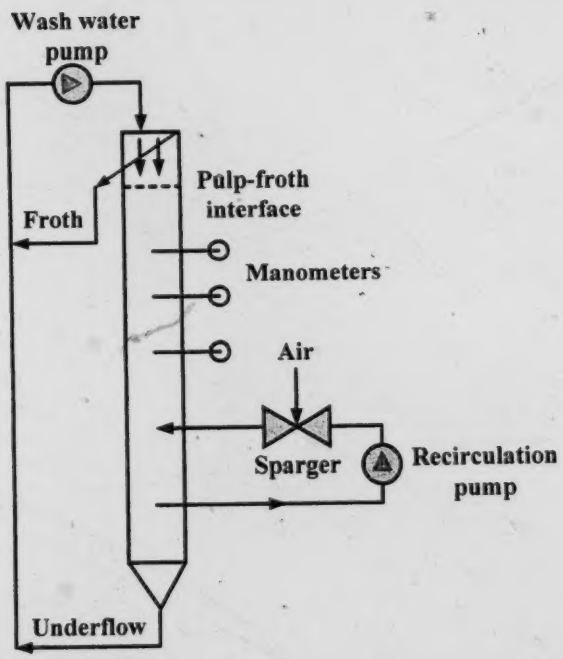

Figure 3-3. A schematic of the flotation column used for this study, including dimensions.

Tygon tubing was used as all the connecting tubing and for the manometers. The calibrations equations, along with the methods used to determine these equations, are included in Appendix C.

For each test, the column was filled with test solution. Both the underflow and froth streams were recycled as wash water and were added to the top of the froth. Air was introduced at 138 kPa into the recirculation stream through a horizontal orifice of 3.1 mm diameter. This type of aeration system, also used by Xu et al. (1996a), is equivalent to a venturi nozzle aerator. It introduces air into a fast flowing slurry stream to create

fine uniform air bubbles. By placing the air sparger in the recirculation line, the slurry is aerated before re-entering the column.

3.4 Materials and procedures

The two-phase systems that were tested included air and either process water that was obtained from the Syncrude Canada Ltd. bitumen extraction process in Fort McMurray, Alberta or de-ionized water with different concentrations of MIBC as frother. A material safety data sheet (MSDS) of MIBC is shown in Appendix D, along with general information on the use of the frothers. Table 3-1 gives the properties of the process water used for testing.

Table 3-1. Properties of the process water used for the two-phase system tests.

Property	Value
Surface Tension (mN/m)	64.93
pH	8.87

The manipulated variables for this study included the flow rates of the wash water, recirculation, and air streams. For the process water tests, the flow rates of the wash water, recirculation, and air streams were set between 0.16 to 0.27 L/min, 2.53 to 4.87 L/min, and 0.31 to 1.76 L/min, respectively. In the tests conducted with MIBC aqueous solutions, the flow rates for the wash water, recirculation, and air streams were set between 0.16 to 0.22 L/min, 2.53 to 2.92 L/min, and 0.41 to 1.09 L/min, respectively. The measured variables included the manometer pressure readings and underflow stream

flow rate. All the experiments were performed at room temperature and measurements were taken at steady state. The height of the pulp-froth interface was kept constant at 4 cm below the top of the froth throughout all the experimental runs and was controlled by the underflow stream flow rate. Details on the column start-up operating procedures are included in Appendix E.

3.5 Results and discussion

All raw and calculated data for the two-phase system tests are included in Appendix F, including data for all figures shown.

For the process water tests, the bubbly zone gas volume fraction ranged from 0.08 to 0.14, while the average bubble diameter ranged from 260 to 960 μm. In the froth zone, the gas volume fraction varied from 0.54 to 0.85, while the average bubble diameter ranged from 300 to 1080 μm. This clearly covers a wide range of column operating conditions.

For tests using MIBC aqueous solutions, the bubbly region calculations yielded a gas volume fraction range of 0.08 to 0.12 and an average bubble diameter range of 320 to 580 μm. The froth region had a gas volume fraction variation of 0.65 to 0.79 with a corresponding average bubble diameter range of 410 to 720 μm.

In all the tests, the bubble shape was spherical for both the bubbly and froth zones, as illustrated in Figures 3-4 and 3-5 respectively. As shown in the two photographs, bubbles are larger and images are sharper in the froth zone than in the bubbly zone, as anticipated.

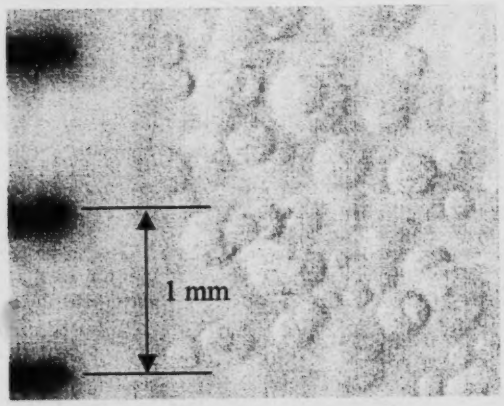

Figure 3-4. A snapshot of the bubbly zone during a process water test, indicating that the bubbles are spherical in shape.

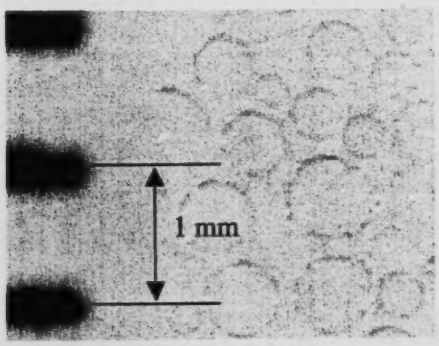

Figure 3-5. A snapshot of the froth zone during a process water test, illustrating that the bubbles are spherical in shape.

Digital images were taken of the bubbly zone in order to compare the calculated bubble diameter to a measured value. The calculation was based on the experimentally

determined gas hold-up using procedures outlined in Figure 3-1. Figure 3-6 shows a comparison between the calculated and measured average bubble diameters within the bubbly zone.

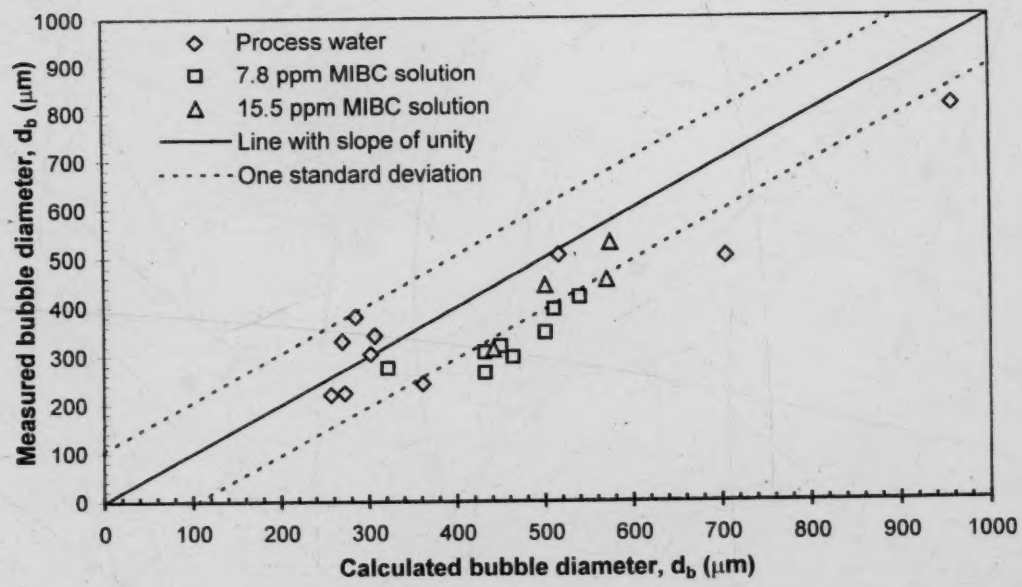

Figure 3-6. A comparison between the measured and calculated average bubble diameters in the bubbly zone for all the tests.

The measured bubble diameter had a tendency to be slightly lower than the calculated value. The discrepancy between the measured and calculated values may be due to the biased selection of digital images for bubble size measurement. Although several images were taken, only those that were perfectly focused were measured. As well, since the images were taken through a circular tube, some degree of distortion due to the tube curvature was inevitable. In addition, the bubbles in a single image were at various depths with respect to the outer wall of the tube and only the foremost bubbles could be counted. Considering the contributions from these two measurement difficulties, the bias

between the calculated and directly measured bubble diameters was considered to be acceptable.

Figure 3-7 summarizes the relationship between the gas flux and the bubbly zone bubble diameter for two series of tests. As expected, when the gas flux (superficial gas velocity) increases, an increase in the bubble diameter is observed. As well, the rate at which the bubble diameter increases with increased gas flux becomes higher at higher fluid velocity.

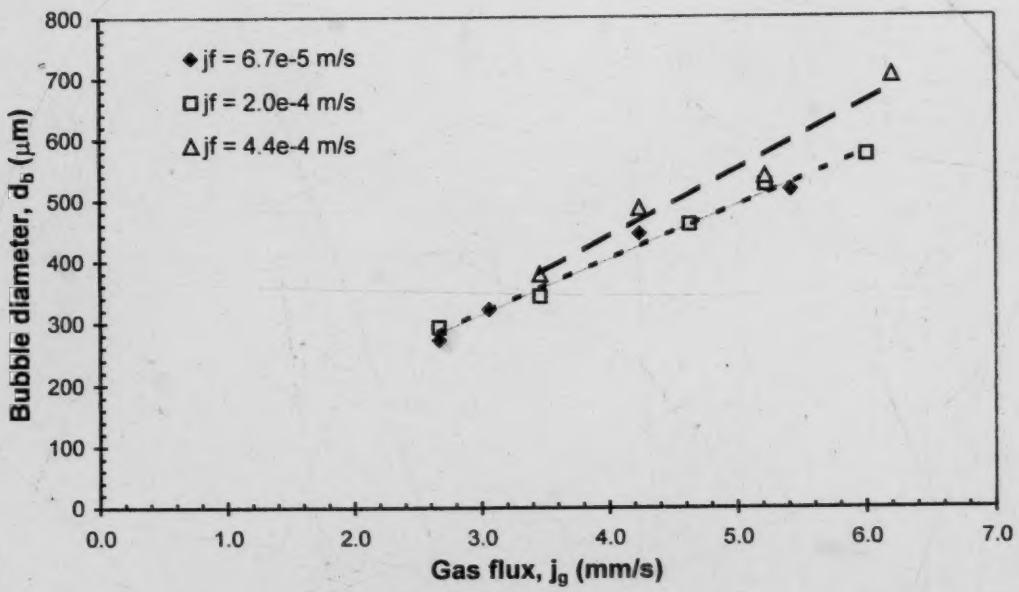

Figure 3-7. The relationship between gas flux and bubble diameter in the bubbly zone for all the tests.

For each test, the operating line was plotted along with the pre-determined gas volume fractions in the bubbly and froth zones. To calculate the terminal velocity used in equation 2-13, the Richardson & Zaki (1954) correlations were used. The characteristic

curves for the bubbly and froth zones were then adjusted by varying the "m" value to intersect the operating line at the locations of the respective gas volume fractions. Figure 3-8 shows an example of the adjusted system characteristic curves for a process water test.

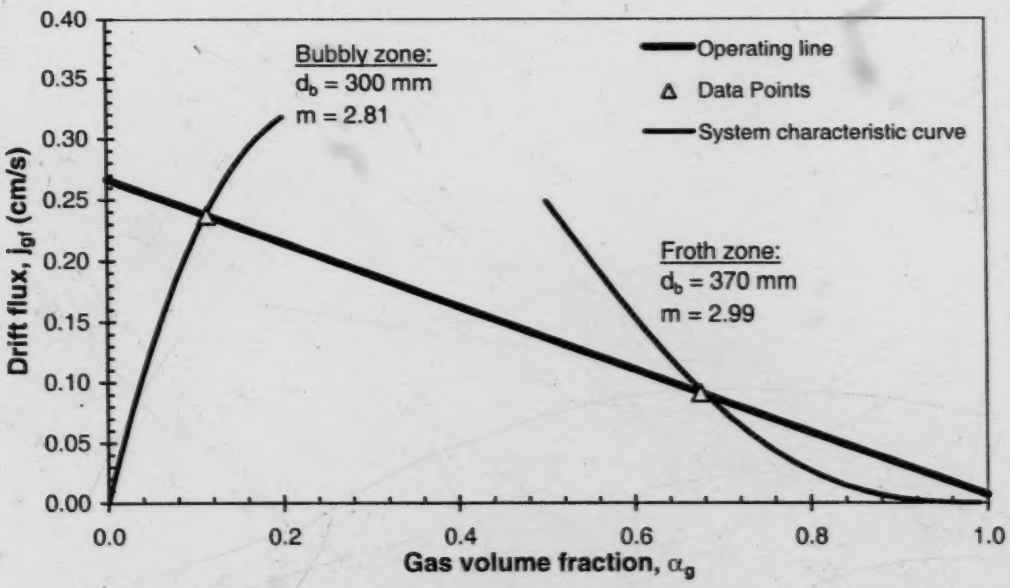

Figure 3-8. An example of a process water test where exponent "m" was adjusted such that the system characteristic curve and the operating line intersected at the locations of the pre-determined gas volume fractions.

In this example, the "m" value for the bubbly zone was found to be 2.81, while the "m" value for the froth zone was 2.99. For each test, an optimal "m" value was found by trial and error for each zone. For the bubbly zone data, Figure 3-9 shows a clear correlation between exponent "m" and bubble Reynolds number. Curve fitting resulted in an empirical correlation of:

$$m = \frac{20.26 + 1.89\,Re_b}{4.38 + Re_b} \qquad (3\text{-}8)$$

It should be noted that this correlation is considered to be valid for both the bubbly and froth zones as long as the bubble Reynolds number is in the range of 5 and 70. Like many other previously reported correlations for exponent "m", as Reynolds number approaches zero, the "m" approaches a constant value of approximately 4.65.

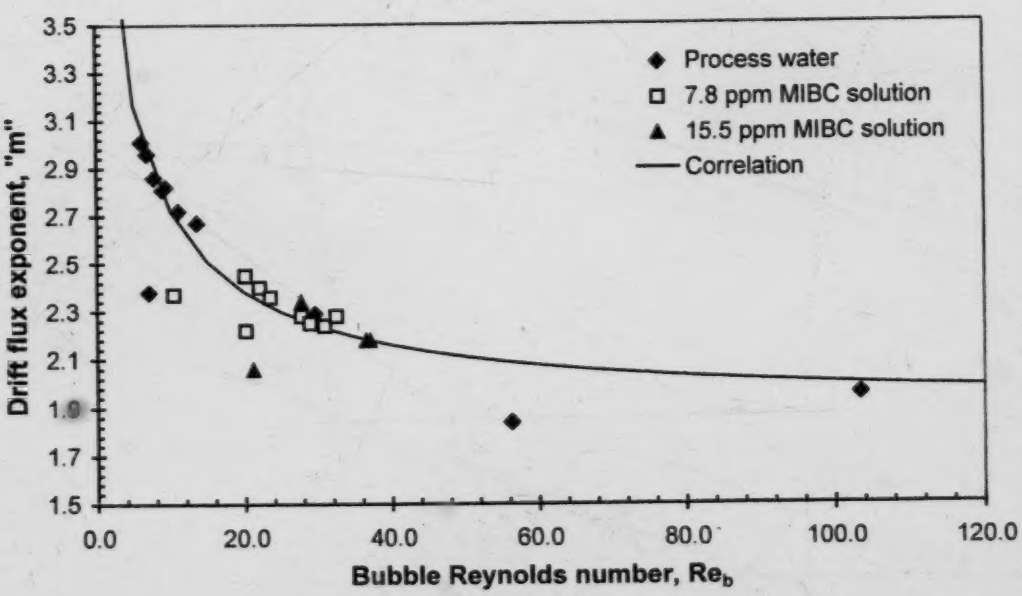

Figure 3-9. A plot of between exponent "m" and bubble Reynolds number for the bubbly zone.

It is evident that the hydrodynamics between the bubbly and the froth zones are not the same and consequently the Reynolds numbers of bubbles in these two zones are anticipated to be different. Although bubble Reynolds numbers in the bubbly zone can

be calculated using the definition of equation 3-4, the calculation of bubble Reynolds number in the froth zone is not available. To find a better estimate for bubble Reynolds number in the froth zone, the derived correlation for exponent "m" was used. Knowing the "m" value for the froth zone (previously found by adjusting the system characteristic curve), equation 3-8 was solved for Reynolds number. The back-calculated Reynolds number from the exponent "m" values of the froth zone was plotted as a function of bubble diameter in the froth zone as shown in Figure 3-10. A correlation between bubble Reynolds number and bubble diameter is evident, as anticipated.

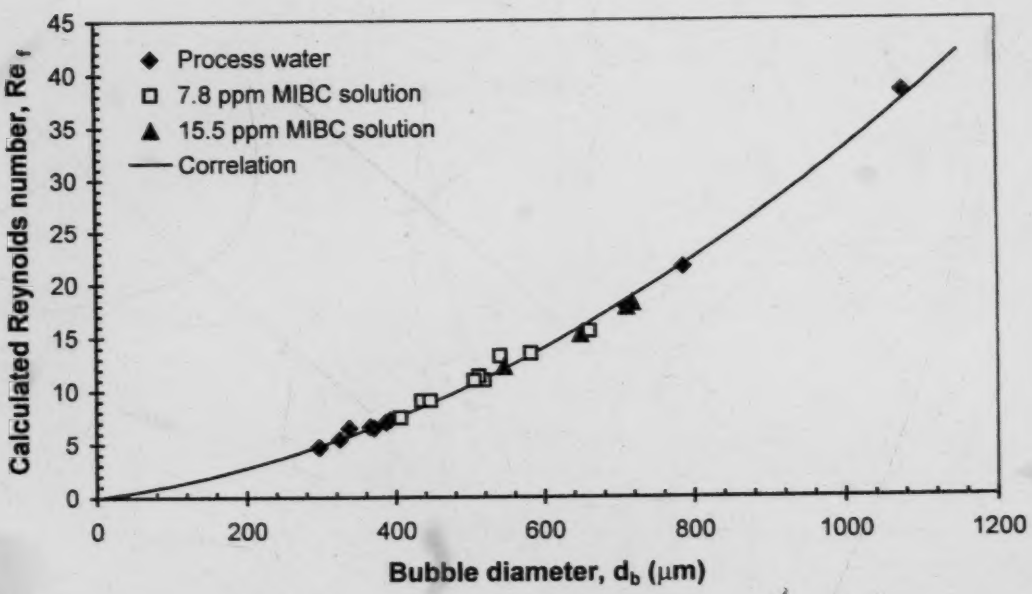

Figure 3-10. A plot of the relationship between froth zone Reynolds number and bubble diameter.

By curve fitting, the resulting correlation between Reynolds number and bubble diameter in the froth zone is given by:

$$\mathrm{Re}_{\text{froth zone}} = 2.38*10^{-5}\left(d_b^2\right)+9.08*10^{-3}\left(d_b\right) \qquad (3\text{-}9)$$

It is interesting to note that this empirical Reynolds number equation has the same form as equation 3-4 for the bubbly zone when the bubble diameter is relatively small. Using the experimentally determined bubble diameter from the froth zone, the Reynolds numbers for the froth zone were calculated using equation 3-9. From these Reynolds numbers, "m" values were calculated using the correlation given by equation 3-8. The "m" values found by adjusting the system characteristic curve are compared with the "m" values calculated using the correlation given by equation 3-8 for both zones and is shown in Figure 3-11.

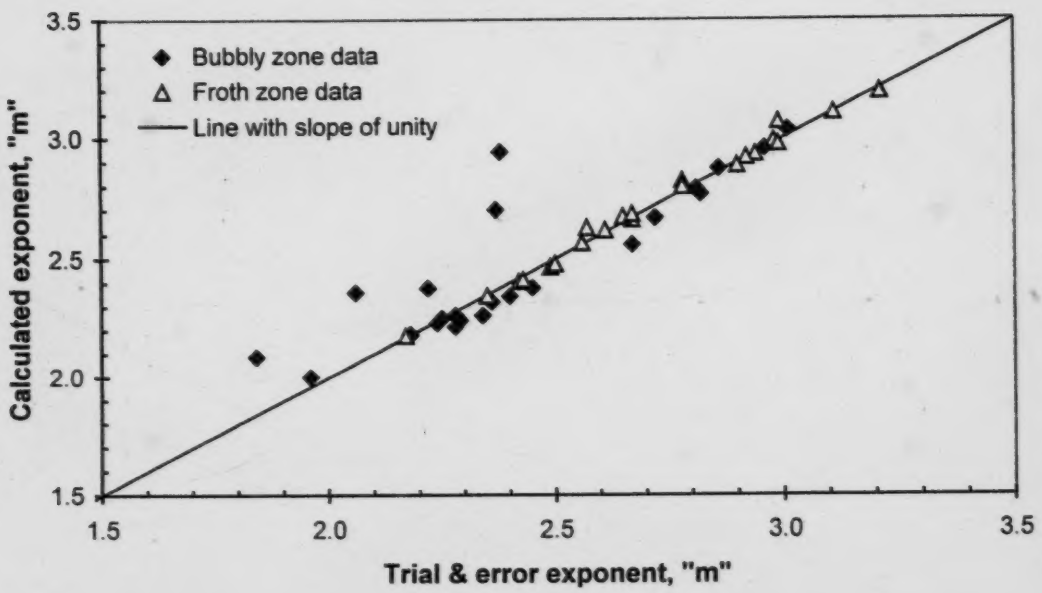

Figure 3-11. Comparison between the trial and error and calculated exponent "m" values for the bubbly and froth zones for all the tests.

Figure 3-11 clearly shows an excellent agreement between the trial and error exponent "m" values and the calculated exponent "m" values. This indicates that the correlation given by equation 3-8 is satisfactory in predicting "m" values.

Another way of verifying that the correlation predicts the bubbly and froth zone gas volume fractions sufficiently well is to provide a drift flux example. The data from a 7.8 ppm MIBC aqueous solution test was re-analyzed using the correlation for exponent "m", along with the new correlation for the Reynolds number in the froth zone. Figure 3-12 shows the resulting curves.

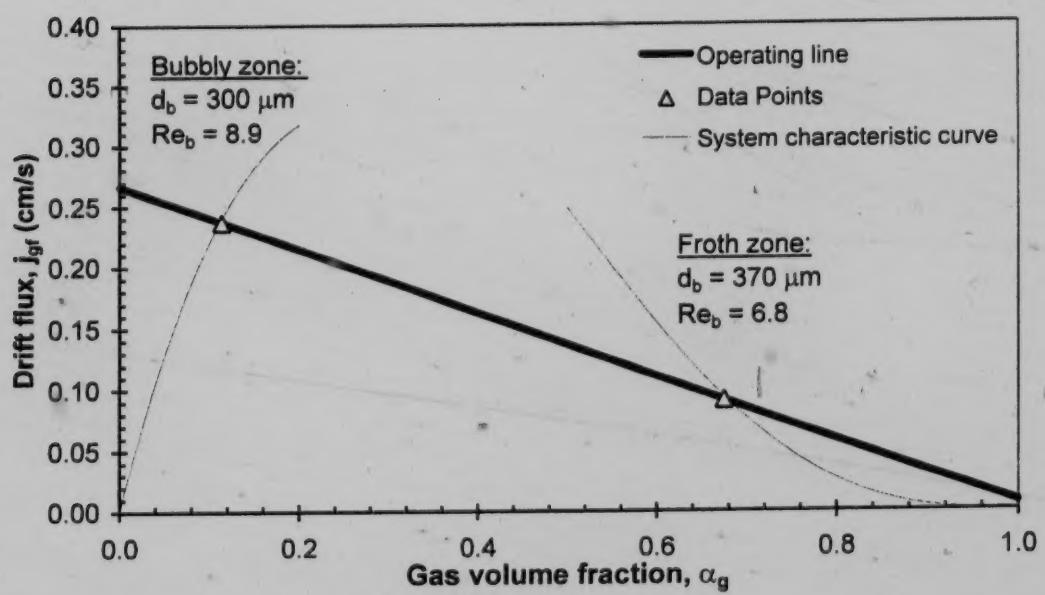

Figure 3-12. An example of the drift flux analysis for a 7.8 ppm MIBC aqueous solution test, using the new correlations.

The gas volume fractions of 0.112 and 0.682 obtained for the bubbly and froth zones from drift flux analysis compares well with the experimentally determined values of 0.114 and 0.675, as anticipated.

3.6 Conclusions

By using a flotation column for the two-phase systems of liquid and air, a new correlation for exponent "m", used in the drift flux system characteristic curve, was found. The new correlation is applicable for a bubble Reynolds number range of 5 to 70 and is given by:

$$m = \frac{20.26 + 1.89\,Re_b}{4.38 + Re_b}$$

Since the bubbly and froth zones have different hydrodynamics, the method of calculating the Reynolds number in the bubbly zone may not be applicable to the froth zone. An empirical correlation for the Reynolds number in the froth zone for our system was found to be:

$$Re_{\text{froth zone}} = 2.38 * 10^{-5}\left(d_b^2\right) + 9.08 * 10^{-3}\left(d_b\right)$$

With these two new correlations, the column operating conditions can be better and more conveniently described over a wider operating range.

4.0 BITUMEN FLOTATION TESTS

The second part of this study deals with the application of the flotation column for recovery of bitumen from oil sand middlings. Initial tests were conducted at the University of Alberta using middlings from the Suncor Energy Inc. separation cells (Sep Cell) within their extraction process. The purpose of the initial tests was to verify that the column could handle an oil sand system without plugging or encountering any major operating complications. After testing at the University of Alberta, the column was transferred to the Syncrude Research Centre in Edmonton, Alberta. Tests were conducted to ensure that the column could operate normally under on-line industrial conditions. In this case the feed was obtained from the middlings stream of the pilot plant primary separation vessel (PSV). The final set of tests was conducted at Suncor Energy Inc. in Fort McMurray, Alberta. The column was used on-line, taking feed from the Sep Cell #6 middlings stream. The objective was to determine the effect of changing feed, recirculation, air, and wash water flow rates on bitumen recovery. Recoveries were compared with the existing flotation system to determine whether improvement was achieved using our flotation column set-up.

4.1 Equipment and set-up

The flotation column for this study was made of glass with a thickness of 3 mm. The column was 1.63 m in height with an inner diameter of 0.062 m and held a volume of 4.8 L. A schematic of the set-up used is shown in Figure 4-1.

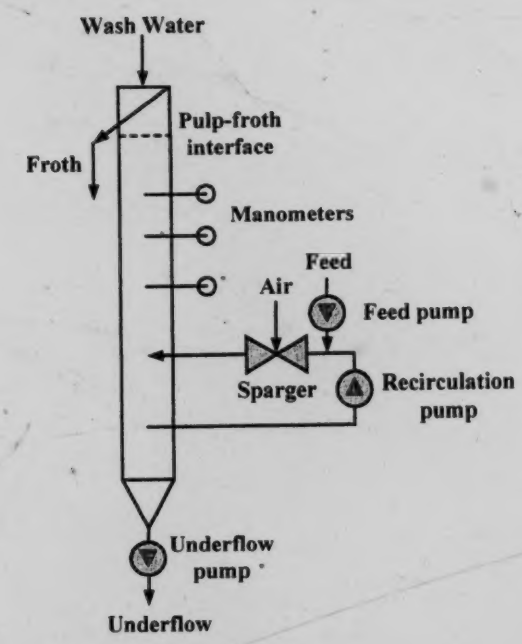

Figure 4-1. Schematic of the flotation column used in the bitumen flotation tests. The column was operated in a continuous mode.

The main feature of this column is that a unique air sparger, shown in Figure 4-2, that was installed in the recirculation loop in order to aerate the slurry before it entered the column.

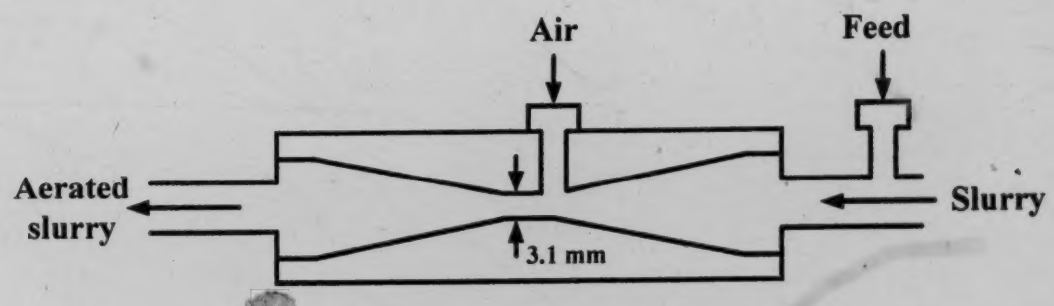

Figure 4-2. Schematic of the air sparger used in the bitumen flotation tests.

In conventional flotation columns, air is usually introduced through rubber spargers or other means of mechanical shearing directly into the column. As shown in Figure 4-1, a peristaltic pump withdrew the recirculating slurry into a recirculation loop that was slightly above the tailings port. The withdrawn slurry was then combined with fresh feed. Next, the combined slurry was injected with air and proceeded through the air sparger to re-enter the column approximately 30 cm above the bottom of the column. The air sparger is designed to first introduce air into the slurry and then force the mixture through a narrow horizontal orifice to aerate the slurry by means of pressure reduction and shear force.

Input streams to the column included the feed, air, and wash water. The outlet streams were the froth and tailings. The only internal line was the recirculation line. Masterflex peristaltic pumps were used for pumping the feed, recirculation slurry, wash water, and tailings streams. The froth stream was drained by gravity. The calibration equations for each pump are shown in Appendix C. Air was regulated to 138 kPa and controlled by a Matheson air rotameter. The pulp-froth interface was controlled by the tailings flow rate and was kept at approximately 1 to 8 cm below the top of the column. Tygon tubing, supplied by either Masterflex or Cole-Parmer, was used to connect the pumps to the column and was changed when necessary. Samples were taken of the feed and tailings streams, and when possible, the froth stream. Pressure was measured in two sections of the bubbly region by three manometers. The location of the manometers with respect to the top of the column was 0.35 m, 0.62 m, and 0.98 m, respectively as shown

in Figure 4-1. Only the lower manometers, at 0.62 m and 0.98 m, were used to determine bubbly zone gas volume fraction. All measurements were gathered at room temperature and under steady-state conditions. Steady-state was identified by establishing minimal oscillation of the pulp-froth interface for five minutes.

4.2 Materials and Procedures

The experimental details of the column flotation tests are given in Appendix E. Briefly before introducing the oil sand feed, the column was started and operated using process water to minimize start-up time. Once the desired operating conditions were reached, the feed line was switched from process water to middlings by-pass stream until the test was completed. Process water was used as wash water for all the tests.

4.2.1 Sample analysis

When analyzed at the University of Alberta, the Dean Stark method was used to determine the bitumen, solids, and water content in the samples. Details on the Dean Stark method are included in Appendix G. By extracting the solids and water from the bitumen, the mass percent of each was determined by:

$$\%\ \text{water} = \frac{\text{water collected}}{\text{sample weight}} * 100 \qquad (4\text{-}1)$$

$$\%\ \text{solids} = \frac{\text{solids collected (entrained solids + dried solids)}}{\text{sample weight}} * 100 \qquad (4\text{-}2)$$

$$\%\,\text{bitumen} = \frac{\text{bitumen collected}}{\text{sample weight}} * 100 \qquad (4\text{-}3)$$

Knowing the weight percent, the recovery was calculated. First, the weight percent values were converted to volume percent. It was assumed that the specific gravity of water and bitumen were approximately unity, while that of solids was close to silica at a value of 2.65. Knowing the volumetric flow rates of each stream, a mass balance around the column was conducted, resulting in the following three equations:

$$m_w^{feed} + m_w^{washwater} - m_w^{froth} - m_w^{tailings} = 0 \qquad (4\text{-}4)$$

$$m_b^{feed} - m_b^{froth} - m_b^{tailings} = 0 \qquad (4\text{-}5)$$

$$m_s^{feed} - m_s^{froth} - m_s^{tailings} = 0 \qquad (4\text{-}6)$$

where the subscript w refers to water, b refers to bitumen, and s refers to solids.

Recovery is then calculated based on the bitumen mass balance, using:

$$\text{Recovery}\,(\%) = \frac{\text{bitumen in froth}}{\text{bitumen in feed}} * 100 \qquad (4\text{-}7)$$

4.3 Experimental techniques

4.3.1 Tests at the University of Alberta

For the preliminary tests at the University of Alberta, Suncor Energy Inc. supplied a middlings sample that was gathered from their extraction process on January 14, 2002 at 15:00. Figure 4-3 shows a schematic of the flotation column set-up used for the University of Alberta tests.

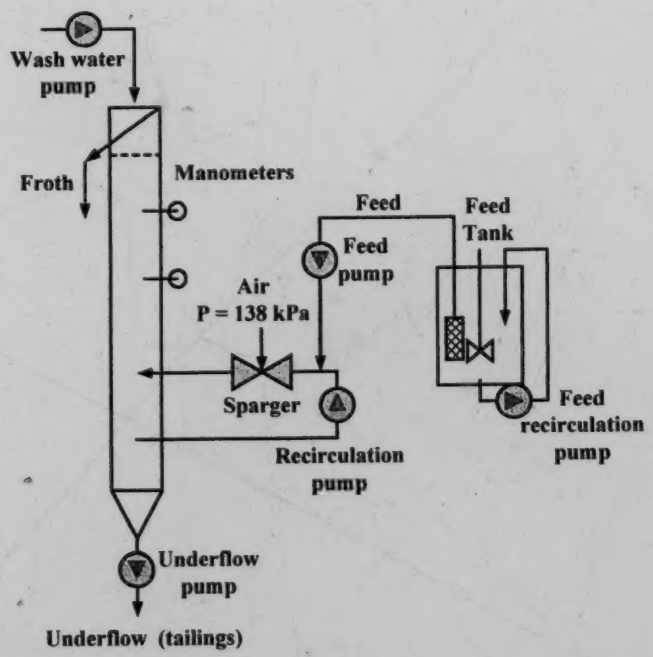

Figure 4-3. Schematic of the experimental set-up used for tests at the University of Alberta.

The feed was placed in a 30 L feed tank and mixed with two stirrers. The feed was withdrawn from the tank through a feed screen with a mesh size of 2 mm and entered the column just before the air sparger in the recirculation loop. The underflow and froth streams were taken off into waste buckets. Process water from the extraction plant at Syncrude Canada Ltd. was used as wash water and introduced just below the froth overflow. The interface level was controlled by the tailings flow rate.

Manipulated variables included the tailings, feed, wash water, air, and recirculation flow rates. Measured variables included the samples taken and the interface level. All tests were conducted at room temperature. The interface was maintained as such that the froth appeared stable, usually within 3 to 6 cm from the top of the column.

4.3.2 Syncrude Research Centre tests

For the second set of tests, the column was transported to the Syncrude Research Centre in Edmonton, Alberta, where a replica pilot plant of the Syncrude extraction process in Fort McMurray is available. Figure 4-4 shows the schematic of the experimental set-up used for the tests here.

The feed from the PSV middlings stream was pumped directly into the column just before the air sparger. A feed screen with a mesh of 2 mm was inserted directly into the PSV at the same level as the pilot plant flotation cell feed port i.e. at the location where the middlings was withdrawn.

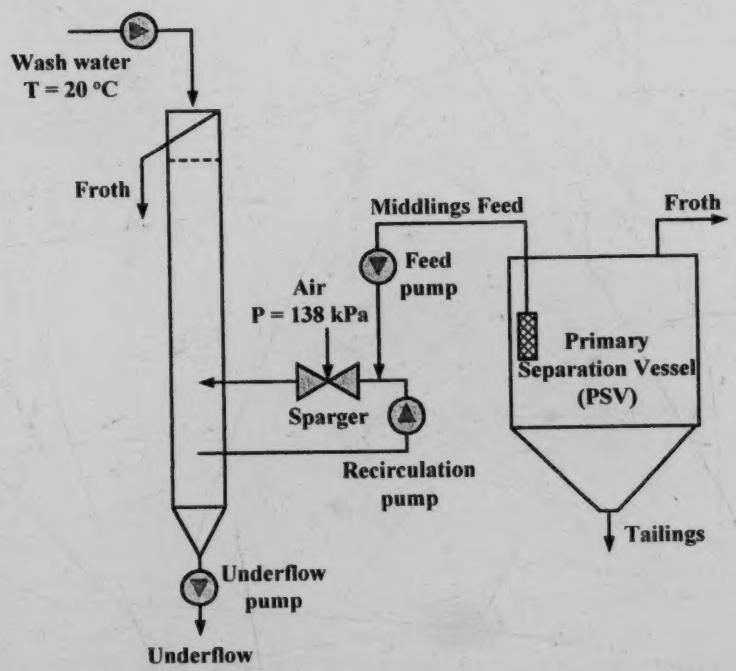

Figure 4-4. Schematic of the flotation column set-up used for the bitumen flotation tests conducted at the Syncrude Research Centre.

Process water at room temperature from the pilot plant supply was placed into 20 L pails and pumped into the column as wash water. The tailings and froth streams were directed to the sump tanks. The froth was gravity drained and cold city water was used to rinse the launder at various intervals to prevent the bitumen-rich froth from plugging the launder outlet. Samples were taken of the feed, tailings, and froth streams, which were analyzed for bitumen, water, and solids content at the Syncrude Research Centre.

The conditions of the pilot plant on the day of testing were recorded, including ore type, ore grade, ore fines, chemical addition, and chemical concentration. The recovery and conditions of the flotation cells were also noted for comparison.

Before the column was assembled, a proper HAZOP was completed to check all possible safety issues. A copy of the issues covered in the HAZOP is included in Appendix H.

4.3.3 Suncor in-plant tests

The final set of tests was completed at Suncor Energy Inc. in Fort McMurray, Alberta. The tests were conducted in the extraction plant using a sample line from the middlings stream of the plant separation cell #6. The sample line was located at the bottom of the middlings pipe. Figure 4-5 shows the set-up used for the bitumen flotation tests conducted at Suncor. The feed, at an approximate temperature of 55 °C, was directed into a 30 L feed tank, which was stirred and pumped through to keep the slurry homogenous and to prevent the slurry from becoming stagnant and sanding. Ensuring that the slurry level was kept above the stirrer within the tank prevented undesired slurry aeration for the test. From the feed tank, the slurry was pumped into the column through a feed screen with a 2 mm mesh opening. Process water at either 15 °C or 60 °C was used as wash water. For the majority of the tests, the colder process water was used, bringing the operating temperature within the column to approximately 20 °C. The interface level was kept within 1 to 5 cm from the top of the column.

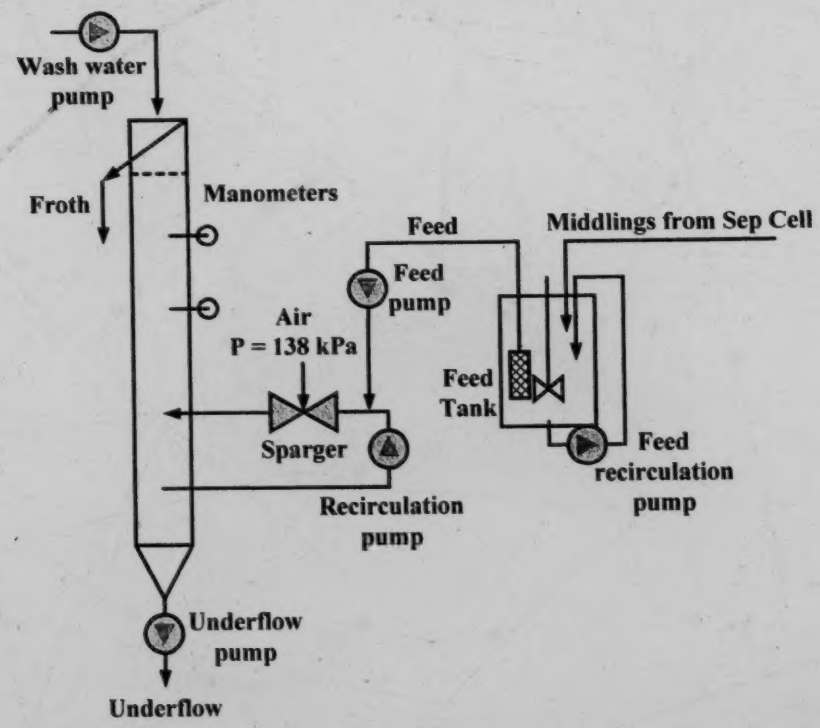

Figure 4-5. Schematic of the flotation column set-up used for the bitumen flotation tests at Suncor.

The recorded variables included the all the flow rates (tailings, feed, air, wash water, and recirculation streams) and the interface level. Assays were also completed for the sampled streams of the feed, tailings, and froth. McMurray Resources Ltd. (MRRT) analyzed the samples for bitumen, water, and solids content. The laboratory sample results were compared with the results from sample analysis conducted at the University of Alberta using the Dean Stark method.

4.4 Results and discussion

The first two sets of tests, at the University of Alberta and at the Syncrude Research Centre, were mainly conducted to eliminate any possible difficulties that may occur when the column was used for the third set of tests (in-plant tests) at Suncor. The majority of the operating difficulties encountered are outlined in this section, along with the operating conditions, results from sample analysis, and bitumen recoveries for each test. All the raw and calculated data are included in Appendix I.

4.4.1 Tests at the University of Alberta

Two tests were completed at the University of Alberta using oil sand middlings from the extraction process at Suncor. The feed was shipped from Fort McMurray in 20 L pails. Since the sample was shipped and not immediately used, the sample was segregated into bitumen, water, and solids. It was observed that bitumen accumulated on the sides and lids of the pails as shown in Figure 4-6. In an attempt to make the feed more homogenous, the middlings were poured into a 30 L feed tank and mixed with a stirrer. During the first test, the feed was not mixed properly and a second stirrer was added to create a more homogeneous slurry in the second test, as shown in Figure 4-7.

Figure 4-6. An example of the bitumen accumulation on the 20 L sample pail that was used to transport the process middling to the University of Alberta.

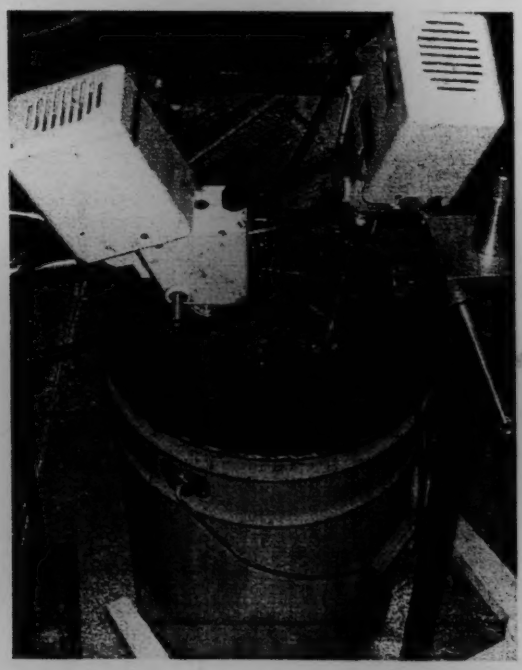

Figure 4-7. The feed stirrers used to create a more homogenous feed for the University of Alberta tests.

During the test, the pulp-froth interface was difficult to identify and was estimated using a bright light to watch the flow patterns and by monitoring the manometer levels. For the first test the interface was at 5 cm, while for the second test the interface was at 8 cm. Table 4-1 shows the operating conditions that were tested for both tests.

Table 4-1. Operating conditions for the initial bitumen flotation tests completed at the University of Alberta.

	Test 1	**Test 2**
Feed (L/min)	0.4	0.5
Recirculation (L/min)	1.8	1.8
Wash water (L/min)	0.5	0.5
Air (L/min)	0.4	0.4

Sample analysis was not completed since the purpose of these tests was to determine if the column would plug or encounter any major operating difficulties. By observation though, the tailings appeared to have a very small amount of bitumen when compared to either the froth or the feed samples. A comparison of the samples taken is shown in Figure 4-8. Clearly recovery of bitumen from middlings by a flotation column is feasible. It was also observed that although there are solids in the froth sample, the majority of the solids did advance to the tailings stream. After completing the tests, it was concluded that the column could handle an oil sand system without plugging.

Figure 4-8. An example of the samples taken during the University of Alberta tests.

4.4.2 Syncrude Research Centre tests

Only three tests were completed at the Syncrude Research Centre. For the most part, the flotation column could only be operated for two or three hours per day, thereby not allowing for extensive testing. A feed screen was inserted into the primary separation vessel (PSV) at the same level where the pilot plant flotation cells draw their middlings as feed (see Figure 4-4). A hot process water line was attached to the feed line by a valve to allow the feed screen to be backflushed before introducing slurry into the column or when the feed screen plugged up. It was found that the backflushing did not actually clean the whole screen, but rather only the bottom 3 mm, as shown in Figure 4-9.

Figure 4-9. The feed screen as it was plugged during the bitumen flotation tests at Syncrude Research Centre, allowing for flow from only the bottom of the screen.

The feed screen would easily plug up after back flushing. This could be contributed to the high bitumen content in the feed stream for the majority of the tests (< 7 wt. %) and lack of continuous cleaning by mixing. Once a bitumen layer accumulated on the screen, the solids would then accumulate on this layer causing even more serious plugging. The screen was eventually replaced after several tests with an exact duplicate. The problem of the feed screen plugging was resolved before the Suncor tests by redirecting the feed into a feed tank first.

The next difficulty encountered was slurry backflow into the air line and rotameter. The air rotameter had to be exchanged and re-calibrated. A check-valve was added to the air supply line just before the air sparger to prevent backflow in the subsequent tests. It was also noted that the air stream pressure fluctuated once the

middlings slurry was introduced into the column. To resolve this problem, the air supply was regulated from 689 kPa to 276 kPa instead of to 138 kPa.

Another major obstacle was that the Tygon tubing tended to plug, especially at locations immediately after the pumps. Since the pumps were peristaltic, the pumping mechanism caused the bitumen droplets to be "squished" together and the resulting larger droplets easily accumulated on the tubing walls. Once bitumen started clogging the tubing, subsequent bitumen easily accumulated, causing the flow to be totally restricted. In these cases, the tubing was replaced. The feed line, which was frequently being clogged, was replaced with larger diameter tubing. There was also a problem with valves and connectors being clogged with bitumen. This did not occur often, but when it did, the connectors were cleaned of the bitumen or replaced if cleaning did not help.

Gathering a sufficient froth sample was also difficult since the bitumen was very sticky, compounded with the wash water distributor location, it was difficult to transfer the froth into a sample bottle. Figure 4-10 shows an example of the top of the column at the location where the froth was sampled. To resolve this issue, city water was used to rinse the lauder periodically. Since excess water was added, the froth sample could not be used for the mass balance. As well, the froth launder outlet hole was found to be too small for continuous froth flow and often had to be cleaned during a test. The launder was modified to have a larger outlet before the Suncor tests were conducted.

Figure 4-10. An example of the froth along with the wash water distributor and launder used to direct the froth stream.

In total, three tests were completed with samples being taken. The feed rate was varied from 0.09 to 1.16 L/min; the recirculation rate was either 1.68 or 7.20 L/min; the air rate was either 0.40 or 0.57 L/min; the tailings rate ranged from 0.45 to 0.71 L/min; and the wash water rate was varied between 0.28 to 0.59 L/min. Samples were taken of the tailings and PSV middlings for every test. A froth sample was taken only for the first test and became too difficult to sample during the other tests. The laboratory at Syncrude Research Centre analyzed the samples for oil, sand, and water content. Table 4-2 summarizes the results for each test run.

For comparison, the recoveries from the flotation cells currently used in the pilot plant were recorded. These were calculated from the regular mass balances that are conducted every day by the operators at Syncrude Research Centre.

Table 4-2. Results for the bitumen flotation tests conducted at the Syncrude Research Centre.

Parameter		Test 1	Test 2	Test 3
Flow rates (L/min)	Feed	0.23	0.09	1.16
	Recirculation	1.68	7.20	7.20
	Air	0.56	0.40	0.40
	Tailings	0.58	0.71	0.45
	Wash water	0.40	0.59	0.28
PSV middlings (wt. %)	Bitumen	2.56	7.53	8.27
	Solids	43.19	38.66	37.51
	Water	54.42	52.94	53.87
Column tailings (wt. %)	Bitumen	0.46	0.06	0.46
	Solids	19.99	4.95	27.13
	Water	80.35	94.67	72.15
Column froth (wt. %)	Bitumen	3.23	N/A	45.65
	Solids	3.37	N/A	17.11
	Water	93.79	N/A	34.57
Recovery	%	63 %	95 %	98 %

The recoveries from the flotation cells for the conditions that the three sets of tests were performed were 90 %, 72 %, and 86 %, respectively. It is evident that in the second and third tests, the flotation column achieved significantly higher bitumen recoveries than the conventional flotation cells.

The conditions of the pilot plant on each testing day were also recorded in case the effect of ore type and chemical addition were evident. The properties of the ore and chemicals added are summarized in Table 4-3.

By comparing the recoveries of the flotation column with the conventional flotation cells, improvement is observed in the second and third tests.

Table 4-3. Summary of the pilot plant conditions at the Syncrude Research Centre during the bitumen flotation tests.

	Test 1	Test 2	Test 3
Type of Ore	Aurora High Grade Estuarine	Aurora - Research Transition Stockpile	Aurora - Research Transition Stockpile (Oil Sand C)
Ore grade	13.3	11.4	11.7
Ore fines	19.7	30.1	29.9
Chemicals added	NaOH; diesel	NaOH; diesel	NaOH; diesel
Chemical concentration	0.01 wt% of ore; 200 ppm of ore	0.01 wt% of ore; 200 ppm of ore	0.01 wt% of ore; 200 ppm of ore

The type of ore or chemical did not seem to affect the recovery when the column was used, but the effect was observed in the mechanical flotation cell. From these tests, it was concluded that the flotation column can assist in improving recovery and can operate under on-line industrial conditions.

4.4.3 Suncor in-plant tests

The goal of the Suncor tests was to determine the effect of varying feed, air, recirculation, and wash water rate on bitumen recovery and to confirm whether the column can be used in an industrial operation. The feed, at an approximate temperature of 55 °C, came from Separation Cell #6 and process water at either 60 °C or 15 °C was added as wash water. To fix the difficulty of bitumen plugging the feed screen that occurred at the Syncrude Research Centre, the feed slurry was placed into a 30 L feed tank and mixed with two stirrers. The feed screen was inserted directly into the tank and the slurry was pumped through the screen into the column. To prevent premature

aeration of the feed slurry, the hose withdrawing the middlings was placed on the side of the tank when filling the tank. If the slurry were allowed to fall from a large height or if any other type of shear force occurred, often air would be introduced into the feed, causing the bitumen to be aerated and pre-maturely separated before entering the column, as shown in Figure 4-11. In contrast, Figure 4-12 shows the slurry in the feed tank when little air was introduced. As well, the level in the feed tank was kept above the stirrers to prevent shear forces from introducing air. In the in-plant test, no problems were encountered with plugging of the feed screen.

Figure 4-11. An example of the feed slurry when air was pre-maturely introduced before entering the flotation column.

Figure 4-12. An example of the feed slurry without pre-mature air introduction, before it entered the flotation column.

Initially difficulties were encountered that were related to the solids content of the feed slurry. The middling sample was taken from the bottom of the middlings transport pipe, and consequently, the feed mainly consisted of settled solids. This high amount of solids in the middling plugged the floor drains, which had to be flushed thoroughly before proceeding with the tests. To prevent this from occurring again, a hot process water line was left running to constantly flush the floor drains and keep the sand from settling. In future tests, a sample port from a higher point in the middlings pipe would be beneficial to provide a more representative sample that would not plug the drains. The sample line that drew slurry from the middlings pipe also tended to clog when unused. To help prevent plugging of the sample line, a high pressure process water line was used to back flush the sample line into the middlings pipe. The slurry from the sample line

was then flushed into the drains for approximately ten minutes to allow the excess water in the sample line to drain before the feed tank was filled.

Since the tests were conducted in-plant and due to time restrictions, repeat test data could not be obtained. As it was, gathering sufficient and adequate test data was difficult due to continuous feed and constantly changing feed properties.

Table 4-4 summarizes the operating conditions and results from the thirteen bitumen flotation tests completed at Suncor. In the first four tests, the feed rate was increased from 0.41 to 1.17 L/min with a recirculation rate of 2.14 L/min. In tests 5 to 8, the same feed rates were tested, but at a higher recirculation rate of 4.87 L/min. It was observed in the first four tests that the interface level was stable at about 1 to 3 cm below the top of the column. In industry, usually a deeper froth bed is desired and to remedy this problem, the recirculation rate was increased from 2.14 L/min to 4.87 L/min. By increasing the recirculation rate, finer bubbles should be generated to help deepen and stabilize the froth bed. For the increased recirculation tests, the interface was observed to be 3 to 5 cm, i.e. a deeper froth was formed. For tests 9 through 11, air rate was increased from 0.30 to 0.55 L/min. The recirculation rate for these tests was chosen at a value of 3.31 L/min, a level between that of the first and second tests. Finally, in the last set of tests the wash water rate was decreased from 0.36 to no wash water addition. Again these tests were conducted at a recirculation rate of 3.31 L/min and at a higher feed rate of 1.17 L/min.

Table 4-4. Summary of the results from the bitumen flotation tests conducted at Suncor (sample analysis completed at the University of Alberta).

		Increasing feed rate (low recirc. rate)				Increasing feed rate (high recirc. rate)				Increasing air rate (med. recirc. rate, high feed rate)			Decreasing wash water rate	
Parameter	**Test**	**1**	**2**	**3**	**4**	**5**	**6**	**7**	**8**	**9**	**10**	**11**	**12**	**13**
Flow rates (L/min)	Feed	0.41	0.67	0.92	1.17	0.43	0.67	0.92	1.17	1.17	1.17	1.16	1.16	1.16
	Recirculation	2.13	2.14	2.14	2.14	4.87	4.87	4.87	4.87	3.31	3.31	3.31	3.31	3.31
	Air	0.45	0.45	0.45	0.45	0.45	0.45	0.45	0.45	0.30	0.45	0.55	0.45	0.45
	Tailings	0.67	0.85	1.22	1.31	0.91	0.91	0.91	1.11	1.05	0.98	0.91	0.91	0.71
	Wash water	0.36	0.36	0.36	0.36	0.36	0.36	0.36	0.36	0.36	0.36	0.36	0.14	0.00
Feed (wt. %)	Bitumen	0.16	0.11	0.13	0.23	0.41	0.45	0.47	1.03	1.20	1.82	0.91	0.74	0.75
	Solids	54.85	52.81	51.92	47.89	45.08	44.31	40.77	46.06	45.26	52.23	52.04	52.59	51.35
	Water	44.91	47.11	47.95	51.87	54.48	55.28	58.78	53.05	53.47	45.95	47.13	46.65	47.88
Tailings (wt. %)	Bitumen	0.02	0.03	0.04	0.05	0.06	0.10	0.15	0.14	0.15	0.30	0.14	0.22	0.16
	Solids	32.21	47.90	43.77	32.42	27.23	29.38	33.84	37.95	33.48	41.43	45.69	49.74	49.57
	Water	67.84	52.01	56.23	67.40	72.76	70.51	66.01	61.85	66.48	57.73	54.18	49.94	50.34
	Recovery (%)	100	100	100	100	70	72	71	83	86	87	88	86	83

The samples were analyzed for bitumen, solids, and water content by both MRRT (McMurray Resources Ltd. Research & Testing) and at the University of Alberta. Figure 4-13 shows an example of the feed and tailings samples that were taken. Table 4-4 shows the weight percent of the solids, bitumen, and water from the analysis completed at the University of Alberta. The recoveries calculated using the data from the two laboratories were similar. It was assumed that when bitumen levels were below 0.1 wt%, there was virtually little to no bitumen in the sample. Since the Dean Stark method is highly reliable on accurate weight measurements, this assumption is reasonable.

Figure 4-13. An example of the feed and tailings samples for Test 1 conducted at Suncor.

In the first set of tests, where flow rate was increased at a lower recirculation rate, the recovery was almost 100 % (judged by < 0.1 wt. % bitumen in the tailings sample). Figure 4-13 shows the feed and tailings samples from Test 1. As observed, there is little to no bitumen in the tailings sample, which qualitatively indicates a high bitumen recovery. In the second set of tests, the same feed rates were tested as in the first set of tests, except now the recirculation rate was set at a higher rate of 4.87 L/min. In this case as the feed rate was increased, a slight but significant increase in recovery was observed. This is expected at high recirculation and feed flow rates, since high feed flow rates tend to induce larger bitumen droplets. With minimal formation of fine bitumen droplets that are difficult float, recovery is expected to increase. Comparing the tests in sets 1 and 2, it is apparent that higher recirculation flow rates result in a lower recovery. It is possible that under such a high slurry flow rate, bitumen droplets were sheared excessively to form tiny droplets, which are ineffective to bitumen-bubble attachment. More importantly, at such a high slurry flow rate, extremely fine bubbles are generated and attached to tiny bitumen droplets. Under operation conditions with wash water addition, the bitumen – loaded fine bubbles are unable to escape from entering the tailings stream as visually observed, resulting in a low bitumen recovery. The change in bitumen recovery trend for the third set of tests (increasing air rate) is fairly small and shows an increase in bitumen recovery with increasing aeration rate. This recovery trend indicates that the lowest aeration rate of 0.3 L/min for the feed and recirculation rates of 1.17 and 3.31 L/min, respectively, was already sufficient and introduction of additional air was inconsequential. Finally in the last set of tests where wash water rate was decreased, the

recovery decreases as well. This indicates the importance of wash water in helping improve recovery levels. For Test 13, when no wash water was introduced, the froth appeared unstable as shown in Figure 4-14. From Figure 4-14, it is clear that the froth was not rich and a lower bitumen recovery would result. This is possibly due to the lack of cooling action the wash water provided. At higher operating temperature, the froth was found to be less stable, as anticipated.

Figure 4-14. The froth during Test 13 where no wash water was introduced.

4.5 Conclusions

From the tests at the University of Alberta and at the Syncrude Research Centre, it is concluded that the flotation column set-up is suitable for processing oil sand middlings in an on-line situation. The recoveries at the Syncrude Research Centre indicate that the flotation column can potentially produce higher recovery rates than the conventional flotation cells. It is concluded from the tests at Suncor that the column can be successfully applied to the oil sand middlings stream. As expected, the bitumen recovery

increases with increased feed flow rate. It decreases with decreasing wash water rate. Recoveries ranged from approximately 70 % to 100 %, depending on operating conditions. The optimal conditions were at a desired recirculation rate (2.14 L/min) with higher feed flow rate (1.17 L/min) and air flow rate (0.55 L/min).

5.0 CONCLUSIONS

1. Using drift flux analysis on a two-phase system within a flotation column, a correlation for exponent "m" relating to Reynolds number was found to be:

$$m = \frac{20.26 + 1.89\,\mathrm{Re}_b}{4.38 + \mathrm{Re}_b}$$

2. The correlation for exponent "m" was tested using different two-phase systems and was found to better predict the bubbly and froth region conditions for changing operating conditions than current exponent "m" correlations. The two-phase systems were tested over a Reynolds numbers range of 5 to 70.

3. For our experimental set-up using a laboratory flotation column, a new correlation for Reynolds number in the froth zone was found to be:

$$\mathrm{Re}_{\text{froth zone}} = 2.38 * 10^{-5}\left(d_b^2\right) + 9.08 * 10^{-3}\left(d_b\right)$$

4. The flotation column can be successfully applied to an oil sand middlings system under industrial conditions without any major operating difficulties.

5. Preliminary studies show that the flotation column set-up presented in this thesis allows better bitumen recovery than current conventional flotation cells used at the Syncrude Research Centre.

6.0 RECOMMENDATIONS

1. In this study, underflow and froth flow rates were all measured manually. For better accuracy, computer process control could be utilized for measurements of flow rates.

2. Since the oil sand industry is moving towards lower temperature processes, effect of temperature on bitumen recovery in column flotation should be studied.

3. Due to shallow froth, the gas volume fraction in the froth zone was not measured, but calculated instead. The gas hold-up in the froth zone should be measured instead.

4. The air sparger used for this study had a 3.1 mm diameter gap. Since the gap was so narrow, a feed screen had to be utilized to prevent the aerator from plugging. Development of an air sparger that could handle direct oil sand feed without plugging would be beneficial.

5. If our column set-up were to be used in-plant permanently, the laboratory column would have to be scaled to industrial size. For scale-up, the following would have to be tested:

- carrying capacity (maximum throughput)
- optimal column height using an in-line aeration system
- optimal operating conditions for maximum bitumen recovery

6. Despite testing limitations, the flotation column allowed for a unique opportunity. More extensive in-plant tests would be beneficial, examining more systematically the effect of bubble generators, wash water addition, feed rate, recirculation rate, etc.

REFERENCES

Akita, K.; and Yoshida, F., 1973, *Ind. Engng Chem. Proc. Des. Dev.*, **12(1)**, 76. (Referred to in: Dobby & Finch, 1985).

Alexander, B.F.; and Shah, Y.T., 1976, "Axial Dispersion Coefficients in Bubble Columns", *The Chemical Engineering Journal*, **11**, 153-156.

Anfruns, J.F.; and Kitchener, J.A., 1977, "Rate of Capture of Small Particles in Flotation", *Trans. Instn. Min. Metall.*, C9-C15.

Banisi, S.; and Finch, J.A., 1994, "Technical Note: Reconciliation of Bubble Size Estimation Methods using Drift Flux Analysis", *Minerals Engineering*, **7(12)**, 1555-1559.

Banisi, S.; Finch, J.A.; and Laplante, A.R., 1995a, "Effect of Solid Particles on Gas Holdup in Flotation Columns – 1. Measurement", *Chemical Engineering Science*, **50(14)**, 2329-2334.

Banisi, S; Finch, J.A.; and Laplante, A.R., 1995b, "Effect of Solid Particles on Gas Holdup in Flotation Columns – 2. Investigation of Mechanisms of Gas Holdup Reduction in Presence of Solids", *Chemical Engineering Science*, **50(14)**, 2335-2342.

Bhaga, D.; and Weber, M.E., 1972, *Canadian Journal of Chemical Engineering*, **50**, 323.

Biesheuvel, A.; and Gorissen, W.C.M., 1990, "Void Fraction Disturbances in a Uniform Bubbly Fluid", *International Journal of Multiphase Flow*, **16(2)**, 211-231.

Burstein, M.A.; and Flint, I.M., 2000, *Flotation*, Academic Press.

Clift, R.; Grace, J.R.; and Weber, M.E., 1978, "Bubbles, Drops, and Particles", *Academic Press*, New York. (Referred to in Dobby et al., 1988).

Concha, F.; and Almendra, E.R., 1979, "Settling Velocities of Particulate Systems, 1. Settling Velocities of Individual Spherical Particles", *International Journal of Mineral Processing*, **5**, 349-367.

Davidson, J.F.; and Harrison, D., 1966, "The Behaviour of a Continuously Bubbling Fluidised Bed", *Chemical Engineering Science*, **21**, 731-738.

Degner, V.R.; and Sabey, J.B., 1988, "WEMCO/LEEDS Flotation Column Development", *Column Flotation '88*, K.V. Sastry (editor), SME, Littleton, CO, 267-279.

Dobby, G.S.; and Finch, J.A., 1991, "Column Flotation: A Selected Review Part 2", *Minerals Engineering*, **4(7-11)**, 911-923.

Dobby, G.S.; and Finch, J.A., 1986, "Flotation Column Scale-up and Modeling", *CIM Bulletin*, **79(889)**, 89-96.

Dobby, G.S.; and Finch, J.A., 1985, "Mixing Characteristics of Industrial Flotation Columns", *Canadian Metallurgical Quarterly*, **25(1)**, 9-13.

Dobby, G.S.; Yianatos, J.B.; and Finch, J.A., 1988, "Estimation of Bubble Diameter in Flotation Columns from Drift Flux Analysis", *Canadian Metallurgical Quarterly*, **27(2)**, 85-90.

Falutsu, M., 1994, "Column Flotation Froth Characteristics – Stability of the Bubble-Particle System", *International Journal of Mineral Processing*, **40**, 225-243.

Falutsu, M.; and Dobby, G.S., 1989, "Direct Measurement of Froth Dropback and Collection Zone Recovery in a Laboratory Flotation Column", *Minerals Engineering*, **2(3)**, 377-386.

Finch, J.A., 1995, "Column Flotation: A Selected Review – Part IV: Novel Flotation Devices", *Minerals Engineering*, **8(6)**, 587-602.

Finch, J.A.; and Dobby, G.S., 1990, *Column Flotation*, Pergamon Press, Oxford, New York.

Finch, J.A.; and Dobby, G.S., 1991, "Column Flotation: A Selected Review, Part I", *International Journal of Mineral Processing*, **33**, 343-354.

Gomez, C.O.; Escudero, R.; and Finch, J.A., 2000, "Determining Equivalent Pore Diameter for Rigid Porous Spargers", *The Canadian Journal of Chemical Engineering*, **78**, 785-792.

Gorain, B.K., 1997, "The Effect of Bubble Surface Area Flux in Flotation Columns from the Physical Characteristics of Rigid Spargers", *Paper presented at the CIM/CMMI/MIGA meeting*, The Met. Soc. Of CIM, Montreal. (Referred to in Tavera et al., 2001).

Gourram-Badri, F.; Conil, P.; and Morizot, G., 1997, "Measurements of Selectivity due to Coalescence between two Mineralized Bubbles and Characterization of MIBC action on Froth Flotation", *International Journal of Mineral Processing*, **51**, 197-208.

Gray, M.P.; Harbort, G.J.; and Murphy, A.S., "Flotation Circuit Design Utilising the Jameson Cell", www.mimpt.com.au/downloads/jc_flotation.pdf, taken June 12, 2002.

Green, D.; and Cox, C., 1993, "Flotation of Copper with an Outokumpu HG Tank Cell Prior to Gold Leaching", *Randol Gold Forum Beaver Creek '93*, 125-130.

Griffith, P.; and Wallis, G.B., 1961, "Two-Phase Slug Flow", *ASME Transactions Journal of Heat Transfer*, **83**, 307-320.

Honaker, R.Q.; and Paul, B.C., 1995, "A Comparison Study of Column Flotation Technologies for Cleaning Illinois Coal", *Final Technical Report*, Illinois Clean Coal Institute, Carterville, Illinois. (Referred to in: Mohanty & Honaker, 1999).

Ityokumbul, M.T., 1996, "What really Determines the Height in Column Flotation?", *Minerals and Metallurgical Processing*, 36-40.

Ityokumbul, M.T.; Bulani, W.; and Kosaric, N., 1988, "Flotation Kinetics for Titanium, Zirconium, and Bitumen Recovery from Oilsand Tailings", *The Canadian Journal of Chemical Engineering*, **66**, 382-385.

Ityokumbul, M.T.; Salama, A.I.A.; and Taweel, A.M.A., 1995, "Estimation of Bubble Size in Flotation Columns", *Minerals Engineering*, **8(1-2)**, 77-89.

Kawatra, S.K.; and Eisele, T.C., 1995, "Baffled-Column Flotation of a Coal Plant Fine Waste Stream", *Minerals and Metallurgical Processing*, 138-142.

Killmeyer et al., 1989, U.S. DOE sponsored study. (Referred to in: Mohanty & Honaker, 1999).

Lapidus, L.; and Elgin, J.C., 1957, "Mechanics of Vertical-moving Fluidized Systems", *AIChE Journal*, **3(1)**, 63-68.

Masliyah, J.H., 1979, "Hindered Settling in a Multi-Species Particle System", *Chemical Engineering Science*, **34**, 1166-1168.

Mattenella, L.E.; and Zapiola, C.R., 2001, "Technical Note: Holdup Models from Experimental Conductance Data in a Bubble Column", *Minerals Engineering*, **14(2)**, 257-262.

Mohanty, M.K.; and Honaker, R.Q., 1999, "A Comparative Evaluation of the Leading Advanced Flotation Technologies", *Minerals Engineering*, **12(1)**, 1-13.

Pal, R.; and Masliyah, J., 1989, "Flow Characterization of a Flotation Column", *The Canadian Journal of Chemical Engineering*, **67**, 916-923.

Peebles, F.N.; and Garber, H.J., 1953, *Chem. Eng. Progr.*, **49**, 88. (Referred to in: Zhou & Egiebor, 1993).

Persechini, M.A.M.; Jota, F.G.; and Peres, A.E.C., 2000, "Dynamic Model of a Flotation Column", *Minerals Engineering*, **13(14-15)**, 1465-1481.

Richardson, J.F.; and Zaki, W.N., 1954, "Sedimentation and Fluidization: Part I", *Trans. Instn. Chem. Engrs.*, **32**, 35-53.

Ross, V.E.; and Van Deventer, J.S.J., 1988, "Mass Transport in Flotation Column Froths", *Column Flotation '88*, K.V. Sastry (editor), SME, Littleton, CO, 129-139.

Rubio, J., 1996, "Modified Column Flotation of Mineral Particles", *International Journal of Mineral Processing*, **48**, 183-196.

Sasaki, H.; Matsukawa, H.; Usui, S.,; and Matijevic, E., 1986, *J. Colloid Interface Sci.*, **113(2)**, 500. (Referred to in: Dobby et al., 1988).

Schiller, L.; and Naumann, A., 1933, *Z. Ver. dt Ing.*, **77**, 318. (Referred to in: Banisi & Finch, 1994).

Shah, Y.T.; Kelker, B.G.; and Godbole, S.P., 1982, "Design Parameters Estimations for Bubble Column Reactors", *AIChE Journal*, **28(3)**, 353-379.

Tavera, F.J.; Escudero, R.; and Finch, J.A., 2001, "Gas Holdup in Flotation Columns: Laboratory Measurements", *International Journal of Mineral Processing*, **6**, 23-40.

Turner, J.C.R., 1966, "On Bubble Flow in Liquids and Fluidised Beds", *Chemical Engineering Science*, **21**, 971-974.

Wallis, G.B., 1969, *One-Dimensional Two-Phase Flow*, McGraw-Hill Inc., New York.

Xu, M.; Quinn, P.; and Stratton-Crawley, R., 1996a, "A Feed-line Aerated Flotation Column Part I: Batch and Continuous Testwork", *Minerals Engineering*, **9(5)**, 499-507.

Xu, M.; Quinn, P.; and Stratton-Crawley, R., 1996b, "A Feed-line Aerated Flotation Column Part 2: Modeling and Scale-up", *Minerals Engineering*, **9(6)**, 655-666.

Xu, M.; Uribe-Salas, A.; Finch, J.A.; and Gomez, C.O., 1989, "Gas Rate Limitation in Column Flotation", *Processing of Complex Ores*, Dobby, G.S. and Rao, S.R. (editors), Pergamon Press, Toronto, ON, 397-407.

Yang, D.C., 1988, "A New Packed Column Flotation System", *Column Flotation '88*, K.V. Sastry (editor), SME, Littleton, CO, 257-265.

Yianatos, J.B., 1987, "Column Flotation Froths", *Ph.D.Thesis*, McGill University, Montreal. (Referred to in: Falutsu, 1994).

Yianatos, J.B.; and Bergh, L.G., 1995, "Troubleshooting Industrial Flotation Columns", *Minerals Engineering*, **8(12)**, 1593-1605.

Yianatos, J.B.; Bergh, L.G.; and Cortés, G.A., 1998, "Froth Zone Modeling of an Industrial Flotation Column", *Minerals Engineering*, **11(5)**, 423-435.

Yianatos, J.B.; Finch, J.A.; Dobby, G.S.; and Xu, M., 1988, "Bubble size Estimation in a Bubble Swarm", *Journal of Colloid Interface*, **126(1)**, 37 – 44.

Yianatos, J.B.; Finch, J.A.; and Laplante, A.R., 1986, "Holdup Profile and Bubble Size Distribution of Flotation Column Froths", *Canadian Metallurgical Quarterly*, **25(1)**, 23-29.

Zhou, Z.A.; and Egiebor, N.O., 1993, "A Gas-Liquid Drift-Flux Model for Flotation Columns", *Minerals Engineering*, **6(2)**, 199-205.

Zhou, Z.A.; Egiebor, N.O.; and Plitt, L.R., 1992, "Frother Effects on Single Bubble motion in a Water Column", *Canadian Metallurgical Quarterly*, **31(1)**, 11-16.

Zuber, N.; and Hench, J., 1962, "Steady-State and Transient Void Fraction of Bubbling Systems and their Operating Limits", General Electric Co., Rept. No. 62GL100, Schenectady, New York. (Referred to in: Pal & Masliyah, 1989).

APPENDIX A

This appendix contains a sample calculation used to find the bubbly zone bubble diameter based on experimentally measured data from the two-phase system tests. The calculations follow the flow chart outlined in Figure 3-1.

A.1 Sample calculation to find bubble diameter in the bubbly zone

Banisi and Finch (1994) summarized the main methods used to calculate bubble diameter from gas volume fraction. The method used in this study is similar to that of Yianatos et al. (1988) and follows the flow chart in Figure 3-1. To better illustrate how to use the equations, an example is given.

The example given is based on the data from a 7.8 ppm MIBC aqueous solution test. The lower manometer reading was 0.032 m. The pump settings were 4.1 for the wash water pump, 4.0 for the recirculation pump, and 13% for the air rotameter. The tailings flow rate was based on a volume of 22 mL measured in a time of 9.75 s.

Using the wash water pump calibration equation defined in Appendix C,

$$\text{Wash water flow rate (mL/min)} = 56.418(\text{pump setting}) - 13.711 \qquad \text{(A-1)}$$

$$56.418(4.1) - 13.711 = 217.603 \text{ mL/min}$$

$$\text{Wash water flow rate} = 0.218 \text{ L/min}$$

Using the recirculation pump calibration equation defined in Appendix C,

$$\text{Recirculation flow rate (L/min)} = 0.7773(\text{pump setting}) - 0.576 \qquad \text{(A-2)}$$

$$0.7773(4.0) - 0.576 = 2.533 \text{ L/min}$$

$$\text{Recirculation flow rate} = 2.533 \text{ L/min}$$

Using the air calibration equation defined in Appendix C,

$$\text{Air flow rate (L/min)} = 0.0712(\text{rotameter setting}) - 0.3004 \qquad \text{(A-3)}$$

$$0.0712(13\%) - 0.3004 = 0.625 \text{ L/min}$$

$$\text{Air flow rate} = 0.625 \text{ L/min}$$

To find the underflow flow rate, a known volume was taken for a certain amount of time.

$$\text{Underflow flow rate} = \frac{\text{volume}}{\text{time}} \qquad \text{(A-4)}$$

$$\frac{22mL}{9.75s} = 2.267\frac{mL}{s}$$

$$\text{Underflow flow rate} = 0.135 \text{ L/min}$$

To convert the pressure reading to gas volume fraction, the following was used:

$$\alpha_g = \frac{h}{L} \qquad \text{(A-5)}$$

$$\alpha_g = \frac{0.032m}{0.370m} = 0.086$$

The gas flux was based on the air flow rate, while the liquid flux was based on the underflow flow rate, both of which are based on equation 3-1.

$$j_f = \frac{\text{underflow flow rate}}{\text{x - sectional area}} \qquad \text{(A-6)}$$

First, the cross sectional area of the flotation column was determined using:

$$\text{Cross sectional area} = \pi r^2$$

$$3.14(0.031\text{m})^2 = 0.003 \text{ m}^2$$

cross sectional area = 0.003 m^2

Next using equation A-6, the liquid flux was calculated by:

$$j_f = \frac{\text{underflow flow rate}}{\text{x - sectional area}} \qquad \text{(A-7)}$$

$$j_f = \frac{0.135 \frac{L}{\min}\left(\frac{m^3}{1000L}\right)\left(\frac{\min}{60s}\right)}{0.003m^2} = 0.000747\frac{m}{s}$$

j_f = 0.000747 m/s

The gas flux was found using the following:

$$j_g = \frac{\text{air flow rate}}{\text{x - sectional area}} \qquad \text{(A-8)}$$

$$j_g = \frac{0.135 \frac{L}{\min}\left(\frac{m^3}{1000L}\right)\left(\frac{\min}{60s}\right)}{0.003m^2} = 0.00345\frac{m}{s}$$

j_g = 0.00345 m/s

The following calculations are outlined in Figure 3-1.

1. Estimate d_b

d_b = 1000 μm

2. Calculate α_g (equation 3-2) and slip velocity, U_{gf} (equation 3-3)

$$\alpha_g = \frac{h}{L} \qquad \text{(A-9)}$$

$$\alpha_g = \frac{0.032}{0.370} = 0.086$$

$$U_{gf} = \frac{j_g}{\alpha_g} + \frac{j_f}{(1-\alpha_g)} \tag{A-10}$$

$$U_{gf} = \frac{0.00345\frac{m}{s}}{0.086} + \frac{0.000747\frac{m}{s}}{(1-0.086)} = 0.0407\frac{m}{s}$$

3. Calculate terminal velocity, U_t

   a. Estimate U_t

$$U_t = 0.122 \text{ m/s}$$

   b. Calculate Re_b (equation 3-4)

$$Re_b = \frac{d_b U_t \rho_f}{\mu_f} \tag{A-11}$$

$$Re_b = \frac{(0.001m)\left(0.122\frac{m}{s}\right)\left(1000\frac{kg}{m^3}\right)}{(0.001Pa*s)}$$

$$Re_b = 122$$

   c. Calculate U_{tCALC}. If the tolerance between the calculated and estimated terminal velocity values are within 10^{-8}, proceed to the next step. If the tolerance is below 10^{-8}, then U_{tCALC} is used as the next estimate and the iterative process (Step 3) is repeated.

$$U_t = \frac{g d_b^2 (\rho_f - \rho_b)}{18\mu_f (1 + 0.15 Re_b^{0.687})} \tag{A-12}$$

$$U_t = \frac{\left(9.81\frac{m}{s^2}\right)(0.001m)^2\left(1000\frac{kg}{m^3} - 1\frac{kg}{m^3}\right)}{18(0.001Pa*s)\left(1+0.15(122)^{0.687}\right)}$$

$$U_t = 107.4\frac{m}{s}$$

tolerance = abs($U_t - U_{tCALC}$)

tolerance = abs(0.122 – 107.4 m/s)

tolerance = 107.3

After iterating until tolerance is below 10^{-8}, the values for terminal velocity and Reynolds number are:

U_t = 0.112 m/s

Re_b = 112.4

4. Calculate "m" (Richardson & Zaki, 1954) (equations 2-24 to 2-26). Then calculate Reynolds number based on slip velocity, Re_{bs}, using equation 3-5.

$$m = \left(4.45 + 18\frac{d_b}{d_c}\right)\mathrm{Re}_b^{-0.1} \qquad \text{(A-13)}$$

$$m = \left(4.45 + 18\frac{(0.001m)}{(0.062m)}\right)(112.4)^{-0.1}$$

m = 2.956

$$\mathrm{Re}_{bs} = \frac{d_b U_{sg}\rho_f(1-\alpha_g)}{\mu_f} \qquad \text{(A-14)}$$

$$\mathrm{Re}_{bs} = \frac{(0.001m)\left(0.0407\frac{m}{s}\right)\left(1000\frac{kg}{m^3}\right)(1-0.0806)}{(0.001Pa*s)}$$

$$\mathrm{Re}_{bs} = 37.42$$

5. Calculate U_{gf} (Schiller & Naumann, 1933) using equation 2-18. Compare the calculated and experimental slip velocities. If the tolerance between the two values is within 10^{-8}, the iterative process is stopped. If the tolerance is not reached, a new estimate for bubble diameter is found using d_{bCALC} and the iterative process repeated.

$$U_{gf} = \frac{g d_b^2 (\rho_f - \rho_b)(1-\alpha_g)^{n-1}}{18\mu_f\left(1+0.15\mathrm{Re}_{bs}^{0.687}\right)} \qquad \text{(A-15)}$$

$$U_{gf} = \frac{\left(9.81\frac{m}{s^2}\right)(0.001m)^2\left(1000\frac{kg}{m^3} - 1\frac{kg}{m^3}\right)(1-0.0806)^{(2.956-1)}}{18(0.001Pa*s)\left(1+0.15(37.42)^{0.687}\right)}$$

$$U_{gf} = 164.6\frac{m}{s}$$

$$\text{tolerance} = \text{abs}(U_{gf} - U_{gfCALC})$$

$$\text{tolerance} = \text{abs}(0.0407 - 164.5 \text{ m/s})$$

$$\text{tolerance} = 164.5$$

Since the tolerance was not reached, a new estimate for bubble diameter is caluclted by rearranging equation A-15:

$$d_{bCALC} = \left(\frac{18\mu_f U_{gf}\left(1+0.15\mathrm{Re}_{bs}^{0.687}\right)}{g(\rho_f - \rho_b)(1-\alpha_g)^{n-1}}\right)^{0.5} \qquad \text{(A-16)}$$

$$d_{bCALC} = \left(\frac{18(0.001Pa*s)\left(0.0407\frac{m}{s}\right)\left(1+0.15(37.42)^{0.687}\right)}{\left(9.81\frac{m}{s^2}\right)\left(1000\frac{kg}{m^3}-1\frac{kg}{m^3}\right)(1-0.0806)^{(2.956-1)}} \right)^{0.5}$$

$$d_{bCALC} = 4.97*10^{-4}\,m$$

Once the tolerance was reached, the resulting values were:

$\alpha_g = 0.0865$

$U_{gf} = 0.0407$ m/s

$U_t = 0.466$ m/s

$Re_b = 20.14$

$Re_{bs} = 16.07$

m = 3.39

$d_b = 432.1$ μm

A.2 Visual Basic program

A program in Visual Basic (Excel programming language) was written to calculate the bubble diameter within the bubbly zone based on the experimentally measured data. The following is a copy of the Excel program.

```
Sub BDiameter()
' This function will determine the bubble diameter for a flotation column for a given gas
' hold-up in the bubbly zone.
' The numerical method will be a simple iterative method
' It was written by Jessica Zinterer in May 2001 @ U of A, Version 4 completed
07/11/2002
```

```
' Declare all variables
Dim Jg As Double, JL As Double, pf As Double, pb As Double, uf As Double
Dim dL1 As Double, dL2 As Double, dh1 As Double, dh2 As Double, pw As Double
Dim g As Double, dc As Double
Dim Ut As Double, Utcalc As Double, eg As Double, Usg As Double, F As Double
Dim d As Double, m As Double, dcalc As Double, Reb As Double, Rebs As Double
Dim tol1 As Double, tol2 As Double, I As Integer, J As Integer, Usgcalc As Double

' Initialize all variables, create reference variables
Jg = Range("D5").Value
JL = Range("D6").Value
pf = Range("D7").Value
pb = Range("D8").Value
uf = Range("D9").Value
dc = Range("D10").Value
dL1 = Range("D11").Value
dL2 = Range("D12").Value
dh1 = Range("D13").Value
dh2 = Range("D14").Value
pw = Range("D15").Value
g = 9.81

' For LOWER MANOMETER ONLY
' Initial guesses for d, Ut, and tolerances to be used
d = 0.001
dcalc = d
Ut = 0.144
Utcalc = 0.122
Usgcalc = 0.1
tol1 = 0.00000001
tol2 = 0.00000001

' Determine Gas Hold-up
' eg = (h/L)

eg = (dh1 / dL1)

' Determine Slip Velocity
' Usg = Jg/eg + Jl/(1-eg)

Usg = Jg / eg + JL / (1# - eg)

While Abs(Usg - Usgcalc) > tol1 And d > 0#
   d = dcalc
   Reb = (d * Ut * pf) / uf
   Utcalc = (g * d ^ 2 * (pf - pb)) / (18 * uf * (1 + 0.15 * Reb ^ 0.687))
```

```
  While Abs(Ut - Utcalc) > tol2
    Ut = Utcalc
' Determine Reynold's number
    Reb = (d * Ut * pf) / uf
' Determine Terminal velocity of particle (Ut) using iterative method
' Ut = (g*d^2*pw)/(18*uf*(1+0.15*Reb^0.687))

    Utcalc = (g * d ^ 2 * (pf - pb)) / (18 * uf * (1 + 0.15 * Reb ^ 0.687))
  Wend

  Reb = (d * Ut * pf) / uf

' Calculate exponent "m" based on Richardson & Zaki (1954) correlations
' m = (4.45 + (18*d/dc))*Reb^(-0.1)

  If Reb < 200# Then
    m = (4.45 + (18# * d / dc)) * Reb ^ (-0.1)
  Else
    m = 4.45 * Reb ^ (-0.1)
  End If

' Calculate Rebs based on slip velocity
' Rebs = (d*Usg*pf*(1-eg))/uf

  Rebs = (d * Usg * pf * (1# - eg)) / uf

' Determine calculated Usg to compare to experimental Usg value
  Usgcalc = (g * d ^ 2 * (pf - pb) * (1 - eg) ^ (m - 1)) / (18 * uf * (1# + 0.15 * Rebs ^
0.687))

' Determine calculated d value
  dcalc = ((Usg * 18# * uf * (1# + 0.15 * Rebs ^ 0.687)) / ((pf - pb) * (1 - eg) ^ (m - 1) *
g)) ^ (0.5)

Wend
d = dcalc

' Recalculate Values based on final d value
  Ut = 0.144
  While Abs(Ut - Utcalc) > tol2
    Ut = Utcalc
    Reb = (d * Ut * pf) / uf
    Utcalc = (g * d ^ 2 * (pf - pb)) / (18 * uf * (1 + 0.15 * Reb ^ 0.687))
  Wend
  Reb = (d * Ut * pf) / uf
  If Reb < 200# Then
```

```
    m = (4.45 + (18# * d / dc)) * Reb ^ (-0.1)
  Else
    m = 4.45 * Reb ^ (-0.1)
  End If

  Rebs = (d * Usg * pf * (1# - eg)) / uf

' Send information to Excel worksheet
' I corresponds to row number, J corresponds to column number

I = 5#
J = 8#
Cells(I, J) = eg
Cells(I + 1, J) = Usg
Cells(I + 2, J) = Ut
Cells(I + 3, J) = Reb
Cells(I + 4, J) = Rebs
Cells(I + 5, J) = m
Cells(I + 7, J) = d

End Sub
```

APPENDIX B

This appendix contains a sample calculation and the formulae used to determine the gas volume fraction in the froth region, used during the two-phase system tests. The calculations are based on the average bubble diameter determined from digital images. The bubble diameter was found using the program SigmaScan with 300 or more bubble diameters statistically averaged to find an overall froth zone bubble diameter for each test.

B.1 Sample calculation to find the gas volume fraction in the froth zone

The procedure to find the gas volume fraction in the froth region follows the calculations outlined in Figure 3-2. A sample calculation based on a 7.8 ppm MIBC aqueous solution test is shown. The average froth bubble diameter was 434.6 μm. The gas flux was 0.00345 m/s and the fluid flux was 0.000747 m/s.

1. Calculate terminal velocity, U_t

   a. Estimate U_t

   $$U_t = 0.122 \text{ m/s}$$

   b. Calculate Re_b (equation 3-4)

   $$Re_b = \frac{d_b U_t \rho_f}{\mu_f} \tag{B-1}$$

   $$Re_b = \frac{(0.000434m)\left(0.122\frac{m}{s}\right)\left(1000\frac{kg}{m^3}\right)}{(0.001Pa*s)}$$

   $$Re_b = 52.9$$

   c. Calculate U_{tCALC} using equation 2-18 and calculate the tolerance between the estimated terminal velocity and the calculated value. If the tolerance is not within 10^{-8}, set $U_t = U_{tCALC}$ and repeat the iterative process.

   $$U_t = \frac{g d_b^2 (\rho_f - \rho_b)}{18\mu_f\left(1 + 0.15\,Re_b^{0.687}\right)} \tag{B-2}$$

$$U_t = \frac{\left(9.81\frac{m}{s^2}\right)(0.000434m)^2\left(1000\frac{kg}{m^3} - 1\frac{kg}{m^3}\right)}{18(0.001Pa*s)\left(1+0.15(52.9)^{0.687}\right)}$$

$$U_t = 1.04*10^{-4}\frac{m}{s}$$

After iterating until tolerance is below 10^{-8}, the values for terminal velocity and Reynolds number are:

$$U_t = 0.0469 \text{ m/s}$$

$$Re_b = 20.41$$

2. Calculate exponent "m" (Richardson & Zaki, 1954) (equations 2-24 to 2-26):

$$m = \left(4.45 + 18\frac{d_b}{d_c}\right)\text{Re}_b^{-0.1} \qquad \text{(B-3)}$$

$$m = \left(4.45 + 18\frac{(0.000434m)}{(0.062m)}\right)(20.41)^{-0.1}$$

$$m = 3.385$$

3. Estimate α_g

$$\alpha_g = 0.2$$

4. Calculate values for U_{gf} (equation 3-3) and Re_{bs} (equation 3-5)

$$U_{gf} = \frac{j_g}{\alpha_g} + \frac{j_f}{(1-\alpha_g)} \qquad \text{(B-4)}$$

$$U_{gf} = \frac{0.00345\frac{m}{s}}{0.2} + \frac{0.000747\frac{m}{s}}{(1-0.2)} = 0.0182\frac{m}{s}$$

$$\mathrm{Re}_{bs} = \frac{d_b U_{gf} \rho_f (1-\alpha_g)}{\mu_f} \qquad \text{(B-5)}$$

$$\mathrm{Re}_{bs} = \frac{(0.000434m)\left(0.0182\frac{m}{s}\right)\left(1000\frac{kg}{m^3}\right)(1-0.2)}{(0.001Pa*s)}$$

$$\mathrm{Re}_{bs} = 6.32$$

5. Calculate bubble diameter and calculate the tolerance. If the tolerance between the calculated and experimental bubble diameter is not within 10^{-8}, a new estimate for gas volume fraction is calculated.

$$d_{bCALC} = \left(\frac{18\mu_f U_{gf}\left(1+0.15\,\mathrm{Re}_{bs}^{0.687}\right)}{g(\rho_f - \rho_b)(1-\alpha_g)^{(m-1)}}\right)^{0.5} \qquad \text{(B-6)}$$

$$d_{bCALC} = \left(\frac{18(0.001Pa*s)\left(0.0182\frac{m}{s}\right)\left(1+0.15(6.32)^{0.687}\right)}{\left(9.81\frac{m}{s^2}\right)\left(1000\frac{kg}{m^3} - 1\frac{kg}{m^3}\right)(1-0.2)^{(3.385-1)}}\right)^{0.5}$$

$$d_{bCALC} = 2.95*10^{-4}m$$

$$\text{tolerance} = \text{abs}(d_b - d_{bCALC})$$

$$\text{tolerance} = \text{abs}(434.6 - 295.0\ \mu\text{m})$$

$$\text{tolerance} = 139.6$$

Since the tolerance is not within 10^{-8}, a new estimate for gas volume fraction was found.

$$\alpha_{gCALC} = 1 - \left(\frac{18\mu_f U_{sf} \left(1 + 0.15 \mathrm{Re}_{bs}^{0.687}\right)}{g\left(\rho_f - \rho_b\right)\left(1-\alpha_g\right)^{(m-2)} d_b^2} \right) \tag{B-7}$$

$$\alpha_{gCALC} = 1 - \left(\frac{18(0.001Pa*s)\left(0.0182\frac{m}{s}\right)\left(1+0.15(6.32)^{0.687}\right)}{\left(9.81\frac{m}{s^2}\right)\left(1000\frac{kg}{m^3} - 1\frac{kg}{m^3}\right)(1-0.2)^{(3.385-2)}\left(2.95*10^{-4}m\right)} \right)$$

$$\alpha_{gCALC} = 0.999$$

$$\alpha_g = \frac{\alpha_g + \alpha_{gCALC}}{2} \tag{B-8}$$

$$\alpha_g = \frac{0.2 + 0.999}{2} = 0.600$$

Using the bisection method to find a new estimate and repeating the process until the tolerance between the calculated and experimental bubble diameter was 10^{-8}, the value for gas volume fraction was eventually found to be 0.645.

B.2 Visual Basic program

A Visual Basic program (Excel programming language) was developed to calculate the gas volume fraction in the froth region based on the bubble diameter and the component fluxes. If the gas volume fraction was out of the range of the program, a trial and error method was used, limited to the same tolerances. The code used in the program is shown below.

```
Sub GasHoldup()
' This function will determine the gas hold-up for a flotation column
' in the froth zone, from a known bubble diameter.
' The numerical method will be a simple iterative method
' It was written by Jessica Zinterer in July 2001 @ U of A, Revision 1 August 15, 2001
```

```
' Declare all variables

Dim Jg As Double, JL As Double, pf As Double, pb As Double, uf As Double
Dim dc as Double, pw As Double, g As Double, eg1 As Double
Dim Ut As Double, Utold As Double, dL1 As Double, dL2 As Double, eg As Double
Dim Usg As Double, Db As Double, m As Double, dh1 As Double
Dim Reb As Double, Rebs As Double, Dbtemp As Double, egnew As Double
Dim tol As Double, I As Integer, J As Integer, Answer As Double

' Initialize all variables, create reference variables
Jg = Range("C7").Value
JL = Range("C8").Value
pf = Range("C9").Value
pb = Range("C10").Value
uf = Range("C11").Value
dc = Range("C12").Value
dL1 = Range("C13").Value
dL2 = Range("C14").Value
pw = Range("C15").Value
Db = Range("C16").Value
g = 9.81

' Initial guesses for Ut, eg and tolerances to be used
Ut = 0.03
tol = 0.00000000001

' Determine Terminal Velocity (Ut)
Reb = (Db * Ut * pf) / uf
Ut = (g * Db ^ 2 * (pf - pb)) / (18 * uf * (1 + 0.15 * Reb ^ 0.687))
While Abs(Ut - Utold) > tol
   Utold = Ut
' Determine Reynold's number
   Reb = (Db * Utold * pf) / uf
' Determine Terminal velocity of particle (Ut) using iterative method
' Ut = (g*dp^2*pw)/(18*uf*(1+0.15*Reb^0.687))

   Ut = (g * Db ^ 2 * (pf - pb)) / (18 * uf * (1 + 0.15 * Reb ^ 0.687))
Wend

' Determine m value based on Richardson & Zaki (1954) correlations
If Reb < 200# Then
   m = (4.45 + (18# * Db / dc)) * Reb ^ (-0.1)
Else
   m = 4.45 * Reb ^ (-0.1)
End If
```

```
' Output current answers to Excel worksheet
' I corresponds to the row number, J corresponds to the column number
I = 7#
J = 8#
Cells(I, J) = Db
Cells(I + 2, J) = Ut
Cells(I + 3, J) = Reb
Cells(I + 4, J) = m


' If difference between the calculated and experimental db is not within tolerance, use
' bisection method to find a better estimate for eg and re-iterate.
' Initialize values
   Dbtemp = 0.0007
   eg = 0.8
   Usg = 0.01
   While Abs(Dbtemp - Db) > tol

   ' Determine Slip Velocity
   ' Usg = Jg/eg + Jl/(1-eg)
      Usg = Jg / eg + JL / (1# - eg)
      Rebs = (Db * Usg * pf * (1# - eg)) / uf
      Dbtemp = ((18# * Usg * uf * (1# + 0.15 * Rebs ^ 0.687)) / (g * (pf - pb) * (1 - eg) ^
(m - 1))) ^ 0.5

   ' Determine new eg value
      egnew = 1 - ((Usg * 18# * uf * (1 + 0.15 * Rebs ^ 0.687)) / ((pf - pb) * (1 - eg) ^ (m
- 2) * g * Db ^ 2))
      eg = (eg + egnew) / 2
   Wend

' Recalculate values based on final eg value
Rebs = (Db * Usg * pf * (1# - eg)) / uf
Usg = Jg / eg + JL / (1# - eg)

' Send information to Excel worksheet
' I corresponds to the row number, J corresponds to the column number
I = 7#
J = 8#
Cells(I + 6, J) = Rebs
Cells(I + 7, J) = Usg
Cells(I + 8, J) = eg

End Sub
```

APPENDIX C

This appendix contains the procedures used to calibrate the peristaltic pumps and the air rotameters. An example is given of each, along with the calibration equations used for each set of tests conducted.

C.1 Pump Calibration

All the Masterflex peristaltic pumps were calibrated in the same manner. Setting the pump to a specific setting, a known volume of water was pumped through for a recorded amount of time and the flow rate calculated. By repeating this procedure for all the pump settings, a calibration equation was found that can be interpolated for any setting within the range tested. If different size Tygon tubing was used in the pump, than the pump had to be recalibrated using the new tubing.

An example of the data used to calibrate the feed pump used in the two-phase system tests is shown in Table C-1 and the calibration curve is shown in Figure C-1.

Table C-1. Data gathered to calibrate the Matheson I/P wash water pump used for the two-phase system tests.

Setting	Volume (mL)	Avg. Volume (mL)	Time (s)	Avg. Time (s)
2	197	194	118.1	117.1
	191		116.1	
3	212	206	82.1	80.5
	200		79.0	
4	205	203	59.1	57.6
	200		56.1	
5	208	208	46.0	45.5
	208		45.1	
6	200	197	37.1	36.6
	194		36.1	
7	209	213	33.1	33.6
	216		34.1	

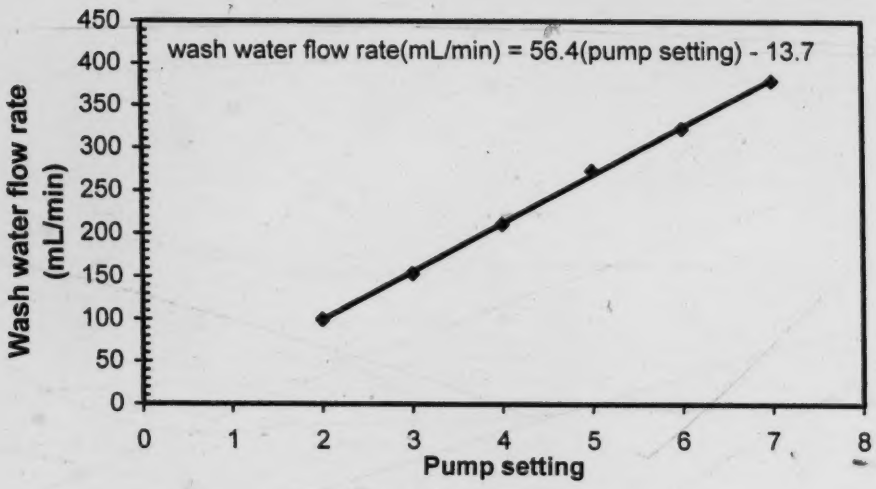

Figure C-1. Calibration curve used for the wash water pump.

C.2 Air rotameter calibration

The air rotameter was calibrated using regular dish soap. Soap was placed into the rotameter and air was then introduced. Once a soap bubble was formed, the distance it traveled in the rotameter, which correlated to volume, was timed. From the distance and time, a calibration curve for air rate was generated based on the rotameter settings. Table C-2 gives an example of the data gathered for calibration. From the data in Table C-2, Figure C-2 was plotted to derive a calibration equation.

Table C-2. Calibration data for the Matheson air rotameter used in the two phase system test.

Rotameter Setting	Flow rate (L/min)
10	0.42
20	1.13
30	1.79
40	2.57

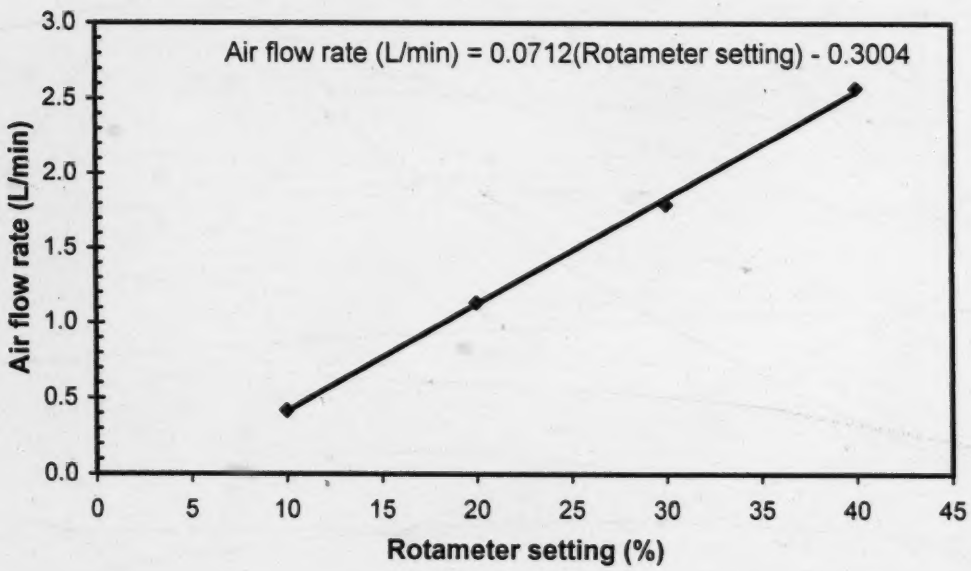

Figure C-2. Calibration curve for the Matheson air rotameter used in the two-phase system tests.

C.3 Summary of all the calibration equations

The pump calibration equations, along with the rotameter calibration equations are summarized in Table C-3 for each corresponding test.

Table C-3. Summary of all the calibration equations used for the corresponding test.

Type of test	Test stream	Calibration equation
Two-phase system	Wash water	$\text{flow rate}\left(\frac{\text{L}}{\text{min}}\right) = 0.0564(\text{pump setting}) - 0.0137$
	Recirculation	$\text{flow rate}\left(\frac{\text{L}}{\text{min}}\right) = 0.7773(\text{pump setting}) - 0.576$
	Air	$\text{flow rate}\left(\frac{\text{L}}{\text{min}}\right) = 0.0712(\text{rotameter setting}) - 0.3004$
Bitumen flotation: University of Alberta	Feed	$\text{flow rate}\left(\frac{\text{L}}{\text{min}}\right) = 0.0564(\text{pump setting}) - 0.0137$
	Recirculation	$\text{flow rate}\left(\frac{\text{L}}{\text{min}}\right) = 0.7773(\text{pump setting}) - 0.576$
	Underflow (tailings)	N/A
	Wash water	$\text{flow rate}\left(\frac{\text{L}}{\text{min}}\right) = 0.0646(\text{pump setting}) - 0.0569$
	Air	$\text{flow rate}\left(\frac{\text{L}}{\text{min}}\right) = 0.0712(\text{rotameter setting}) - 0.3004$
Bitumen flotation: Syncrude Research Centre	Feed	$\text{flow rate}\left(\frac{\text{L}}{\text{min}}\right) = 0.0814(\text{pump setting}) - 0.255$ $\text{flow rate}\left(\frac{\text{L}}{\text{min}}\right) = 0.0383(\text{pump setting}) - 0.103$
	Recirculation	$\text{flow rate}\left(\frac{\text{L}}{\text{min}}\right) = 0.7773(\text{pump setting}) - 0.576$

Type of test	Test stream	Calibration equation
	Underflow (tailings)	$\text{flow rate}\left(\frac{\text{L}}{\text{min}}\right) = 0.133(\text{pump setting}) - 0.353$
	Wash water	$\text{flow rate}\left(\frac{\text{L}}{\text{min}}\right) = 0.0646(\text{pump setting}) - 0.0569$
	Air	$\text{flow rate}\left(\frac{\text{L}}{\text{min}}\right) = 0.00647(\text{rotameter setting}) + 0.112$
Bitumen flotation: Suncor	Feed	$\text{flow rate}\left(\frac{\text{L}}{\text{min}}\right) = 0.0646(\text{pump setting}) - 0.0569$ $\text{flow rate}\left(\frac{\text{L}}{\text{min}}\right) = 0.123(\text{pump setting}) - 0.0675$ $\text{flow rate}\left(\frac{\text{L}}{\text{min}}\right) = 0.0814(\text{pump setting}) - 0.255$
	Recirculation	$\text{flow rate}\left(\frac{\text{L}}{\text{min}}\right) = 0.7773(\text{pump setting}) - 0.576$
	Underflow (tailings)	$\text{flow rate}\left(\frac{\text{L}}{\text{min}}\right) = 0.133(\text{pump setting}) - 0.353$
	Wash water	$\text{flow rate}\left(\frac{\text{L}}{\text{min}}\right) = 0.0383(\text{pump setting}) - 0.103$ $\text{flow rate}\left(\frac{\text{L}}{\text{min}}\right) = 0.0646(\text{pump setting}) - 0.0569$
	Air	$\text{flow rate}\left(\frac{\text{L}}{\text{min}}\right) = 0.00647(\text{rotameter setting}) + 0.112$

APPENDIX D

This appendix contains safety information on the use of the frother, methyl isobutyl carbinol (MIBC).

D.1 Material Safety Data Sheet (MSDS)

This Material Safety Data Sheet (MSDS) can be found at the following website: www.fishersci.ca. The following gives a brief overview of the major characteristics of MIBC, taken from the website www.fishersci.ca on May 14, 2002.

General Overview:

Physical state:	Liquid
Appearance:	Clear, Colorless
Vapor density:	3.52
Boiling point:	148 °C @ 760.00 mm_{Hg}
Specific gravity/density (g/cm^3):	0.8240
Molecular formula:	C_6H_{140}
Molecular weight (g/mol):	102.18

Stability and Reactivity:

Chemical stability:	Stable under normal temperatures and pressures
Conditions to avoid:	Incompatible materials, ignition sources, excess heat, strong oxidants
Incompatibilities with other materials:	Acids, acid chlorides, oxidizing agents
Hazardous decomposition products:	Carbon monoxide, irritating and toxic fumes and gases, carbon dioxide

Potential Health Effects and First Aid Measures:

Body Part	Potential Health Effects	First Aid	PPE to be used
Eye	Causes eye irritation. May cause chemical conjunctivitis and corneal damage	Immediately flush eyes with plenty of water for at least 15 minutes, occasionally lifting the upper and lower eyelids. Get medical aid.	Wear appropriate protective eyeglasses or chemical safety goggles.
Skin	May cause irritation and dermatitis. May cause cyanosis of the extremities.	Get medical aid. Flush skin with plenty of soap and water for at least 15 minutes while removing contaminated clothing and shoes. Wash clothing before reuse.	Wear appropriate protective gloves to prevent skin exposure. Wear appropriate protective clothing to prevent skin exposure.
Ingestion	May cause gastrointestinal irritation with nausea, vomiting and diarrhea. May cause liver and kidney damage. May be harmful if swallowed. May cause central nervous system depression. Ingestion o large amounts may cause	Never give anything by mouth to an unconscious person. Get medical aid. Do NOT induce vomiting. If Conscious and alert., rinse mouth and drink 2 – 4 cupfuls of milk or water.	

Body Part	Potential Health Effects	First Aid	PPE to be used
	CNS depression.		
Inhalation	May cause respiratory tract irritation. May cause liver and kidney damage. Aspiration may lead to pulmonary edema. Vapors may cause dizziness or suffocation. May cause cardiac abnormalities. Exposure may produce metabolic acidosis. Inhalation at high concentrations may cause CNS depression and asphyxiation. May cause burning sensation in the chest.	Remove from exposure to fresh air immediately. If breathing is difficult, give oxygen. Get medical aid. Do NOT use mouth-to-mouth resuscitation. If breathing has ceased apply artificial respiration using oxygen and a suitable mechanical device such as a bag and a mask.	A respiratory protection program that meets Standard Safety requirements.

Fire and Spills:

For small fires, use dry chemical, carbon dioxide, water spray or alcohol-resistant foam. For large fires, use water spray, fog, or alcohol-resistant foam. Use water spray to cool fire-exposed containers. Water may be ineffective. Do NOT use straight streams of water.

Absorb spill with inert material (e.g. vermiculite, sand, or earth), then place in suitable container. Avoid runoff into storm sewers and ditches that lead to waterways. Clean up

spills immediately, observing precautions in the Protective Equipment section. Remove all sources of ignition. Use a spark-proof tool. Provide ventilation. A vapor suppressing foam may be used to reduce vapors.

Handling:

Wash thoroughly after handling. Use with adequate ventilation. Ground and bond containers when transferring material. Use spark-proof tools and explosion proof equipment. Avoid contact with eyes, skin, and clothing. Empty containers retain product residue, (liquid and/or vapor), and can be dangerous. Keep container tightly closed. Avoid contact with heat, sparks, and flame. Avoid ingestion and inhalation. Do not pressurize, cut, weld, braze, solder, drill, grind, or expose empty container to heat, sparks, or open flames.

D.2 General information on frothers

MIBC is a surfactant molecule in which the hydroxide group (-OH) corresponds to a hydrophilic head. MIBC will adsorb at an air-water interface and tend to form a monolayer, which will decrease the surface tension of the bubble and reduce the chances of coalescence. Since coalescence decreases, smaller gas bubbles are easier to produce when using a frother. Frothers are also known to reduce the bubble rise velocity, although the influence of frothers depends on the type and concentration. MIBC frothing properties are linked to mineral hydrophobicity (Gourram-Badri et al. 1997).

APPENDIX E

This appendix contains the procedures used to operate the flotation column. The first section describes the operational procedures used for the two-phase system tests. The second section deals with the procedures used for operating the column for the bitumen flotation tests.

E.1 Two-phase system test operating procedure

For the two-phase system tests, the tailings and froth streams were recycled and re-introduced into the column as wash water. The interface was set at 4 cm below the top of the froth. All measurements were made at equilibrium and room temperature.

To start the column, air was introduced first to prevent back pressure from causing slurry to enter the air line. The air supply was regulated to a pressure 137.9 kPa (20 psi) before entering the column. The slurry was introduced next via the wash water pump. To fill the column rapidly, the pump setting was at its maximum. The underflow stream, which did not use a pump, was used to control the pulp-froth interface level and was adjusted such that the interface was approximately 4 cm below the top of the froth. Once the column was filled to the interface level, the wash water pump was set to a low setting and the recirculation pump was started, also at a low pump setting. Both the recirculation and wash water pump setting were slowly incremented to the desired test setting. If the pumps were set directly at the desired setting, the column experienced unsteady-state conditions. Once equilibrium was reached at the desired settings, the interface was more accurately adjusted to 4 cm below the top of the froth. Before taking measurements, steady-state had to be ensured by watching the amount of oscillation in the pulp-froth interface level. If no oscillation was observed for 15 consecutive minutes, steady-state was reached. After equilibrium was reached, the manometer readings were taken, the pump settings recorded, and the digital images taken.

To shut down the column, all the pumps were set to zero. The air rotameter was left at the operating setting to prevent the slurry from entering the air lines. Once the pumps were turned off, the column was drained via the tailings line.

E.2 Bitumen flotation test operating procedure

The flotation column was operated continuously for the bitumen flotation tests. When used in industry, the column will be operated in a continuous manner and the start-up and shut down procedures are vital. The column set-up follows the schematic shown in Figure 4-1. The feed was introduced in the recirculation line just before the air sparger, while the underflow (tailings) and froth streams were not recycled and sent to the sump pump. There were pumps for the feed, recirculation, wash water, and underflow (tailings) streams.

The flotation column was first started using process water instead of the oil sand slurry. This allowed the system to reach equilibrium more efficiently. Start-up followed the procedure for the two-phase system tests outlined in Section D.1. Once equilibrium was reached at the desired test settings, the feed line was switched from process water to oil sand slurry. From here, the tailings pump setting was adjusted to cause the pulp-froth interface to be within 1 to 8 cm of the top of the froth. Once equilibrium was reached at the desired settings, measurements and samples were taken.

To shut down the column, the pump settings were all turned to zero, except the tailings pump and the wash water pump. The slurry was pumped out the column via the tailings pump. The wash water was used to rinse the column of any excess slurry. Between testing locations, the column and the equipment was thoroughly cleaned of bitumen using solutions of toluene.

APPENDIX F

This appendix contains the raw data and results from the two-phase system tests using systems of air and either process water or de-ionized water with low concentrations (7.8 or 15.5 ppm) MIBC.

F.1 Two-phase system test data

The raw data for the first set of tests is displayed in Table F-1. The results from the drift flux analysis tests are displayed in Table F-2. The other tables include the data used for the figures in Chapter 3.0.

Table F-1. Raw data for two-phase system tests.

	Pump/rotameter settings			
Medium	**Feed**	**Recirculation**	**Air (%)**	**Manometer height (m)**
Process Water	5	6	32	0.051
	3	4	20	0.032
	5	7	11	0.048
	3	6	11	0.042
	3	6	10	0.043
	3	6	12	0.049
	3	4	12	0.036
	3	4	8.5	0.029
	3	5	9.5	0.042
	3	4	29	0.037
	3	4	17	0.038
7.8 ppm MIBC solution	4.1	4	13	0.032
	4.1	4	16	0.04
	4.1	4	15	0.038
	4.1	4	18	0.043
	3	4.5	15	0.04
	3	4.5	10	0.031
	3	4.1	16	0.035
	3	4.1	17.5	0.037
	4.1	4	18	0.04
15.5 ppm MIBC solution	3	4	19.5	0.04
	3	4	18	0.036
	3.5	4	16	0.036
	3.5	4	13	0.031

Table F-2. Results for the two-phase system tests.

Medium	J_g (m/s)	J_f (m/s)	Diameter (μm)	Gas volume fraction	Re_b	Diameter (μm)	Gas volume fraction	Re_b	"m"
Process Water	3.46E-03	3.65E-04	330	0.14	11	337	0.54	12	2.95
	6.20E-03	4.38E-04	705	0.09	56	786	0.80	70	2.29
	2.67E-03	2.20E-04	285	0.13	8	365	0.65	14	2.71
	2.67E-03	6.72E-05	302	0.11	9	371	0.68	14	2.74
	2.27E-03	1.37E-04	270	0.12	7	324	0.63	11	2.87
	3.06E-03	4.71E-05	307	0.13	9	387	0.67	16	2.69
	3.06E-03	8.61E-05	361	0.10	14	392	0.68	16	2.84
	1.68E-03	3.04E-04	272	0.08	7	296	0.61	9	3.09
	2.08E-03	4.88E-05	257	0.11	6	298	0.62	9	3.00
	9.74E-03	3.25E-05	958	0.10	103	1077	0.85	130	2.12
	5.02E-03	5.30E-04	516	0.10	30	710	0.79	57	2.21
7.8 ppm MIBC solution	3.45E-03	7.47E-04	432	0.09	20	435	0.65	20	2.78
	4.63E-03	1.26E-04	464	0.11	2	506	0.71	28	2.61
	4.24E-03	4.38E-04	450	0.10	22	512	0.71	29	2.56
	5.42E-03	6.21E-05	501	0.12	28	518	0.70	30	2.63
	4.24E-03	1.41E-05	432	0.11	20	446	0.68	22	2.74
	2.27E-03	3.33E-04	321	0.08	10	406	0.70	18	2.65
	4.63E-03	4.47E-04	511	0.09	29	660	0.78	49	2.32
	5.22E-03	1.83E-04	540	0.10	32	582	0.74	38	2.51
	5.42E-03	1.74E-04	527	0.11	31	540	0.71	32	2.61
15.5 ppm MIBC solution	6.01E-03	2.03E-04	575	0.11	37	710	0.79	57	2.29
	5.42E-03	4.56E-04	571	0.10	36	718	0.79	58	2.27
	4.63E-03	4.46E-04	501	0.10	28	648	0.77	47	2.32
	3.45E-03	7.84E-04	442	0.08	21	546	0.79	33	2.44

Table F-3. Data used in generating Figure 3-6, a comparison between the bubbly zone measured and calculated average bubble diameters.

	Pump/Rotameter Settings				
Medium	**Feed**	**Recirc.**	**Air (%)**	**Calculated d_b (mm)**	**Measured d_b (mm)**
Process water	5	6	32	330	N/A
	3	4	20	705	502
	5	7	11	285	381
	3	6	11	302	305
	3	6	10	270	331
	3	6	12	307	342
	3	4	12	361	243
	3	4	8.5	272	224
	3	5	9.5	257	220
	3	4	29	958	811
	3	4	17	516	505
7.8 ppm MIBC solution	4.1	4	13	432	265
	4.1	4	16	464	298
	4.1	4	15	450	320
	4.1	4	18	527	N/A
	3	4.5	15	432	308
	3	4.5	10	321	275
	3	4.1	16	511	395
	3	4.1	17.5	540	420
	4.1	4	18	501	348
15.5 ppm MIBC solution	3	4	19.5	575	530
	3	4	18	571	455
	3.5	4	16	501	443
	3.5	4	13	442	314

Note: In some cases, the measured bubble diameter is not given (replaced by "N/A"). This is due to the fact that the digital images were out of focus and a representative sample of bubbles could be averaged.

Table F-4. Data used in generating Figure 3-7, the relationship between gas flux and the bubbly zone bubble diameter.

j_f (m/s)	j_g (m/s)	Calculated d_b (μm)	Medium tested
6.72E-05	2.67E-03	273	Process water
	3.06E-03	323	Process water
	4.24E-03	445	7.8 ppm MIBC solution
	5.42E-03	518	7.8 ppm MIBC solution
2.03E-04	2.67E-03	293	Process water
	3.46E-03	343	Process water
	4.63E-03	461	7.8 ppm MIBC solution
	5.22E-03	526	7.8 ppm MIBC solution
	6.01E-03	575	15.5 ppm MIBC solution
4.38E-04	3.46E-03	379	Process water
	4.24E-03	488	7.8 ppm MIBC solution
	5.22E-03	540	7.8 ppm MIBC solution
	6.20E-03	705	Process water

Table F-5. Bubbly zone data used in generating Figure 3-9, relationship between exponent "m" and bubble Reynolds number.

Medium	jg (m/s)	jf (m/s)	α_g	j_{gf} (cm/s)	d_b (μm)	U_t (m/s)	Re_b	m
Process water	3.46E-03	3.65E-04	0.138	0.303	330.0	0.0333	11.0	2.72
	6.20E-03	4.38E-04	0.086	0.570	705.1	0.0798	56.3	1.84
	2.67E-03	2.20E-04	0.130	0.235	285.0	0.0274	7.8	2.86
	2.27E-03	1.37E-04	0.116	0.202	269.8	0.0254	6.8	2.96
	2.67E-03	6.72E-05	0.114	0.237	301.9	0.0296	8.9	2.81
	3.06E-03	4.71E-05	0.132	0.266	306.8	0.0303	9.3	2.82
	1.68E-03	3.04E-04	0.078	0.157	272.3	0.0257	7.0	2.38
	3.06E-03	8.61E-05	0.097	0.277	361.3	0.0375	13.5	2.67
	2.08E-03	4.88E-05	0.114	0.185	256.8	0.0236	6.1	3.01
	5.02E-03	5.30E-04	0.103	0.456	516.3	0.0572	29.6	2.29
	9.74E-03	2.70E-04	0.100	0.879	958.0	0.1079	103.4	1.96
7.8 ppm MIBC	5.42E-03	6.21E-05	0.116	0.479	500.6	0.0553	27.7	2.28
solution	3.45E-03	7.47E-04	0.086	0.322	432.1	0.0466	20.1	2.22
	4.24E-03	4.38E-04	0.103	0.385	450.0	0.0489	22.0	2.4
	4.63E-03	1.26E-04	0.108	0.414	463.7	0.0506	23.5	2.36
	5.42E-03	1.74E-04	0.108	0.485	526.8	0.0585	30.8	2.24
	2.27E-03	3.33E-04	0.084	0.211	321.5	0.0322	10.4	2.37
	4.24E-03	1.41E-05	0.108	0.378	431.6	0.0466	20.1	2.45
	4.63E-03	4.47E-04	0.095	0.423	510.6	0.0565	28.9	2.25
	5.22E-03	1.83E-04	0.100	0.472	539.6	0.0601	32.4	2.28
15.5 ppm MIBC	5.42E-03	4.56E-04	0.097	0.493	570.6	0.0639	36.5	2.18
solution	6.01E-03	2.03E-04	0.108	0.538	574.8	0.0644	37.0	2.18
	4.63E-03	4.46E-04	0.097	0.422	500.7	0.0553	27.7	2.34
	3.45E-03	7.84E-04	0.084	0.323	441.6	0.0478	21.1	2.06

Table F-6. Data used to generate Figure 3-10, the relationship between Reynolds number and bubble diameter in the froth zone.

Medium	j_g (m/s)	j_f (m/s)	d_b (μm)	m (trial & error)	Re_f (back calculated)	Re_f (re-calculated)	m (re-calculated)
Process Water	3.4587E-03	3.6517E-04	337.4	2.99	6.51	5.78	3.07
	6.2028E-03	4.3811E-04	786.0	2.35	21.62	21.87	2.35
	2.6653E-03	2.1959E-04	365.4	2.98	6.61	6.50	2.99
	2.2722E-03	1.3680E-04	324.4	3.11	5.44	5.45	3.11
	2.6653E-03	6.7236E-05	370.7	2.99	6.51	6.64	2.98
	3.0583E-03	4.7059E-05	387.0	2.94	7.02	7.08	2.93
	1.6826E-03	3.0397E-04	296.1	3.21	4.69	4.78	3.20
	3.0583E-03	8.6136E-05	392.3	2.92	7.25	7.23	2.92
	2.0757E-03	4.8790E-05	297.6	3.21	4.69	4.81	3.19
	5.0236E-03	5.2968E-04	710.3	2.43	17.78	18.48	2.41
	9.7403E-03	2.7042E-04	1077.3	2.17	38.28	37.46	2.18
7.78 ppm MIBC	5.4167E-03	6.2054E-05	518.1	2.67	10.97	11.11	2.66
	3.4514E-03	7.4739E-04	434.6	2.78	9.07	8.45	2.82
	4.2375E-03	4.3775E-04	511.6	2.65	11.37	10.89	2.67
	4.6306E-03	1.2617E-04	505.6	2.67	10.97	10.69	2.68
	5.4167E-03	1.7376E-04	539.9	2.57	13.22	11.86	2.63
	2.2722E-03	3.3313E-04	406.3	2.9	7.48	7.62	2.89
	4.2375E-03	1.4070E-05	446.1	2.78	9.07	8.79	2.80
	4.6306E-03	4.4740E-04	660.1	2.49	15.56	16.38	2.47
	5.2201E-03	1.8342E-04	581.7	2.56	13.48	13.35	2.57
15.6 ppm MIBC	5.4167E-03	4.5599E-04	717.9	2.42	18.19	18.81	2.41
	6.0063E-03	2.0292E-04	710.1	2.43	17.78	18.47	2.41
	4.6306E-03	4.4561E-04	648.0	2.5	15.24	15.90	2.48
	3.4514E-03	7.8435E-04	545.6	2.61	12.24	12.05	2.62

APPENDIX G

This appendix contains information on the Dean Stark method used to analyze samples for the weight percentage of oil, water, and solids.

G.1 Dean Stark method

The Dean Stark method is used to analyze samples for oil, water, and solids content. The following outlines the procedure used to complete this process.

Samples are gathered in glass jars. Before starting the procedure, a few of the materials used are weighed. The materials that are weighed include: the empty glass jar that supports the thimble while transferring the sample, the empty filter thimble including three kim-wipes, and the empty plastic water jar. The empty filter thimble is then placed into the empty glass jar, which catches any liquids that soak through the thimble. Now, the sample is transferred from the original sample jar into the filter thimble. If there the sample is large or contains excess amounts of sand, two or more thimbles may be used for the single sample. Each thimble should only be filled to approximately two-thirds to prevent the thimble from rupturing from the weight. If using several thimbles, one thimble should be used for the bitumen and another for the water. While transferring the sample, often the bitumen is hard to remove. Toluene can dissolve the bitumen first and the bitumen-toluene solution can more easily transferred into the thimble. The sand should be transferred last. The kim-wipes that were weighed with the empty thimble are used last to ensure all the sample is removed from the jar. Once the kim-wipes are used, they should be placed in the full thimble as far down as possible.

Now that the sample is transferred, the thimble is moved from the holding jar into a wire holder. If the thimble is saturated with water, it may be hard to move without

tearing it. If there is a large amount of sand and water in the sample, it is often wise to place the empty thimble into the wire frame prior to transferring the sample. Once the thimble is situated in the wire frame, a wire top is placed on it. The wire frame and thimble are then placed within a distillation flask that is situated within a heater, as shown in Figure G-1.

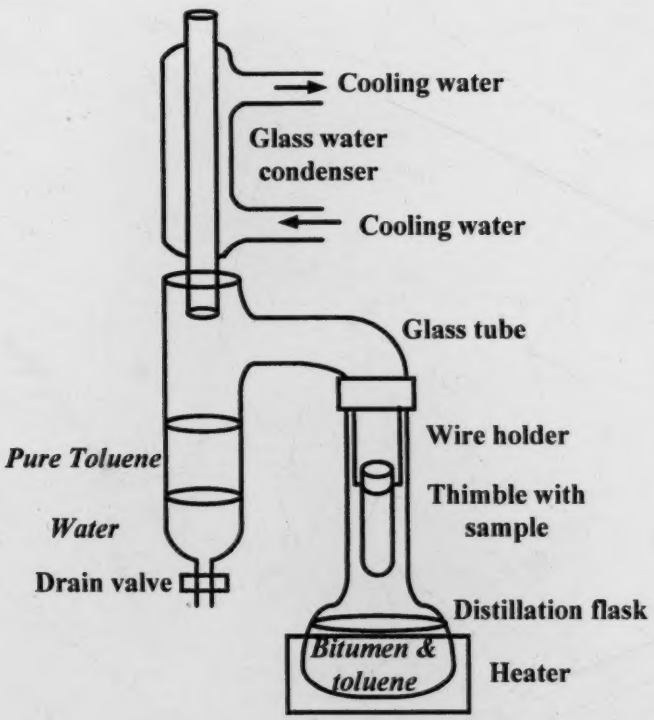

Figure G-1. Schematic of separation process used in the Dean Stark method.

The excess liquid from the holding jar is then placed in the round-bottom distillation flask. To ensure all the sample is transferred, the holding jar is rinsed with toluene. The toluene used to rinse the jar is also placed into the distillation flask. Once the sample is in place and all the liquids transferred to the flask, the flask is then filled with toluene to

the same level as the outer metal heater (approximately 150 mL total toluene). After the distillation flask is filled with toluene and the sample in place, the distillation flask is stoppered with a glass tube, as shown in Figure G-1. This glass tube consists of a holding tube with a drain valve on the bottom of it. Be sure that the drain is closed. Once the glass tube is in place, the glass water condenser is placed on top of the glass tube. The condenser should be slightly loose to prevent pressure build-up. Now that all the equipment is in place, the separation process can begin.

First the cooling water is introduced into the water condenser. Once it is circulating, the heater that the distillation flask is placed in is set to 90 °C. The sample is then left to distill until fully separated. Full distillation depends on the size of the sample, but is approximately three to four hours. To determine when distillation is complete, the water and toluene that has gathered in the glass tube will appear clear with no water droplets rising through it for ten consecutive minutes.

The theory behind this procedure is that the toluene and water will evaporate from the sample. As the water and toluene evaporate, the droplets contact the water condenser causing the droplets to condense into the glass tube. Since the water is denser than toluene, the water will settle below the pure toluene and can be drained off into the plastic water jar (that was weighed in the beginning). The thimble should now only contain solids while the bottom of the distillation flask should contain a solution of toluene-bitumen.

Once the sample has finished distilling, all products should be left to cool to room temperature. After cooling, the plastic water jar should be weighed. To determine the water content in the sample, the following calculation is used:

$$\%\ \text{water} = \frac{\text{full plastic water jar - empty plastic water jar}}{\text{full filter thimble - empty filter thimble}} * 100 \qquad \text{(G-1)}$$

To determine the amount of solids in the sample, the full thimble (including the solids) must be dried in a vacuum oven (if temperature is set at 40 °C it will take about eight hours while at 60 °C it takes about four hours). Once the thimble has been dried, it is stored in a decicator and is later weighed. The solids content then determined using:

$$\%\ \text{solids} = \frac{\text{dried full thimble - empty filter thimble}}{\text{full filter thimble - empty filter thimble}} * 100 \qquad \text{(G-2)}$$

To find the bitumen content, the solution of toluene-bitumen is transferred to a 250 mL volumetric flask. If there are any solid particles in the bitumen-toluene solution, the solution is centrifuged before proceeding. The solution in the volumetric flask is then diluted to 250 mL with toluene and thoroughly mixed. A dry filter paper is weighed at this point. The filter paper is than placed on a glass dish. A 5 mL pipette is filled with the bitumen-toluene solution and discharged to cover the filter paper. Once the filter paper is doused, it is left to dry in the fume hood for approximately 15 minutes. It is than weighed. To find the bitumen content, the following is used:

$$\%\ \text{bitumen} = \frac{\frac{250}{5} * (\text{dried bitumen on filter paper - dry filter paper})}{\text{full filter thimble - empty filter thimble}} * 100 \qquad \text{(G-3)}$$

APPENDIX H

This appendix contains a general HAZOP completed at Syncrude Research Ltd. for the possible safety issues in operating the flotation column.

H.1 HAZOP for flotation column

Possible Hazard	Measures taken to prevent Injury
Plugged lines	Spare tubing available
Plugged feed screen	An extra screen is available. A flush system was installed on the feed line to allow backflushing with hot process water to help rinse screen.
Broken glass tubing	Glass is fairly sturdy, and no past problems with the possibility of cutting, or cracking of the glass.
Rotating pump parts	Rotating guards are installed on all the pumps.
Light	Light comes with a cover to prevent splash back on the bulb. It is a regular 60 Watt bulb, and poses no threat as a heat source.
Electrical wiring	All electrical lines are CSA approved.

APPENDIX I

This appendix includes the raw and resultant data for the bitumen tests. There were three sets of tests done: University tests, Syncrude Research tests, and Suncor tests.

I.1 Tests at the University of Alberta

For the university tests, only two tests were completed. The following tables show the raw and resulting data.

Table I-1. The raw data collected for the University bitumen flotation tests.

Parameter		Test 1	Test 2
	Date:	Feb. 2002	Feb. 2002
Pump settings	Feed	7	9
	Recirculation	3	3
	Air (%)	9.8	9.8
	Underflow (RPM)	240	290
	Wash water	8.6	8.6

Table I-2. The resultant data collected for the University bitumen flotation tests.

Flow rates (L/min)	Test 1	Test 2
Feed	0.4	0.5
Recirculation	1.8	1.8
Air	0.4	0.4
Underflow	N/A	N/A
Wash water	0.5	0.5

I.2 Syncrude Research tests

The following show the raw and resultant data for the tests completed at the Syncrude Research Centre. Only three tests were completed. The laboratory at Syncrude Research completed the sample analysis.

Table I-3. Raw data for bitumen flotation tests conducted at the Syncrude Research Centre.

Parameter		Test 1	Test 2	Test 3
	Date	March 14/02	March 18/02	March 19/02
Pump settings	Feed	6	5	10
	Recirculation	3	10	10
	Air (%)	70	44	44
	Underflow	7	8	6
	Wash water	7	10	10
Samples Taken	Froth	yes	no	no
	Underflow	yes	yes	yes
	Feed	yes	yes	yes
	PSV Middlings	yes	yes	yes

Table I-4. Resultant data for bitumen flotation tests conducted at the Syncrude Research Centre.

Parameter		Test 1	Test 2	Test 3
Flow rates (L/min)	Feed	0.23	0.09	0.28
	Recirculation	1.68	7.20	7.20
	Air	0.56	0.40	0.40
	Underflow	0.58	0.71	0.45
	Wash water	0.40	0.59	0.59
PSV middlings (wt. %)	Bitumen	2.56	7.53	8.27
	Solids	43.19	38.66	37.51
	Water	54.42	52.94	53.87
Column tailings (wt. %)	Bitumen	0.46	0.06	0.46
	Solids	19.99	4.95	27.13
	Water	80.35	94.67	72.15
Column froth (wt. %)	Bitumen	3.23	N/A	45.65
	Solids	3.37	N/A	17.11
	Water	93.79	N/A	34.57
Recovery (%)		63	95	98

Also recorded were the pilot plant testing conditions on the days that the flotation column was operated. Table I-5 shows the type of ore and chemicals added to the system.

Table I-5. Pilot plant conditions on the same day as the bitumen flotation tests, including ore type, grade, and fines, as well as chemical type and concentration.

Parameter	Test 1	Test 2	Test 3
Type of Ore	Aurora High Grade Estuarine	Aurora - Research Transition Stockpile	Aurora - Research Transition Stockpile (Oil Sand C)
Ore grade	13.3	11.4	11.7
Ore fines	19.7	30.1	29.9
Chemicals added	NaOH; diesel	NaOH; diesel	NaOH; diesel
Chemical concentration	0.01 wt% of ore; 200 ppm of ore	0.01 wt% of ore; 200 ppm of ore	0.01 wt% of ore; 200 ppm of ore

I.3 Suncor in-plant tests

Raw data and results from the Suncor tests are shown in the tables below. There were thirteen tests completed. Sample analysis was done by McMurray Resources Ltd. Research & Testing and was compared to samples analyzed using the Dean Stark Method at the University of Alberta.

Table I-6 Raw data for the tests completed at Suncor.

		Pump and Rotameter Settings					Samples Taken		
Test	Date	Feed	Recirc.	Air (%)	Underflow	Wash water	Froth	Underflow	Feed
1	04/18/02	7.2	3.5	52.0	7.7	12.0	no	yes	yes
2	04/18/02	6.0	3.5	52.0	9.0	12.0	no	yes	yes
3	04/18/02	8.0	3.5	52.0	11.8	12.0	no	yes	yes
4	04/18/02	10	3.5	52	12.5	12	yes	yes	yes
5	04/18/02	4	7	52	8.5	12	yes	yes	yes
6	04/18/02	6	7	52	9.5	12	yes	yes	yes
7	04/18/02	8	7	52	9.5	12	yes	yes	yes
8	04/18/02	10	7	52	11	12	yes	yes	yes
9	04/19/02	10	5	29	10.5	12	yes	yes	yes
10a	04/19/02	17.5	5	52	10	6.5	yes	yes	yes
10b	04/19/02	17.5	5	52	10	6.5	yes	yes	yes
11	04/19/02	17.4	5	68	9.5	3	yes	yes	yes
12	04/19/02	17.4	5	52	9.5	3	yes	yes	yes
13	04/19/02	17.4	5	52	8	0	yes	yes	yes

Table I-7. Raw data for feed sample analysis completed at the University of Alberta for all the tests conducted at Suncor.

	Test	1	2	3	4	5	6	7	8	9	10	11	12	13
Water	Full water jar (g)	253.5	316.7	360.1	317.2	263.1	355.2	192.4	N/A	N/A	N/A	368.5	315.1	350.5
	Empty water jar (g)	49.4	49.8	56.2	49.6	44.3	74.2	48.9	N/A	N/A	N/A	68.6	43.9	68.2
	Full jar (g)	716.8	836.4	877.7	808.4	658.2	768.4	424.3	N/A	N/A	N/A	673.5	641.9	666.2
	Empty jar (g)	253.0	264.9	251.6	253.8	254.1	253.3	181.2	N/A	N/A	N/A	57.9	57.8	58.2
	Empty thimble + jar (g)	473.4	465.7	473.2	471.3	467.6	467.7	311.3	N/A	N/A	N/A	623.2	465.6	464.1
	Water (wt.%)	44.0	46.7	48.5	48.3	54.1	54.5	59.0	50.6	53.5	46.0	48.7	46.4	46.4
Solids	Dried thimble with solids + jar (g)	727.2	766.3	788.0	751.7	648.7	694.3	408.3	N/A	N/A	N/A	928.6	770.1	781.4
	Empty thimble + jar (g)	473.4	465.7	473.2	471.3	467.6	467.7	311.3	N/A	N/A	N/A	623.2	465.6	464.1
	Full jar (g)	716.8	836.4	877.7	808.4	658.2	768.4	424.3	N/A	N/A	N/A	673.5	641.9	666.2
	Empty jar (g)	253.0	264.9	251.6	253.8	254.1	253.3	181.2	N/A	N/A	N/A	57.9	57.8	58.2
	Solids (wt.%)	54.7	52.6	50.3	50.6	44.8	44.0	39.9	46.4	45.3	52.2	49.6	52.1	52.2
Bitumen	Dried filter paper + bitumen (g)	1.1	1.1	1.1	1.1	1.1	1.2	1.1	N/A	N/A	N/A	1.2	1.2	1.2
	Dried filter paper (g)	1.1	1.1	1.1	1.1	1.1	1.1	1.1	N/A	N/A	N/A	1.1	1.1	1.1
	Full jar (g)	716.8	836.4	877.7	808.4	658.2	768.4	424.3	N/A	N/A	N/A	673.5	641.9	666.2
	Empty jar (g)	253.0	264.9	251.6	253.8	254.1	253.3	181.2	N/A	N/A	N/A	57.9	57.8	58.2
	Empty thimble + jar (g)	473.4	465.7	473.2	471.3	467.6	467.7	311.3	N/A	N/A	N/A	623.2	465.6	464.1
	Bitumen (wt.%)	0.2	0.2	0.2	0.3	0.5	0.6	0.5	1.0	1.2	1.8	1.2	1.2	0.8

Table I-8. Raw data for the underflow sample analysis completed at the University of Alberta for the flotation tests conducted at Suncor.

	Test	1	2	3	4	5	6	7	8	9	10	11	12	13
Water	Full water jar (g)	249.8	253.7	258.3	291.0	278.1	301.1	281.1	N/A	148.4	199.6	204.7	194.3	200.9
	Empty water jar (g)	56.6	49.6	49.4	44.1	43.9	49.8	49.5	N/A	25.0	49.7	43.5	49.5	49.5
	Full jar (g)	562.8	634.5	631.3	627.4	575.9	614.8	616.1	N/A	371.3	439.8	473.5	472.5	478.6
	Empty jar (g)	262.7	250.0	251.4	253.0	249.4	252.4	254.0	N/A	182.2	180.2	181.3	181.4	181.5
	Empty thimble + jar (g)	318.9	310.1	316.3	310.7	320.3	316.4	311.1	N/A	310.4	310.2	309.7	309.3	313.6
	Water (wt. %)	64.4	53.1	55.0	65.9	71.8	69.3	64.0	62.1	65.3	57.7	55.2	49.7	51.0
Solids	Dried thimble with solids + jar (g)	426.4	487.5	484.4	435.8	407.5	424.1	435.7	N/A	374.3	417.8	439.2	456.1	457.4
	Empty thimble + jar (g)	318.9	310.1	316.3	310.7	320.3	316.4	311.1	N/A	310.4	310.2	309.7	309.3	313.6
	Full jar (g)	562.8	634.5	631.3	627.4	575.9	614.8	616.1	N/A	371.3	439.8	473.5	472.5	478.6
	Empty jar (g)	262.7	250.0	251.4	253.0	249.4	252.4	254.0	N/A	182.2	180.2	181.3	181.4	181.5
	Solids (wt.%)	35.8	46.2	44.2	33.4	26.7	29.7	34.4	37.7	33.8	41.4	44.3	50.5	48.4
Bitumen	Dried filter paper + bitumen (g)	1.1	1.1	1.1	1.1	1.1	1.1	1.1	N/A	1.1	1.1	1.1	1.1	1.1
	Dried filter paper (g)	1.1	1.1	1.1	1.1	1.1	1.1	1.1	N/A	1.1	1.1	1.1	1.1	1.1
	Full jar (g)	562.8	634.5	631.3	627.4	575.9	614.8	616.1	N/A	371.3	439.8	473.5	472.5	478.6
	Empty jar (g)	262.7	250.0	251.4	253.0	249.4	252.4	254.0	N/A	182.2	180.2	181.3	181.4	181.5
	Empty thimble + jar (g)	318.9	310.1	316.3	310.7	320.3	316.4	311.1	N/A	310.4	310.2	309.7	309.3	313.6
	Bitumen (wt. %)	0.1	0.1	0.1	0.1	0.1	0.1	0.2	0.2	0.2	0.3	0.2	0.3	0.2

Table I-9. Results from the tests conducted at Suncor.

		Increasing feed rate (low recirc. rate)				Increasing feed rate (high recirc. rate)				Increasing air rate (med. recirc. rate, high feed rate)			Decreasing wash water	
Parameter	**Test**	**1**	**2**	**3**	**4**	**5**	**6**	**7**	**8**	**9**	**10**	**11**	**12**	**13**
Flow rates (L/min)	Feed	0.41	0.67	0.92	1.17	0.43	0.67	0.92	1.17	1.17	1.17	1.16	1.16	1.16
	Recirculation	2.13	2.14	2.14	2.14	4.87	4.87	4.87	4.87	3.31	3.31	3.31	3.31	3.31
	Air	0.45	0.45	0.45	0.45	0.45	0.45	0.45	0.45	0.30	0.45	0.55	0.45	0.45
	Tailings	0.67	0.85	1.22	1.31	0.91	0.91	0.91	1.11	1.05	0.98	0.91	0.91	0.71
	Wash water	0.36	0.36	0.36	0.36	0.36	0.36	0.36	0.36	0.36	0.36	0.36	0.14	0.00
Feed (wt. %)	Bitumen	0.16	0.11	0.13	0.23	0.41	0.45	0.47	1.03	1.20	1.82	0.91	0.74	0.75
	Solids	54.85	52.81	51.92	47.89	45.08	44.31	40.77	46.06	45.26	52.23	52.04	52.59	51.35
	Water	44.91	47.11	47.95	51.87	54.48	55.28	58.78	53.05	53.47	45.95	47.13	46.65	47.88
Tailings (wt. %)	Bitumen	0.02	0.03	0.04	0.05	0.06	0.10	0.15	0.14	0.15	0.30	0.14	0.22	0.16
	Solids	32.21	47.90	43.77	32.42	27.23	29.38	33.84	37.95	33.48	41.43	45.69	49.74	49.57
	Water	67.84	52.01	56.23	67.40	72.76	70.51	66.01	61.85	66.48	57.73	54.18	49.94	50.34
	Recovery (%)	100	100	100	100	70	72	71	83	86	87	88	86	83